

ABSTRACT

Title of dissertation: EVOLUTION OF FACETED CRYSTAL SURFACES:
 MODELING AND ANALYSIS

Kanna Nakamura, Doctor of Philosophy, 2014

Dissertation directed by: Professor Dionisios Margetis
 Department of Mathematics
 Professor Antoine Mellet
 Department of Mathematics

Nanoscale materials hold the promise of leading to breakthroughs in the development of electronics. These materials are of great interest especially at low temperatures due to their thermal stability. In order to predict the evolution of crystal surfaces at such precision, physical effects across a wide range of scales, from atomistic processes to large-scale thermodynamics, must be consolidated [71, 73].

This thesis aims to incorporate the microscale information carried by the atomic dynamics to the evolution of an apparently smooth surface at macroscopic scale. At the nanometer scale, the motion of atomic defects in the surface is described by ordinary differential equations (ODEs). At larger scale, the atomic roughness is no longer detectable and the surface evolution can be described by a smooth function for the surface height on some reference plane. This height function satisfies certain partial differential equations (PDEs) on the basis of the thermodynamic principles. These ODEs and PDEs separately yield predictions of distinct characteristics for the morphological evolution of a surface. While modeling at small scale has the advantage of simple physical principles, observation at the larger scale offers more tangible intuition for the topographic evolution and it is often more suitable for relating to experiments [53].

A principal theme of this thesis is to understand the difference or error between these two predictions. The error can be conveniently assessed numerically but this is not sufficient to achieve a deeper understanding of the problem. To this end, this thesis addresses both quantitative notion of the error through numerics and systematic and conceptual notion of the error. In order to give a concrete notion to this “difference”, it is crucial to carefully interpret what is meant by a solution of the evolution PDEs; the subtlety pertains to the choice of method used to solve the PDE. Recently, it has been shown that the solutions of PDEs obtained solely from the thermodynamic principles are prone to deviate from the underlining microscopic dynamics. This thesis investigates the cause of this discrepancy and propose a reconciliation by exploring a new continuum model that may plausibly incorporate microscopic influences.

EVOLUTION OF FACETED CRYSTAL SURFACES:
MODELING AND ANALYSIS

by

Kanna Nakamura

Dissertation submitted to the Faculty of the Graduate School of the
University of Maryland, College Park in partial fulfillment
of the requirements for the degree of
Doctor of Philosophy
2014

Advisory Committee:

Professor Dionisios Margetis, Chair/Advisor

Professor Antoine Mellet, Co-Advisor

Professor Matei Machedon

Professor David Levermore

Professor John Weeks, Deans Representative

© Copyright by
Kanna Nakamura
2014

Dedication

To my loving parents Makie and Fujio and to my dear Rin.

Acknowledgments

First and foremost, I am most grateful to my advisor Professor Dionisios Margetis. The amount of time and patience he has kindly offered to me in the five years I learnt from him was far beyond my expectation. Especially at the beginning of my apprenticeship, we would regularly have five hours long meetings and I have no idea how he tolerated me for so long. He has been the most generous and understanding advisor I could possibly ask for. Besides our interactions, I am thankful that he provided me with so many opportunities to interact with other researchers and immerse myself in the academic world, which was invaluable to writing this thesis.

I also owe great many thanks to my co-advisor Professor Antoine Mellet. He has co-advised me practically for more than a year and he taught me a lot during this time. Throughout my career in mathematics, I jumped from a topic to topic and there was a vast gap in my knowledge that needed to be filled in order to complete this thesis. I cannot thank Antoine enough for stepping in the role to help me through. He was always so incredibly generous with his time and effort. I think that the fact that he made time to work with me even on his moving day to France speaks for itself.

I would like to express my deep appreciation to Professors Yoshikazu and Miho Giga as well. This thesis would have taken a very different shape without their previous work. There is no doubt that, after my advisors, they had the most influence on this thesis. I also appreciate their hospitality to meet with me and allow me to speak at University of Tokyo.

I am indebt to numerous colleagues and professors for sharing their knowledge and ideas with me. I would like to especially thank Professors Robert Kohn, Inwon Kim, Peter Smereka, Tim Schulze, and Eitan Tadmor for our interactions and their valuable advices.

I would like to thank my thesis committee members Professors Matei Machedon, David Levermore, and John Weeks for finding time to join me in their busy schedule and for their helpful comments.

I also thank the Graduate School at the University of Maryland for providing me with a financial support through awards such as Graduate Student Summer Research Fellowship, Monroe H. Martin Graduate Research Fellowship, and Graduate Deans Award.

I am truly obliged to Satvik Beri for his encouragement. If it were not for his kind words, I would have given up on mathematics years ago. I also thank my dear friends Edward Phillips and Cameron Mozafari for opening their home to me when I most needed.

Finally my most sincere love and gratitude goes to my family in Japan. I thank them for letting me pursue my passion for mathematics. Their unlimited love and support mean the world to me. And thanks for all the epic care packages.

Kanna Nakamura

August 2014

Table of Contents

List of Abbreviations	viii
1 Introduction	1
1.1 Physical description of crystal surfaces	1
1.2 Multiscale modeling in the presence of facet	2
1.3 Burton-Cabrera-Frank model	5
1.4 Thermodynamic approach	8
1.5 Continuum limit of step flow in 1D	11
1.6 Mathematical addendum	12
1.6.1 Elements of subgradient formalism	13
1.6.2 Idea of viscosity solution	15
1.7 Overview	15
2 Long, straight steps	18
2.1 Formulation: step motion laws	20
2.1.1 Evaporation-condensation process	21
2.1.2 Surface diffusion	22
2.2 Compatibility of microscopic and macroscopic predictions	26
2.3 Limit of discrete scheme and near-facet expansions	27
2.3.1 Evaporation-condensation kinetics	27
2.3.2 Surface diffusion	32
2.3.2.1 DL kinetics	32
2.3.2.2 ADL kinetics	36
3 Evaporation-condensation in radial geometry	39
3.1 Formulation	41
3.1.1 Geometry	42
3.1.2 Discrete equations of motion	43
3.2 Formal continuum limit outside facet	47
3.3 Existence of unique discrete solution	50
3.3.1 Case with zero step interactions, $g = 0$	50
3.3.2 Case with repulsive step interactions, $g > 0$	53
3.4 Subgradient formalism and free-boundary conditions	56
3.4.1 Subgradient formalism	57
3.4.2 Natural boundary conditions	57

3.4.3	Alternate condition: flux jump at facet edge	58
3.4.4	Initial data	61
3.4.5	Exactly solved case: zero step interaction ($g = 0$)	61
3.4.5.1	Continuous flux ξ	62
3.4.5.2	Discontinuous flux ξ	63
3.5	Numerical simulations	63
3.5.1	Numerics for $g=0$	64
3.5.1.1	Non-geometric step mobility (M1)	65
3.5.1.2	Geometry-induced step mobility (M2)	65
3.5.2	Numerics for $g > 0$	68
3.5.2.1	Numerics for M1	72
3.5.2.2	Numerics for M2	73
3.5.3	Approximation by boundary layer theory	73
4	Shock-wave formalism	78
4.1	Facet height as shock	79
4.2	Convergence of discrete schemes for $g = 0$	81
4.3	Proof of convergence of step schemes for $g = 0$	83
5	Introduction (Part II)	88
5.1	The gradient flow approach	92
5.1.1	Case of M1, $g \geq 0$	92
5.1.2	Case of M2, $g = 0$	94
5.2	Case of M2, $g > 0$	94
6	Proper viscosity solutions: definitions	98
7	Comparison Principle	110
7.1	Case I	112
7.2	Case II	118
8	Existence	122
8.1	Regularized equations	122
8.2	Bound for h_r	123
8.3	Application of Arzelà-Ascoli theorem	124
8.4	Far-field condition	127
8.5	Proper viscosity solution	128
A	Computations for facets in (1+1)D	135
A.1	Second-order difference scheme	135
A.2	Extensions	136
A.2.1	Multipole nearest-neighbor step interactions	136
A.2.2	Special kinetics of extremal step	137
A.2.3	Fourth-order difference scheme	140
A.3	Iterations of integral equations	142
A.3.1	Evaporation-condensation	142
A.3.2	DL kinetics	144
B	Evaporation model as limit of BCF-type model in radial setting	146

C	On discrete equations with $g = 0$ in radial setting	149
C.1	Model M1	149
C.2	Model M2	151
D	Continuum solutions for $g = 0$ in radial setting	153
E	Formal boundary layer analysis for facets in radial setting	155
F	On near-facet expansion for $\mathbf{m}(\eta)$	157
	Bibliography	159

List of Abbreviations

$BV(\Omega)$	Set of bounded variation on Ω .
\mathbf{R}^N	N-dimensional Euclidean space.
$W^{k,p}(\Omega)$	Sobolev space of order k based on the space $L^p(\Omega)$.
$C^k(\Omega)$	Set of k-times continuously differentiable functions.
$\mathcal{O}(f)$	Order of magnitude of f .
\mathbf{N}	Set of all natural numbers.
\mathbf{R}	Set of all real numbers.
$B^d(\mathbf{r}, \delta)$	Open ball of radius $\delta > 0$ centered at point \mathbf{r} in the Euclidean space \mathbf{R}^d .
$\mathcal{D}(E)$	Effective domain of a function/functional E .
∂E	Subdifferential of a function/functional E .
$\mathcal{D}(\partial E)$	Domain of the subdifferential ∂E .
$\text{int}E$	Interior of E .
\bar{E}	Closure of E .

Chapter 1: Introduction

1.1 Physical description of crystal surfaces

The development of small and precise electric devices requires an accurate manipulation of crystal surfaces at nano- to micron-scale. In this so-called mesoscale regime, physical principles in various scales are indispensable and the separation of scales become ambiguous. Establishing a methodological procedure for such multiscale modeling is a challenging and long-standing problem in material science, physics, and mathematics. Interestingly, the crystal surfaces exhibit very distinct morphologies depending on whether the surface is above or below its “roughening transition temperature”. To unlock the potential of stable nano-scale material, it is especially important to develop theories for the systems below the roughening transition temperature; to this end, we describe surface relaxation in such regime in three scales in the next few paragraphs.

At the atomistic scale, atoms on the crystal surface with sufficient energy may break the neighbor bonds and hop to another site on the surface or leave the vicinity of the surface to the surrounding vapor. When the number of these moving atoms, called adsorbed atoms (adatoms), is large, it is reasonable to study the concentration of adatoms on the surface rather than the motion of individual atoms. In this thesis, we study the relation of the adatom concentration and the evolution of the surface in the following scenario: For temperatures below the roughening transition, even a small crystalline miscut from

the plane of symmetry may introduce thermally stable line defects (steps) [53]. In epitaxial phenomena, this leads to a simple structure consisting of mono-layers of adatoms (terraces) separated by steps of atomic height. In the absence of external forcing, the surface is expected to relax and the atom concentration is described by a diffusion process on the surface and desorption, supplemented with the attachment and detachment of atoms to the step edges.

On the other hand, atomistic effects are no longer observable at the macroscale; the surface appears smooth and is expected to follow the thermodynamic principles [22, 51, 53]. Yet this approach is not complete in the presence of flat regions called facets. It turns out that the formulation of facet has a global influence in the surface evolution. The difficulty posed by the formulation of facet is explained in the next section.

1.2 Multiscale modeling in the presence of facet

At the microscale, the step motion is dictated by (i) the motion of atoms (ii) adatom attachment and detachment to the step edges, and (iii) step line-tension and entropic and elastic-dipole repulsive step-step interactions [61, 78]. Although the step flow model offer the advantage of simple and unambiguous physical principles, even after considerable simplifications it leads to expensive computations. Also, this approach is not suited to tracking topographic changes at long length and times scales.

On the other hand, observations at the macroscale have the merit of less computational complexity and a concise description of the surface topography. In this view, the evolution of a smooth crystal surface is characterized by its tendency to lower its free energy [8, 43, 55, 68, 97]. The facet has a precise description within the continuum

framework [9, 28, 62, 94, 95, 97, 98] as a flat region at which the free energy develops a cusp singularity thus a conventional thermodynamic approach is inadequate to study a surface with a facet. In order to clarify the ambiguity associated with this singularity, various potential remedies have been proposed.

One approach to circumventing the singularity in the free energy is to treat a facet edge as the moving boundary for the evolution partial differential equation (PDE) of the smooth part of the surface. The main objective of this approach is to assign appropriate boundary conditions at the facet edge; however, the criteria for these boundary conditions is not adequately understood. We adopt the viewpoint that microscopic theories provide a guiding principle. In order to investigate the near-facet behavior of continuum-scale variables consistent with the underlying step motion, the theory of homogenization [45] may be applied to the discrete picture. The main idea of homogenization is to extract information from a microscopic structure that influences the system at a large scale.

Interestingly, the dependence of facet motion on the discrete dynamics appears to rely on whether the facet height is conserved or not. In this respect, we investigate two distinct, corresponding geometries:

- We start with a monotone train of N steps separating two semi-infinite facets at fixed heights. The limiting behavior of discrete schemes for steps to nonlinear macroscopic laws for crystals is studied via formal asymptotics in one space dimension. We consider evaporation-condensation kinetics; and surface diffusion via the Burton, Cabrera and Frank(BCF) model where adsorbed atoms diffuse on terraces and attach-detach at steps. *Nearest-neighbor* step interactions are included. Under the assumption of the existence of self-similar solutions for

discrete slopes, we show how boundary conditions for the continuum slope and flux, and expansions in the height variable near facets, may emerge from the algebraic structure of discrete schemes as $N \rightarrow \infty$. For this purpose, we convert the discrete schemes to sum equations and further reduce them to nonlinear integral equations for the continuum-scale slope. Approximate solutions to the continuum equations near facet edges are constructed by direct iterations. For elastic-dipole step interactions, the continuum slope is found in agreement with a previous hypothesis of “local equilibrium” and the boundary conditions are in agreement with Spohn’s thermodynamic approach [97] in this particular geometry.

- The other geometry of interest is an axisymmetric crystal mound. The relaxation of the surfaces with a facet is studied via an ad hoc evaporation-condensation model. Unlike long straight steps, the number of steps is not necessarily conserved in this setting: the top (extremal) atomic layers may shrink and eventually collapse successively, which decreases the height of the entire profile. At the microscale, the discrete scheme consists of a large system of differential equations for the radii of repulsively interacting steps separated by terraces. Each step velocity is proportional to the step chemical potential, the variation of the total step free energy; the relevant discrete mobility is assumed linear in the width of the upper terrace. We focus on two step flow models: In one model (called M1) the discrete mobility is simply proportional to the upper-terrace width; in another model (M2) the mobility is altered by an extra *geometric factor*. At the macroscale, both step models give rise to free-boundary problems for a second-order PDE. By invoking self similarity at long time, we numerically demonstrate that: (i) in M1, discrete slopes follow closely a continuum thermodynamics approach with “natural

boundary conditions” at the facet edge; (ii) in contrast, predictions of M2 deviate from results of the above continuum approach; (iii) this discrepancy can be eliminated via a continuum boundary condition with a *geometry-induced jump* for *top-step collapses*; (iv) This jump is equivalent to the Rankine-Hugoniot condition in the Lagrangian coordinates in the special case of non-interacting steps. In this limited case, we prove the convergence of the discrete schemes M1 and M2 to its respective continuum limits. (v) In the presence of step interaction, we propose a continuum theory that reveals that the formula for the flux jump at the step edge is independent of the strength of step interaction. In particular, the formula we obtained as a limit of non-interacting steps remains valid for the interacting steps in the conjectured continuum limit.

1.3 Burton-Cabrera-Frank model

In this section, the surface evolution under the roughening transition regime is described at the microscale. Before we continue, we will briefly review the role of roughening transition temperature. Above the roughening transition temperature, atoms have high energy and steps are formed and collapse instantaneously so they are not observable. This atomic roughness translates to a smooth macroscopic picture with no singularity in the surface free energy. On the other hand, well-below the roughening temperature T_R , steps become thermally stable and their lifetime is long enough to be experimentally observed. Here we focus on the under roughening transition regime. A basic geometric picture is the following: Terraces are formed by a large number of surface atoms at one height. The edge of the terrace with an adjacent terrace (say, a terrace at height = ia where a is the diameter of atom and at height = $(i + 1)a$) is called a step. These steps resemble

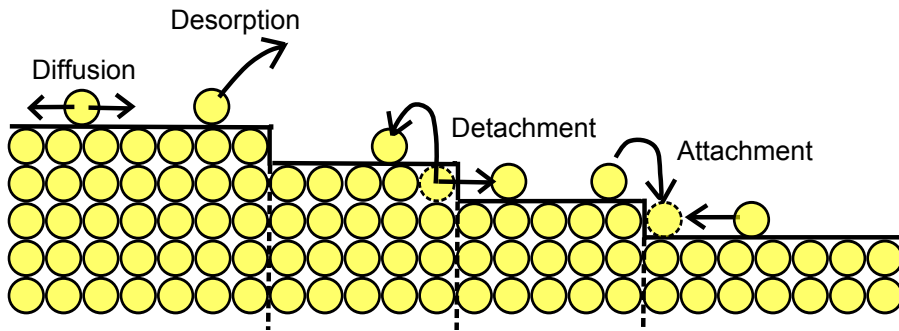


Figure 1.1: Diagram of the side view of steps illustrating diffusion and desorption on terraces, attachment-detachment at step edges. The step at x_i will retreat to the left as atoms detach, while the steps at x_{i+1} will advance to the right as atoms attach from above and below.

smooth curves and we assume that they are countable.

The Burton-Cabrera-Frank (BCF) framework is the starting point of our model, which was first introduced in 1951 [6]. Three basic ingredients of the BCF model for surface diffusion are: (i) motion of steps by mass conservation; (ii) diffusion of adsorbed atoms (adatoms) on terraces; and (iii) attachment and detachment of atoms at steps. The main assumption of BCF is that there are enough adatoms on the terraces to define adatom concentration $\rho_i(x, t)$ on the i th terrace. The evolution of $\rho_i(x, t)$ is characterized by the diffusion rate D_s through a diffusion equation,

$$\partial_t \rho_i(x, t) = \text{div} (D_s \nabla \rho_i(x, t)) - \frac{\rho_i(x, t)}{\tau} + f \quad (1.1)$$

where τ is the mean desorption time and f is the flux of atoms arriving from the vapor to the surfaces. The step velocity v_i at the i th step, $i = 1, \dots, N$, is proportional to the difference in the adatom flux $J_i = -D_s \nabla \rho_i$ arriving from the top and bottom terrace:

$$v_i(x, t) = -\frac{\Omega}{a} (J_i - J_{i-1}), \quad (1.2)$$

where Ω is atomic volume and a is step height.

In this thesis, we follow the BCF approach in the absence of nucleation and external material deposition from above. In principle, the material parameters included in these kinetics depend on the individual steps and terraces. However, this thesis addresses only isotropic surfaces for which the material parameters are uniform among steps. For some work on anisotropic surfaces, see [47, 74, 77].

Remark 1. Instead of the step velocity law being described in terms of the adatom fluxes on top of the terraces, the step velocity law for evaporation-condensation case describe an exchange of adatoms between step edges and the surrounding vapor. In the evaporation condensation kinetics, $v_i(x, t)$ is proportional to the difference in the chemical potential of the step edges and the vapor. This model can be formally derived as an extension of the BCF model (see, Appendix B).

The boundary conditions for (1.1) is given by Robin conditions:

$$-J_i(x, t) = k_u (\rho_i - \rho_i^{eq}), \quad x \in x_i \quad (1.3)$$

$$J_i(x, t) = k_d (\rho_i - \rho_{i+1}^{eq}), \quad x \in x_{i+1} \quad (1.4)$$

where $k_u(k_d)$ is an attachment-detachment rate from upper-(lower-)terrace. ρ_i^{eq} is the equilibrium density at the i th step given through a chemical potential via Gibbs-Thomson relation [46]. The chemical potential μ_i is the change of free energy at $x = x_i$. The total free energy is the combination of the line tension energy $E_{line}(t)$ and the pairwise step-step interaction energy $E_{int}(t)$. $E_{int}(t)$ results from steps' inclination to repel each other entropically and as elastic dipoles [53]. Detailed description of the

free energy is provided in later chapters. For example, in the special case of straight steps with zero curvature, line tension is absent. See chapters 2 and 3 for details.

1.4 Thermodynamic approach

Another description of the surface evolution can be given through the thermodynamic principles. These principles are based on macroscopic topography so it does not capture atomistic details but it is useful for longer observation time. The first surface evolution model was proposed by Mullins in 1958 [68]. In his original work, Mullins wrote the normal velocity of the surface to be proportional to the surface Laplacian of the surface mean curvature. Instead, we adopt the graph theory and define the height profile $h(x, t)$ at point $x = (x_1, x_2)$ on the coordinate plane \mathbf{R}^2 . In chapters 2 and 4, we will also utilize the Lagrangian coordinate system as opposed to the Euclidean coordinate system. The main idea of the thermodynamic approach is that the system evolves in a way to minimize the surface free energy on a surface S :

$$E[h] = \int_S \gamma(\nabla h) ds = \int_A \gamma(\nabla h) \sqrt{1 + |\nabla h|^2} dx dy. \quad (1.5)$$

where the surface energy density $\gamma(\nabla h)$ is the energy per unit area of the surface. The local slope of the surface ∇h is often assumed to be relatively small so $\gamma(\nabla h)$ may (formally) be replaced by its second order expansion. Also, A is the projection of S onto the reference plane. In his description, Mullins assumed $T > T_R$ and the existence of a smooth free energy function. Mullin's theory serves as a motivation for the study of the continuum limit of step structure at $T < T_R$ and we adapt (1.5) with non-smooth $\gamma(\nabla h)$. The evolution of surface is driven by the surface chemical potential $\mu(x, y)$, which is the change in the free energy due to redistribution of atoms at point (x, y)

$$\mu(x, y) = \Omega \frac{\delta E}{\delta h} \quad (1.6)$$

where Ω is the atomic volume and $\frac{\delta E}{\delta h}$ is the functional derivative of the free energy $E[h]$. Note that Equation (1.6) may not be taken literally when $T < T_R$ and $E[h]$ is not globally smooth. In such case, the energy density $\gamma(\nabla h)$ has a singular term proportional to $|\nabla h|$, which plays a crucial role in macroscopic models and makes the evolution PDEs (1.7) and (1.8) ill-defined on the region on which $\nabla h = 0$ (facet). As a matter of fact, the interpretation of chemical potential for non-smooth $E[h]$ is the main theme of this thesis. Next, we introduce various mass transport mechanisms. In surface diffusion, the surface profile changes due to the motion of the atoms across the surface. In other words, the surface profile evolves due to the redistribution of atoms on the surface so we employ the conservation law:

$$h_t = -\operatorname{div} J \quad (1.7)$$

where J is the continuum surface flux proportional to the gradient of the chemical potential, $J = -M\nabla\mu$, where the surface mobility M in principle may depend on the slope; however, we focus on isotropic surface with a constant mobility.

We also consider the evaporation condensation regime. In contrast to the case of surface diffusion, the surface morphology under the evaporation-condensation regime changes due to the exchange of atoms between surface and vapor. So the mass of atoms in the vicinity of surface is no longer conserved and the transportation equation is a second-order PDE, viz.,

$$h_t = -\mu(\nabla h). \quad (1.8)$$

Now we elaborate on the role of facet in surface evolution. In his ground-breaking paper, Spohn [97] formulated the surface evolution as a free boundary problem. This approach consists of two elements: (a) a PDE for the height profile satisfied outside facets defined by (1.7) or (1.8); and (b) boundary conditions at the facet edge, which are derived as an extension of continuum thermodynamics principles. His free boundary approach has the merit of keeping the form of the PDE that is in agreement with ODEs outside facets while singling out the influence of facets through the boundary conditions.

Another attempt at deriving a continuum theory in presence of facets is made through subgradient theory. Subgradient theory is purely based on the thermodynamic principles and functional operator theory. This approach does not require an explicit tracing of the facet motion. Despite this advantage, the application of subgradient theory may not be suited for our purposes as the solution depends on the form of the subgradient system.

In other words, the choice of the energy and the Hilbert space in the formulation is crucial. To the author's knowledge, there is no obvious determining factor for the choice of subgradient formalism solely at the level of the continuum theory. This approach can be related to the free boundary approach by applying the *natural boundary conditions* found through the solution at the free boundary.

Unfortunately, both the boundary conditions of Spohn's theory and the subgradient theory can be incompatible with solutions of ODEs for steps near facets [71]. In the next section, we take a closer look at the relation between these macroscopic theories with the microscopic approach.

1.5 Continuum limit of step flow in 1D

In the limit of a large number of steps, the ODE system for steps is expected to reduce to evolution PDEs for the surface height and slope profiles away from the facet. In this process, coarse-graining is applied under the set of assumptions: $a \rightarrow 0$, $Na = \mathcal{O}(1)$, $ia \rightarrow x$, $m_i \rightarrow m(x, t) = \mathcal{O}(1)$, $h_i \rightarrow h(x, t) = \mathcal{O}(1)$. In other words, the step size approaches zero while the step density is kept fixed. The idea is to recognize the step position $x_i(t)$ as a level set of the continuum height $h(x, t)$ at height $h = ia$. If the coarse-graining is valid, we expect to see the error between ia and $h(x_i, t)$ to vanish in the limit $N \rightarrow \infty$. However, when steps are sparse, the surface appears flat and has a zero-orientation at the macroscale. As previously mentioned, coarse-graining does not work in such situations.

In order to attain a continuum limit of the ODE system for the whole surface profile including facets, we need to carefully address the meaning of “continuum limit” of a discrete system. There are multitude levels of rigor (besides coarse-graining) at which a continuum limit can be considered: In a phenomenological approach, a continuum limit is obtained through an educated guess. The usage of subgradient theory as a continuum limit often belongs to this category (see, section 1.4).

In another instance of phenomenological comparison of the ODE systems and the PDEs, self-similarity in variables such as slope is often assumed in order to numerically solve the ODE/PDE system. We will make this assumption in some parts of this thesis.

Unfortunately, the availability of rigorous homogenization results is limited. The connection of step flow to continuum theories has been studied analytically for semi-infinite 1D facets at fixed heights in surface diffusion [4, 5, 65]; however, only the

attachment-detachment limited (ADL) regime was addressed rigorously. In this setting, the surface height is a convenient independent variable that allows to eliminate a free boundary for the facet (see, chapter 2. Furthermore, step collapses do not occur and, thus, the total number of steps is preserved. The analysis becomes more involved for periodic 1D surface corrugations [50, 81] and radial geometries [49, 71, 73]¹ in which the facet height changes with time. For such geometries, boundary conditions consistent with step flow are in principle expected to involve microscale parameters (see, chapter 3), e.g., step collapse times, which result from solving discrete schemes for steps [49, 71]. This means that the resulting theory is not fully continuum; however, in Chapter 4, we will prove the convergence of the step dynamics to its continuum limit in the special case of non-interacting steps.

1.6 Mathematical addendum

In this section, we briefly describe elements of the mathematical theories utilized in this thesis. We assume some familiarity of the reader with basic functional analysis. The subgradient formalism provides a means of analyzing evolution laws that have a steepest descent structure with respect to a convex, singular energy functional [55]. An elementary exposition for the surface diffusion case can be found in [81]. On the other hand, the theory of viscosity solutions may be applied to more extensive family of equations that do not necessarily have a steepest descent structure [19].

¹We note that there is a fundamental difference between the 1D periodic setting and radial geometries: in the former, steps on facets can be of opposite sign which in turn may affect the nature of their interactions [50].

1.6.1 Elements of subgradient formalism

Formally speaking, the notion of the subgradient extends the concept of conventional gradient (or derivative) to convex functions or functionals that are not necessarily differentiable everywhere. Let \mathcal{H} be a Hilbert space and F be a convex functional on \mathcal{H} . The subdifferential, $\partial F(x)$, of F at the point x of \mathcal{H} is the set of all vectors v in \mathcal{H} that satisfy the inequality

$$F(x+h) - F(x) \geq \langle v, h \rangle \quad \text{for all } h \text{ in } \mathcal{H}, \quad (1.9)$$

where $\langle v, h \rangle$ denotes the inner product of \mathcal{H} . We call such v the subgradient of $F(x)$.

Consider first the classic example of the convex function $f(x) = |x|$ where $-1 \leq x \leq 1$.

In this case, \mathcal{H} is the one-dimensional space $[-1, 1]$ equipped (trivially) with the product of reals. Since $f(x)$ is differentiable at $x \neq 0$, we find $\partial f(x) = \{\text{sgn}(x)\}$, a singleton,

where $\text{sgn}(x) = x/|x|$ is the sign function. The notion of $\partial f(x)$ becomes particularly useful for $x = 0$, where $f(x)$ is not differentiable. To compute $\partial f(0)$, one notices that for any real h , $f(h) - f(0) = |h| \geq |\varpi h|$ only if $|\varpi| \leq 1$. It is easily deduced that

$\partial f(0) = [-1, 1]$, the set of all possible slopes of linear graphs bounded above by the

graph of $y = |x|$ in the xy plane. This example can be extended to d space dimensions:

Consider $f(\mathbf{x}) = |\mathbf{x}|$, where \mathbf{x} is any point in the d -dimensional Euclidean space, \mathbb{R}^d ;

then, $\partial f(\mathbf{x}) = \{\mathbf{x}/|\mathbf{x}|\}$ if $\mathbf{x} \neq 0$, and $\partial f(0) = B^d(0, 1)$.

The above ideas can be generalized to functionals, i.e., mappings of vectors in \mathcal{H} to real numbers, or more generally to its underlying algebraic field. An abstract formulation suggests that an evolution with the variational structure can be viewed as ‘trajectories’ of elements of \mathcal{H} , in a way analogous to dynamical systems. The associated evolution

PDE for u is replaced globally by a statement of the form

$$\frac{du(t)}{dt} \in -\partial F(u(t)) \quad \text{for all } t > 0, \quad (1.10)$$

with the initial condition $u(0) = u_0 \in \mathcal{H}$. A known theorem of convex analysis asserts that there exists a unique (sufficiently smooth) $u(t)$ in \mathcal{H} for all $t > 0$ provided the functional F satisfies certain conditions such as appropriate convexity [38].

In particular, evolution PDE (3.22) for evaporation-condensation can be recast to form (1.10), where $u = h$ is of bounded variation and $F(h) = \nu\Omega E(h) = \iint \gamma(\nabla h) dA$, the singular surface free energy (3.20). The subgradient $\partial F(h)$ extends the variational derivative of $F(h)$ to the facet ($\nabla h = 0$). A *characterization theorem* for subgradient systems states that, for such a functional F , a function f belongs to $\partial F(h)$ if and only if there is a pair of *continuous* vector-valued functions ξ_1 and ξ_2 in \mathbb{R}^2 satisfying [38]

$$f = \nu\Omega g_1 \operatorname{div}(\xi_1 + g\xi_2), \quad (1.11)$$

where ξ_1 is an element of $\partial J_1(\nabla h)$ and ξ_2 is an element of $\partial J_2(\nabla h)$ with $J_1(\mathbf{p}) = |\mathbf{p}|$ and $J_2(\mathbf{p}) = |\mathbf{p}|^3/3$. This characterization is central in this framework, with direct implications to boundary conditions at the facet. By virtue of

$$\partial J_1(\mathbf{p}) = \begin{cases} \{\mathbf{p}/|\mathbf{p}|\} & \text{if } p \neq 0 \\ B^2(0,1) & \text{if } p = 0 \end{cases}, \quad \partial J_2(\mathbf{p}) = \{|\mathbf{p}|\mathbf{p}\}, \quad (1.12)$$

one can assert that $|\xi_1| \leq 1$ and $\xi_2 = 0$ for $\mathbf{p} = 0$; therefore, $|\xi| \leq 1$ on the facet.

In conclusion, by (1.10)-(1.12), there exists a *continuous* vector-valued ξ such that

$$\partial_t h = -\nu\Omega g_1 \operatorname{div}\xi \quad \text{everywhere}, \quad (1.13)$$

where $g_1\xi$ belongs to $\partial\gamma(\mathbf{p})$ for $\mathbf{p} = \nabla h$. In our radial setting, $|\xi| \leq 1$ for $r < r_f(t)$; and ξ_2 is zero on the facet. These considerations lead to boundary conditions (3.37)

and (3.39) for $g > 0$. Since m is continuous for $g > 0$, so is h . (For $g = 0$, this argument needs to be modified since m ceases to be continuous [55].)

1.6.2 Idea of viscosity solution

Viscosity solutions are a type of weak solutions. Roughly speaking, the idea of weak solution is to pass derivatives that are hard to control onto a smooth test function. Unlike the classical weak solution approach, viscosity solutions are tested point-wise. The primary virtues of the theory of viscosity solutions are that it allows merely continuous functions to be solutions of fully nonlinear equations of second order and provides very general existence and uniqueness theorems. Moreover, these features of viscosity solutions go hand-in-hand with a great flexibility in formulating precise general boundary conditions and passing to limits in various settings [19]. Furthermore, the theory of *classical* viscosity solutions offers relatively simple proofs that are generally through point-wise arguments; however, we are interested in the global effect of the facets; thus we need a theory in which solutions are tested more strictly than just point-wise. To this end, we follow in the footsteps of [31] to study the global behavior of viscosity solutions of degenerate PDEs with a strong singularity.

1.7 Overview

The rest of this thesis is organized as follows:

This thesis is divided into two parts: In Part I, we will focus on the mathematical modeling aspect of this thesis. Micro- and macro-scale models are developed through physical principles and analyzed numerically and heuristically. The analysis in Part I (Ch.2–Ch.4) is mostly formal and it invokes simplifying assumptions without proofs.

Part II (Ch.5–Ch.8) is purely mathematical. The well-posedness of some degenerate parabolic PDEs that describe the evolution of the evaporation-condensation case is established using gradient flow and a generalized notion of viscosity solutions. Each part is self-contained.

Although we only study isotropic surfaces in this thesis, our work on anisotropic surfaces with heterogeneous characteristics can be found in [74, 77]. Also, extensive reviews of elements of epitaxy for crystals can be found in, e.g., [22, 37, 66, 84, 88].

In chapter 2, we study straight long steps under the evaporation-condensation and surface diffusion kinetics. In chapter 3, we study the relaxation of axisymmetric mound under the evaporation-condensation kinetics. In chapter 4, we discuss an interpretation of the facet height as a shock wave, and the convergence of the discrete schemes for non-interacting steps.

In chapter 5, we introduce the degenerate parabolic PDEs and motivate our main problem by studying easier cases via the theory of gradient flow. In chapter 6, we provide a rigorous definition for the solution of the equation. In chapter 7, the comparison principle and uniqueness of proper viscosity solution is established. In chapter 8, the existence of a unique viscosity solution of our specific problem is proven via an approximation by regularized parabolic problems.

PART I: Modeling

Chapter 2: Long, straight steps

In this chapter, we demonstrate a situation in which the moving facet can be treated as a stable (unmoving) boundary for the surface evolution PDE. We adopt the Lagrangian coordinate in which the slopes are written as a function of height. We assume that the heights of facets do not change therefore they are no longer free boundaries in the new coordinate [4]. Specifically, we consider two semi-infinite facets separated by a monotone train of N steps, $N \gg 1$. This setting captures features of a finite crystal and can be conveniently represented by a (1+1)-dimensional model. In this special situation, the analysis can be simplified and the near facet evolution of the surface is studied through power series expansions.

Besides the assumptions listed in section 1.3, self-similarity for finite N is also assumed; presumably, this is reached for long enough times [4, 28] in various kinetic regimes, but this property is not proved here. The persistence of semi-infinite facets and monotone slope during evolution is hypothesized. This formal approach enables us to explore modifications of the energetics and kinetics of the step model.

This work has been inspired by Al Hajj Shehadeh, Kohn, and Weare (AKW) [4]. These authors study rigorously the relaxation of the same step configuration by employing the l^2 -steepest descent of a discrete energy functional under attachment-detachment limited (ADL) kinetics. In this case, the dominant process is the exchange of atoms at step edges. Notably, AKW invoke ordinary differential equations (ODEs) for *discrete slopes*

at the nanoscale, and a PDE for the surface slope as a function of height at the macroscale. In [4], the positivity of discrete slopes and convergence of the discrete self-similar solution to a continuum self-similar one with zero slope at facet edges are proved; the condition of zero flux emerges as a “natural boundary condition” from the steepest descent. An analogous method for DL kinetics appears elusive at the moment. Israeli, Jeong, Kandel and Weeks [48] study self-similar slope profiles under evaporation-condensation and surface diffusion with ADL kinetics for three 1D step geometries. Their step trains are semi-infinite and thus differ from the *finite* step train studied here and in [4]. For this reason, direct comparisons to results of [48] are not compelling. By contrast to our setting, the self-similar slopes in [4] do not decay with time. In the same work [48], the condition of zero slope at the facet edge along with a power series expansion of a certain form for the slope are imposed at the outset. Because of the different boundaries involved, their scaling exponent (in the self-similarity variable) and form of the power series for evaporation-condensation are different from ours.

We adopt the use of the height as an independent variable [4], which is a convenient Lagrangian coordinate of motion [27, 28]. An advantage of this choice in the present setting, where facets are at fixed heights, is the elimination of free boundaries, as pointed out by AKW. We invoke equations for the discrete slopes, following AKW as well as Israeli and Kandel [49, 50].

In surface-diffusion, adatoms move by diffusing on terraces and attaching/detaching to/from the step edges. On the other hand, in evaporation condensation, atoms are exchanged between step edges and vapor. Although we separate these two mechanisms, they coexist in realistic mechanical systems.

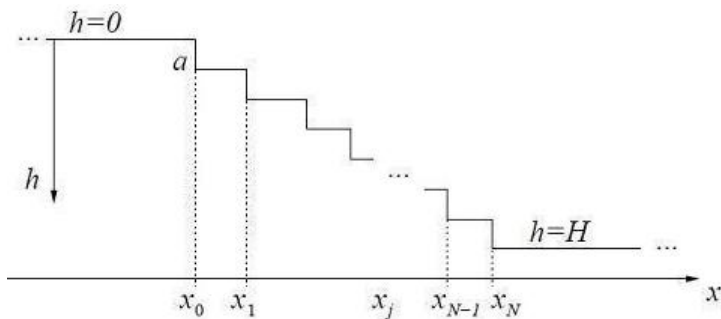


Figure 2.1: Geometry in 1D (cross section): the step height is a ; the step position is x_j ; and the semi-infinite facets are located at heights $h = 0$ (top) and $h = H$ (bottom).

2.1 Formulation: step motion laws

Consider a stepped surface with N steps as shown in Fig. 2.1. The step positions are denoted by $x = x_j(t)$ where $j = 0 \dots N$ and $t \geq 0$. Each step has a height of atomic length a . The step train ends with a semi-infinite facets on the each side. Thus we set $h = 0$ for $x < x_0(t)$ and $h = H := aN$ for $x > x_N(t)$; cf. [4, 28].

For the ease of computation, non-dimensionalize the variables by substituting $\tilde{x} = x/H$ and $\tilde{h} = h/H$ and drop the tildes. The atomic length a is replaced by a small parameter $\epsilon = a/H$ so $(N + 1)\epsilon = 1$ (where $N \gg 1$ and $\epsilon \ll 1$), $0 \leq h \leq 1$. The discrete slope m_j is defined by

$$m_j(t) := \frac{\epsilon}{x_{j+1}(t) - x_j(t)} > 0, \quad j = 0, 1, \dots, N - 1. \quad (2.1)$$

m_j , are assumed to be positive for all $t > 0$, given that $m_j > 0$ at $t = 0$.

To explain the step dynamics, first thermodynamic elements of step motion are described. For entropic and elastic-dipole step interactions, the energy of the step train

is [53, 78]

$$E_N = \frac{1}{2} \sum_{i=0}^{N-1} \left(\frac{\epsilon}{x_{i+1} - x_i} \right)^2 = \frac{1}{2} \sum_{i=0}^{N-1} m_i^2. \quad (2.2)$$

The chemical potential of the j th step is the change of the energy per unit volume [53]

$$\mu_j = \frac{\delta E_N}{\delta x_j} = \epsilon^{-1} \left[\left(\frac{\epsilon}{x_{j+1} - x_j} \right)^3 - \left(\frac{\epsilon}{x_j - x_{j-1}} \right)^3 \right] = \epsilon^{-1} (m_j^3 - m_{j-1}^3) \quad (2.3a)$$

if $j = 1, \dots, N - 1$. For the extremal steps at $x = x_0, x_N$ the chemical potential is set to be

$$\mu_0 = \epsilon^{-1} m_0^3, \quad \mu_N = -\epsilon^{-1} m_{N-1}^3. \quad (2.3b)$$

The step velocity law depends on the choice of kinetics. Following BCF and considering special cases of the BCF model, the step dynamics for surface diffusion and evaporation-condensation are written down.

2.1.1 Evaporation-condensation process

In evaporation-condensation, the step velocity, v_j , is driven by the step chemical potential [53]. The main idea of evaporation-condensation is the atoms move between the step edges and vapor, from a higher chemical potential to a lower chemical potential. Thus, the step velocity law reads [53, 98]

$$v_j(t) = \frac{dx_j(t)}{dt} = \dot{x}_j(t) = -(\mu_j - \mu^0) \quad (j = 0, 1, \dots, N), \quad (2.4)$$

where μ^0 is the chemical potential of the surrounding vapor. For completion, set $\mu^0 = 0$.

In the above equation, a constant mobility has been applied. By combining (2.3) and

(2.4), obtain the discrete scheme:

$$\dot{m}_0 = -\epsilon^{-1}m_0^2(\dot{x}_1 - \dot{x}_0) = \epsilon^{-2}m_0^2(m_1^3 - 2m_0^3), \quad (2.5a)$$

$$\dot{m}_j = \epsilon^{-2}m_j^2(m_{j+1}^3 - 2m_j^3 + m_{j-1}^3), \quad j = 1, \dots, N-2, \quad (2.5b)$$

$$\dot{m}_{N-1} = \epsilon^{-2}m_{N-1}^2(m_{N-2}^3 - 2m_{N-1}^3). \quad (2.5c)$$

Equations (2.5) are merged into a single law

$$\epsilon^{-2}m_j^2(m_{j+1}^3 - 2m_j^3 + m_{j-1}^3) = \dot{m}_j, \quad j = 0, \dots, N-1, \quad (2.6a)$$

along with the termination conditions

$$m_{-1} = 0 = m_N. \quad (2.6b)$$

Furthermore, in order to analyze the discrete scheme, consider a similarity ansatz

$$m_j(t) = p(t) M_j \quad (dM_j/dt \equiv 0, M_j \neq 0). \quad (2.7)$$

Comparing (2.7) and (2.6), it is easy to see that $\dot{p}/p^5 = -C = \text{const.}$ and set $C = 1$ thus,

$P(t) = (4t + K)^{-1/4}$. So, M_j satisfy the second-order difference scheme

$$M_{j+1}^3 - 2M_j^3 + M_{j-1}^3 = -\frac{\epsilon^2}{M_j}, \quad j = 0, \dots, N-1 \quad (M_j > 0), \quad (2.8a)$$

$$M_{-1} = 0 = M_N. \quad (2.8b)$$

2.1.2 Surface diffusion

For surface diffusion, writing down the step velocity law takes more preparation. We start with the adatom density $\rho_j(x, t)$ and a diffusion equation $\partial_t \rho_j + \partial_x(D\partial_x \rho_j) \approx 0$ for $t > 0$ and $\{x_j(t) < x < x_{j+1}(t)\}$. $j = 0, \dots, N-1$. Here, $D > 0$ is the adatom diffusivity. To simplify the model, it is assumed that there is no deposition and

desorption. In the quasi-steady regime [53], where steps move slower than adatoms

diffuse, the diffusion equation is reduced to $\partial_x^2 \rho_j = \frac{1}{D} \partial_t \rho_j \approx 0$.

Therefore the adatom density satisfy a linear relation $\rho_j(x) = A_j x + B_j$ in

$\{x_j < x < x_{j+1}\}$, $j = 0, \dots, N - 1$. Further, we apply linear kinetics for atom

attachment/detachment at steps. Given that atoms attach/detach with a kinetic rate $2k$

(the factor 2 is included for later algebraic convenience) from the upper or lower terrace:

$$-J_j = 2k (\rho_j - \rho_j^{\text{eq}})|_{x_j}, \quad J_j = 2k (\rho_j - \rho_{j+1}^{\text{eq}})|_{x_{j+1}}, \quad (2.9)$$

Here, note that setting the attachment/detachment rate to be equal from the upper and

lower terrace, excludes EhrlichSchwoebel(ES) barrier in this model. Also, an equilibrium

density $\rho_j^{\text{eq}} = 1 + \mu_j$ is the density at which the steps are at dynamical equilibrium; here,

$k_B T$ has been set to 1 [53]. The coefficient A_j is computed with respect to the boundary

condition (2.9):

$$J_j(x) = -A_j = -\frac{k}{1 + k(x_{j+1} - x_j)} (\mu_{j+1} - \mu_j), \quad j = 0, \dots, N - 1. \quad (2.10a)$$

Equation (2.10a) needs to be extended to $j = 0, N$. By taking into account $\rho_j(x)$ for

$j = -1, x < x_0$ and $j = N, x > x_N$, where there are no steps and $\rho_j(x)$ must be bounded

in x , the plateau fluxes are found to be

$$J_{-1}(x) = 0 \quad x < x_0, \quad J_N(x) = 0 \quad x > x_N. \quad (2.10b)$$

In this kinetics, the steps move with respect to the difference in the flux. So the step

velocity law is

$$v_j = \dot{x}_j = \epsilon^{-1} [J_{j-1}(x_j) - J_j(x_j)], \quad j = 1, \dots, N - 1; \quad (2.11)$$

$J_j(x) = -\partial_x \rho_j(x)$ is the adatom flux on the j th terrace, $\{x_j < x < x_{j+1}\}$ (where the

diffusivity is set to unity).

Finally, combine (2.11) and (2.10) with (2.3) to obtain a system of ODEs for m_j :

$$\frac{\dot{m}_0}{m_0^2} = -\epsilon^{-4} \left[\frac{k\epsilon}{m_1 + k\epsilon} m_1 (m_2^3 - 2m_1^3 + m_0^3) - \frac{2k\epsilon}{m_0 + k\epsilon} m_0 (m_1^3 - 2m_0^3) \right], \quad (2.12a)$$

$$\begin{aligned} \frac{\dot{m}_1}{m_1^2} = & -\epsilon^{-4} \left[\frac{k\epsilon}{m_2 + k\epsilon} m_2 (m_3^3 - 2m_2^3 + m_1^3) - \frac{2k\epsilon}{m_1 + k\epsilon} \right. \\ & \left. \times m_1 (m_2^3 - 2m_1^3 + m_0^3) + \frac{k\epsilon}{m_0 + k\epsilon} m_0 (m_1^3 - 2m_0^3) \right], \end{aligned} \quad (2.12b)$$

$$\begin{aligned} \frac{\dot{m}_j}{m_j^2} = & -\epsilon^{-4} \left[\frac{k\epsilon}{m_{j+1} + k\epsilon} m_{j+1} (m_{j+2}^3 - 2m_{j+1}^3 + m_j^3) - \frac{2k\epsilon}{m_j + k\epsilon} m_j (m_{j+1}^3 \right. \\ & \left. - 2m_j^3 + m_{j-1}^3) + \frac{k\epsilon}{m_{j-1} + k\epsilon} m_{j-1} (m_j^3 - 2m_{j-1}^3 + m_{j-2}^3) \right], \\ & j = 2, \dots, N-3, \end{aligned} \quad (2.12c)$$

$$\begin{aligned} \frac{\dot{m}_{N-2}}{m_{N-2}^2} = & -\epsilon^{-4} \left[\frac{k\epsilon}{m_{N-3} + k\epsilon} m_{N-3} (m_{N-4}^3 - 2m_{N-3}^3 + m_{N-2}^3) \right. \\ & - \frac{2k\epsilon}{m_{N-2} + k\epsilon} m_{N-2} (m_{N-3}^3 - 2m_{N-2}^3 + m_{N-1}^3) \\ & \left. + \frac{k\epsilon}{m_{N-1} + k\epsilon} m_{N-1} (m_{N-2}^3 - 2m_{N-1}^3) \right], \end{aligned} \quad (2.12d)$$

$$\begin{aligned} \frac{\dot{m}_{N-1}}{m_{N-1}^2} = & -\epsilon^{-4} \left[\frac{k\epsilon}{m_{N-2} + k\epsilon} m_{N-2} (m_{N-3}^3 - 2m_{N-2}^3 + m_{N-1}^3) \right. \\ & \left. - \frac{2k\epsilon}{m_{N-1} + k\epsilon} m_{N-1} (m_{N-2}^3 - 2m_{N-1}^3) \right]. \end{aligned} \quad (2.12e)$$

We make further simplification by considering two extreme regimes: (i) ADL kinetics [4],

where $m_j \gg k\epsilon$ for all j ; and (ii) DL kinetics [28], where $k\epsilon \gg m_j$.

ADL kinetics. Equations (2.12) are reduced to the ODEs

$$\frac{\dot{m}_j}{m_j^2} = -\epsilon^{-4} (m_{j+2}^3 - 4m_{j+1}^3 + 6m_j^3 - 4m_{j-1}^3 + m_{j-2}^3), \quad (2.13a)$$

for $j = 0, \dots, N-1$, along with the conditions

$$m_{-1} = 0 = m_N, \quad m_0^3 - 2m_{-1}^3 + m_{-2}^3 = 0 = m_{N-1}^3 - 2m_N^3 + m_{N+1}^3. \quad (2.13b)$$

In (2.13a), we have set $k\epsilon = 1$ by appropriately rescaling time.

In particular, by the ansatz $m_j(t) = P(t)M_j$, we find $P(t) = (Ct + K)^{-1/4}$ and set $C = 4$, assuming $M_j > 0$. This solution is approached for long enough times [4].

Consequently, M_j satisfies the *fourth-order* difference scheme

$$M_{j+2}^3 - 4M_{j+1}^3 + 6M_j^3 - 4M_{j-1}^3 + M_{j-2}^3 = \frac{\epsilon^4}{M_j}, \quad j = 0, \dots, N-1, \quad (2.14a)$$

$$M_{-1} = 0 = M_N, \quad M_0^3 - 2M_{-1}^3 + M_{-2}^3 = 0 = M_{N-1}^3 - 2M_N^3 + M_{N+1}^3. \quad (2.14b)$$

DL kinetics. With recourse to (2.12) we obtain the ODEs

$$\begin{aligned} \frac{\dot{m}_j}{m_j^2} = & -\epsilon^{-4}[m_{j+1}(m_{j+2}^3 - 2m_{j+1}^3 + m_j^3) - 2m_j(m_{j+1}^3 - 2m_j^3 + m_{j-1}^3) \\ & + m_{j-1}(m_j^3 - 2m_{j-1}^3 + m_{j-2}^3)], \quad j = 0, \dots, N-1, \end{aligned} \quad (2.15a)$$

where

$$m_{-1} = 0 = m_N, \quad m_{-2}, m_{N+1} : \text{finite}; \quad (2.15b)$$

so, $m_{-1}(m_0^3 - 2m_{-1}^3 + m_{-2}^3) = 0 = m_N(m_{N-1}^3 - 2m_N^3 + m_{N+1}^3)$.

Again, we assume self-similarity: $m_j(t) = P(t)M_j$. Plugging this ansatz into (2.15), we have $\dot{P}(t)/P(t)^6 = -C < 0$ and find $P(t) = (5Ct + K)^{-1/5}$. We set $C = 1$ for algebraic convenience. Given this, we obtain a difference equation for M_j :

$$\begin{aligned} M_{j+1}(M_{j+2}^3 - 2M_{j+1}^3 + M_j^3) - 2M_j(M_{j+1}^3 - 2M_j^3 + M_{j-1}^3) \\ + M_{j-1}(M_j^3 - 2M_{j-1}^3 + M_{j-2}^3) = \frac{\epsilon^4}{M_j}, \quad j = 0, \dots, N-1, \end{aligned} \quad (2.16a)$$

with $M_j > 0$ for $j \in \{0, 1, \dots, N-1\}$ and extreme step conditions

$$M_{-1} = 0 = M_N \quad \text{and} \quad M_{-2}, M_{N+1} : \text{finite}. \quad (2.16b)$$

The choice of the discrete slope at the extreme steps (2.13b)(2.15b) do not automatically imply zero continuum slope and flux at the facet edges. As a matter of fact the choices

made for m_{-1} and m_N have little importance in the continuum limit. This is in agreement with the expectation for a robust continuum theory that such an arbitrary choice in the discrete level should not affect a continuum limit.

2.2 Compatibility of microscopic and macroscopic predictions

The step flow model introduced in section 2.1.2 can be compared with experiments with macroscopic observation time/spacial length in the realm of the continuum limit.

Steps can be considered as an approximation to the level sets of a height function $h(x, t)$.

One may write down a PDE for the slope function $m(x, t)$. Our presentation in this section is strictly phenomenological and we assume such continuum limits exist. In other words, we think of $m_j(t)$ as an interpolation of the continuous function $m(h, t)$ where $h = (j + 1)\epsilon = \mathcal{O}(1)$ as $\epsilon \downarrow 0$, $j \rightarrow \infty$. So set $m_j(t) = m(x, t)$.

One way to view the problem at $\nabla h = 0$ is by looking at it as a free boundary problem [97]. To this end, we investigate the boundary conditions and near-facet expansions for continuum-scale variables consistent with step motion.

We find that in surface diffusion, the large-scale slope and flux vanish at facet edges.

Our technique captures the local behavior of the slope resulting from the structure of discrete schemes for crystal steps.

The discrete schemes are converted to sum equations, which approach integral equations.

The latter reveal power series expansions in the height variable.

Evaporation-condensation and surface diffusion are treated separately in the absence of external material deposition; in fact, the evaporation case is exactly solvable under self-similarity and is invoked for comparisons.

2.3 Limit of discrete scheme and near-facet expansions

In this section the expansions for the continuum-scale slope near facet edges are derived from discrete schemes for steps. The main process involves converting the discrete schemes to sum equations; and show that, in the limit $\epsilon \downarrow 0$ with $h = (j + 1)\epsilon = \mathcal{O}(1)$ and $(N + 1)\epsilon = 1$, the sum equations become integral equations which indicate via iterations the slope behavior as $h \downarrow 0$ and $h \uparrow 1$.

Regarding the behavior of $m(h, t)$ near facets, the *order of limits* should be emphasized.

First, we let $\epsilon \downarrow 0$ with fixed h ; *next*, we allow $h \downarrow 0$ or $h \uparrow 1$.

2.3.1 Evaporation-condensation kinetics

Consider slopes under self-similarity, $m_j(t) = (4Ct + K)^{-1/4}M_j$, and set $C = 1$; more generally, a constant $C \neq 1$ would enter the resulting integral equation for $m(h)$ as a prefactor of the integral term and the analysis is not essentially different if we consider $C \neq 1$.

Rewrite (2.8) by defining $\psi_j := M_j^3$, the relevant difference scheme reads

$$\psi_{j+1} - 2\psi_j + \psi_{j-1} = f_j = -\frac{\epsilon^2}{\psi_j^{1/3}}, \quad \psi_{-1} = 0 = \psi_N, \quad (2.17)$$

where $\psi_j > 0$ and $j = 0, 1, \dots, N - 1$.

Proposition 1. (A continuum limit in evaporation-condensation) *In the limit $\epsilon \downarrow 0$, discrete scheme (2.17) reduces to the integral equation*

$$\psi(h) = m(h)^3 = C_1 h - \int_0^h \frac{h-z}{m(z)} dz \quad 0 < h < 1; \quad (2.18)$$

thus, $\lim_{h \downarrow 0} m(h) = 0$. The constant C_1 is

$$C_1 = \int_0^1 \frac{1-z}{\psi(z)^{1/3}} dz = \int_0^1 \frac{1-z}{m(z)} dz, \quad (2.19)$$

which implies $\lim_{h \uparrow 1} m(h) = 0$. By (2.18), a sufficiently differentiable $m(h)$ satisfies the ODE $m(m^3)_{hh} = -1$ for $0 < h < 1$.

With a slight abuse of notation, we use the symbol $m(h)$ for the space-dependent part of the self-similar slope; i.e., $m(h, t) = P(t)m(h)$. Assume that the integral in (2.18) converges and a solution exists in an appropriate sense.

Proof. By (2.17), express ψ_j in terms of a finite sum over f_j . To this aim, write

$$\psi_j = \frac{1}{j!} \frac{d^j \Psi(s)}{ds^j} \Big|_{s=0} = \frac{1}{2\pi i} \oint_{\Gamma} \frac{\Psi(\zeta)}{\zeta^{j+1}} d\zeta \quad (i^2 = -1), \quad j = 0, \dots, N-1, \quad (2.20)$$

by applying the Cauchy integral formula, where Γ is a smooth simple curve enclosing 0 and $\Psi(s)$ is the generating function (polynomial) defined by

$$\Psi(s) = \sum_{j=0}^{N-1} \psi_j s^j \quad s \in \mathbb{C}. \quad (2.21)$$

This $\Psi(s)$ is computed via (2.17).

By multiplying (A.1) by s^j and summing over j we have

$$s^{-1}[\Psi(s) - \psi_0 + \psi_N s^N] - 2\Psi(s) + s[\Psi(s) + \psi_{-1}s^{-1} - \psi_{N-1}s^{N-1}] = F(s),$$

where $F(s)$ is defined in (2.25). Thus, we obtain

$$\Psi(s) = \frac{\psi_0 - \psi_{-1}s - \psi_N s^N + \psi_{N-1}s^{N+1} + sF(s)}{(1-s)^2} = \frac{\mathcal{P}(s)}{(1-s)^2}, \quad (2.22)$$

which leads to (2.25) by virtue of the termination conditions. The point $s = 1$ is a removable singularity provided $\mathcal{P}(1) = 0 = \mathcal{P}'(1)$, which yield (2.26).

The coefficient of s^j in $\Psi(s)$ is given by (2.20). By restricting the contour Γ in the interior of the unit disk ($|\zeta| < 1$) and eliminating analytic terms, we have

$$\psi_j = \frac{1}{2\pi i} \oint_{\Gamma} \frac{\psi_0 + \zeta F(\zeta)}{(1-\zeta)^2} \frac{d\zeta}{\zeta^{j+1}}, \quad j = 0, \dots, N-1. \quad (2.23)$$

Recalling the binomial expansion $(1 - \zeta)^{-2} = \sum_{k=0}^{\infty} (1+k)\zeta^k$, we find the series

$$\frac{\psi_0 + \zeta F(\zeta)}{(1 - \zeta)^2} = \psi_0 + \sum_{l=0}^{\infty} \zeta^{l+1} \left[l + 2 + \sum_{p=0}^l (1+l-p)f_p \right]. \quad (2.24)$$

The coefficient of ζ^j is singled out for $l = j - 1$; thus, by (A.3) we recover (2.27).

The result is

$$\Psi(s) = \frac{\psi_0 + \psi_{N-1}s^{N+1} + sF(s)}{(1-s)^2}, \quad F(s) = \sum_{j=0}^{N-1} f_j s^j, \quad (2.25)$$

where ψ_0, ψ_{N-1} are such that $s = 1$ is a removable singularity of $\Psi(s)$:

$$\psi_0 = \frac{-NF(1) + F'(1)}{N+1}, \quad \psi_{N-1} = -\frac{F(1) + F'(1)}{N+1}. \quad (2.26)$$

The prime denotes the derivative of $F(s)$. By (2.20), we find (see Appendix A.1)

$$\psi_j = (1+j)\psi_0 + \sum_{p=0}^{j-1} (j-p)f_p = (1+j)\psi_0 - \sum_{p=0}^{j-1} \epsilon [(j+1)\epsilon - (p+1)\epsilon] \psi_p^{-1/3}. \quad (2.27)$$

This is the desired sum equation for ψ_j .

Let us now focus on the limit of (2.27) as $\epsilon \downarrow 0$ with $(j+1)\epsilon = h = \mathcal{O}(1)$. With regard to the computation of ψ_0 by (2.26), note that

$$(N+1)\psi_0 = \sum_{j=0}^{N-1} [(N+1)\epsilon - (j+1)\epsilon] \psi_j^{-1/3} \epsilon \xrightarrow{\epsilon \downarrow 0} \int_0^1 (1-h)\psi(h)^{-1/3} dh, \quad (2.28)$$

assuming that the respective sum and integral are convergent; thus,

$$\lim_{\epsilon \downarrow 0} (\epsilon^{-1}\psi_0) =: C_1 = \int_0^1 \frac{1-h}{\psi(h)^{1/3}} dh = \int_0^1 \frac{1-h}{m(h)} dh. \quad (2.29)$$

Let $z = (p+1)\epsilon$ in (2.27); then, by $\psi_p \rightarrow \psi(z)$, we have

$$\sum_{p=0}^{j-1} [(j+1)\epsilon - (p+1)\epsilon] \psi_p^{-1/3} \epsilon \rightarrow \int_0^h (h-z)\psi(z)^{-1/3} dz. \quad (2.30)$$

This limit is encapsulated in the Euler summation formula; see, e.g., [11]. In view of

(2.29), we wind up with (2.18) and (2.19). The ODE $m(m^3)_{hh} = -1$ ensues by

differentiation (in the usual calculus sense) of the integral equation. This assertion concludes our heuristic derivation. \square

Corollary 1. *The constant C_1 appearing in (2.18) is positive.*

Near-facet expansion. Proposition 1 suggests what the behavior of m near facet edges should be. Notice that the integral in (2.18) produces a subdominant contribution $\mathcal{O}(h^{2-\alpha})$ if $m(h) = \mathcal{O}(h^\alpha)$ as $h \downarrow 0$ for some $0 \leq \alpha < 1$. A formal expansion can be derived by *iteration* of (2.18). (We alert the reader that our construction of a local self-similar solution by iteration is heuristic. A rigorous analysis lies beyond our present scope.) Set $m(h) \sim m^{(n)}(h)$ to $n + 1$ terms as $h \downarrow 0$, where

$$m^{(n+1)}(h)^3 = C_1 h - \int_0^h \frac{h-z}{m^{(n)}(z)} dz; \quad m^{(0)}(h) = (C_1 h)^{1/3}, \quad (2.31)$$

and $n = 0, 1, \dots$. Thus, we derive the three-term expansion

$$m(h) = (C_1 h)^{1/3} - \frac{3}{10} C_1^{-1} h - \frac{171}{1400} C_1^{-7/3} h^{5/3} + \mathcal{O}(h^{7/3}) \quad \text{as } h \downarrow 0; \quad (2.32)$$

higher-order terms are produced directly. Our construction satisfies the estimate $m^{(n+1)} - m^{(n)} = \mathcal{O}(h^{2n/3+1})$. Expansion (2.32) is in agreement with the corresponding exact, global solution; see discussion in Appendix A.3.1.

The formal expansion by iteration can be converted to a power series in $x - x_{f,L}$ where $x_{f,L}(t)$ is the position of the left facet edge. By $\dot{x}_j = -\mu_j = -\epsilon^{-1}(m_j^3 - m_{j-1}^3)$, and the ansatz $m_j(t) = (4t + K)^{-1/4} M_j$, we ascertain that $x_j(t) \sim t^{1/4} X_j$ for large t . Hence, the similarity coordinate is $\eta = xt^{-1/4}$ and we set $h = h(\eta)$; $m(h(\eta)) = h'(\eta)$. By integrating (2.32), after some algebra we obtain

$$C_1^{1/3}(\eta - \eta_{f,L}) = \frac{3}{2} h^{2/3} + \frac{9}{40} C_1^{-4/3} h^{4/3} + \frac{1305}{2800} C_1^{-8/3} h^2 + \mathcal{O}(h^{8/3}) \quad \text{as } h \downarrow 0,$$

where $\eta_{f,L} = x_{f,L}(t)t^{-1/4}$. By inverting in the limit $\bar{\eta} = \eta - \eta_{f,L} \downarrow 0$, we find

$$m(h(\eta)) = \left(\frac{2}{3}\right)^{3/2} C_1^{1/2} \left[\frac{3}{2} \bar{\eta}^{1/2} - \frac{3}{8} C_1^{-1} \bar{\eta}^{3/2} - \frac{971}{1600} C_1^{-2} \bar{\eta}^{5/2} + \mathcal{O}(\bar{\eta}^{7/2}) \right]. \quad (2.33)$$

For the other end point ($h \uparrow 1$), mirror symmetry applies (under $h \mapsto 1 - h$).

Remark 1. Integral equation (2.18) can result from integrating the ODE

$(m^3)_{hh} = -1/m$ via imposing from the outset $m \rightarrow 0$ as $h \downarrow 0$ and $h \uparrow 1$. Here, we let this zero-slope condition emerge by directly resolving the discrete scheme.

Remark 2. It is tempting to extend the above calculation to the full time-dependent setting, with focus on ODEs (2.6). Consider $m_j(t) \rightarrow m(h, t)$. Formally, $1/m(h)$ (under self-similarity) is now replaced by $\partial_t[m(h, t)^{-1}]$ in defining f_j . If the integral converges, the relation for $m(h, t)$ now reads

$$m(h, t)^3 = C_1(t)h - \int_0^h (h - z) \partial_t[m(z, t)^{-1}] dz \quad t > 0 ; \quad (2.34)$$

$C_1(t)$ is given by the t -dependent counterpart of (2.19). Alternatively, differentiate to get the PDE $\partial_t m = m^2 \partial_h^2(m^3)$ [98]. Caution should be exercised though: in principle, (2.34) may not be amenable to iterations in the sense described above, unless t is sufficiently large. So, it is not advisable to iterate (2.34) to study transients of the slope near the facet edge.

Remark 3. This discussion suggests that, for a class of initial data,

$$m(h(x, t), t) = \mathcal{O}((x - x_f(t))^{1/2}) \quad x \rightarrow x_f(t) , \quad (2.35)$$

at the left- and right-facet edge position, $x_f(t)$, for sufficiently long times. Notably, this behavior is in agreement with the condition of local equilibrium at facet edges [10, 52].

Furthermore, the integral equation formulation indicates the *form* of the expansion for $m(h, t)$ and readily provides the leading-order term. For the derivation of higher-order terms (to arbitrary order), it is algebraically convenient to use the respective PDE (or ODE for self-similar slopes). The starting point is the power series expansion

$\sum_{n=1}^{\infty} A_n(x - x_f(t))^{n/2}$, in accord with the iterations of (2.18); see also Section 2.3.2.

This form is to be contrasted with the series used in [48] for a geometry having a single semi-infinite facet, where the self-similar solution for the continuum slope does not decay in time.

2.3.2 Surface diffusion

Our analysis for evaporation-condensation can be extended to surface diffusion with a few (mostly technical) modifications. For DL kinetics, we split the fourth-order discrete scheme into two second-order schemes. This case is discussed in some detail. We present fewer details for ADL kinetics where the fourth-order scheme is treated without analogous splitting.

2.3.2.1 DL kinetics

We first focus on the self-similarity ansatz $m_j(t) = (5t + K)^{-1/5} M_j$ observed in [28], and set $\psi_j = M_j^3$. The fourth-order scheme (2.16) is split as

$$\psi_{j+1} - 2\psi_j + \psi_{j-1} = -\frac{\epsilon^2 \varphi_j}{\psi_j^{1/3}}, \quad \varphi_{j+1} - 2\varphi_j + \varphi_{j-1} = -\frac{\epsilon^2}{\psi_j^{1/3}}; \quad (2.36a)$$

$$\psi_{-1} = 0 = \psi_N, \quad \varphi_{-1} = 0 = \varphi_N; \quad j = 0, 1, \dots, N-1. \quad (2.36b)$$

Recall that φ_j is the adatom flux on the j th terrace, where $x_j < x < x_{j+1}$.

Proposition 2. (A continuum limit in DL kinetics) *In the limit $\epsilon \downarrow 0$, discrete scheme (2.36) reduces to the integral equation*

$$\psi(h) = m(h)^3 = C_1 h - C_2 \int_0^h \frac{z(h-z)}{m(z)} dz + \int_0^h \int_0^z \frac{(h-z)(z-\zeta)}{m(z)m(\zeta)} d\zeta dz, \quad (2.37)$$

for $0 < h < 1$; thus, $\lim_{h \downarrow 0} m(h) = 0 = \lim_{h \downarrow 0} \varphi(h)$ (φ : flux). The constants C_1, C_2 are subject to respective conditions at $h = 1$: $\lim_{h \uparrow 1} m(h) = 0 = \lim_{h \uparrow 1} \varphi(h)$. By (2.37), any sufficiently differentiable $m(h)$ satisfies $m[m(m^3)_{hh}]_{hh} = 1$.

In fact, (2.36) reduces to a pair of integral relations, which yield (2.37). The primary continuum variables are the slope, $m(h)$, and flux, $\varphi(h)$; see (2.40),(2.41). Assume that the integrals in (2.37) converge and a solution exists appropriately.

Proof. We proceed along the lines of Section 2.3.1; recall formulas (2.20) and (2.21) regarding ψ_j in terms of $\Psi(s)$. Our strategy is to express each of the second-order difference equations (2.36a) as a sum equation, treating their right-hand sides as forcing terms, f_j (see Appendix A.1). The first one of (2.36a) leads to

$$\psi_j = (1+j)\psi_0 - \sum_{p=0}^{j-1} [(j+1)\epsilon - (p+1)\epsilon] \frac{\varphi_p}{\psi_p^{1/3}} \epsilon, \quad (2.38a)$$

after applying the first pair of conditions (2.36b); the coefficient ψ_0 is given by

$$(N+1)\psi_0 = \sum_{j=0}^{N-1} [(N+1)\epsilon - (j+1)\epsilon] \frac{\varphi_j}{\psi_j^{1/3}} \epsilon. \quad (2.38b)$$

The second one of equations (2.36a) with the last pair of conditions (2.36b) yield

$$\varphi_j = (1+j)\varphi_0 - \sum_{p=0}^{j-1} \frac{(j+1)\epsilon - (p+1)\epsilon}{\psi_p^{1/3}} \epsilon, \quad (2.39a)$$

where, by analogy with (2.38b),

$$(N+1)\varphi_0 = \sum_{j=0}^{N-1} [(N+1)\epsilon - (j+1)\epsilon] \psi_j^{-1/3} \epsilon. \quad (2.39b)$$

Now let $\epsilon \downarrow 0$ with $(N+1)\epsilon = 1$ and $(j+1)\epsilon = h = \mathcal{O}(1)$. By (2.38), we have

$$\psi_j \rightarrow \psi(h) = m(h)^3 = C_1 h - \int_0^h (h-z) \frac{\varphi(z)}{m(z)} dz \quad 0 < h < 1; \quad (2.40a)$$

$$C_1 := \lim_{\epsilon \downarrow 0} (\epsilon^{-1} \psi_0) = \int_0^1 (1-z) \frac{\varphi(z)}{m(z)} dz. \quad (2.40b)$$

By (2.39), the analogous limit for φ_j is

$$\varphi_j \rightarrow \varphi(h) = C_2 h - \int_0^h \frac{h-z}{m(z)} dz \quad 0 < h < 1; \quad (2.41a)$$

$$C_2 := \lim_{\epsilon \downarrow 0} (\epsilon^{-1} \varphi_0) = \int_0^1 \frac{1-z}{m(z)} dz. \quad (2.41b)$$

By the definitions of C_1 and C_2 , we infer $\lim_{h \uparrow 1} m(h) = 0 = \lim_{h \uparrow 1} \varphi(h)$. The combination of (2.40a) and (2.41a) recovers (2.37). Differentiations of the integral equations entail $m(m^3)_{hh} = -\varphi$, $m\varphi_{hh} = -1$, by which $m(m(m^3)_{hh})_{hh} = 1$. \square

Corollary 2. *The constants C_1, C_2 in (2.37) are positive. Further, for $0 < h < 1$, the flux $\varphi(h)$ is positive; thus, (a twice continuously differentiable) $m(h)^3$ is concave.*

The first statement in Corollary 2 follows from the definitions of C_1, C_2 and the assumed positivity of slope. Note that

$$C_1 = \int_0^1 \frac{1-z}{m(z)} \left[\int_0^z \frac{\zeta(1-z)}{m(\zeta)} d\zeta + \int_z^1 \frac{z(1-\zeta)}{m(\zeta)} d\zeta \right] dz .$$

The positivity of $\varphi(h) = -m(m^3)_{hh}$ follows from (2.41). \square

Near-facet expansion. We notice that if $m(h) = \mathcal{O}(h^\alpha)$ as $h \downarrow 0$ for some $0 \leq \alpha < 1$, the integral terms in (2.37) generate subdominant contributions of orders (from left to right) $\mathcal{O}(h^{3-\alpha})$ and $\mathcal{O}(h^{4-2\alpha})$. This observation motivates an iteration scheme for (2.37), or the system of (2.40a) and (2.41a). Successive local approximations of $m(h)$ as $h \downarrow 0$ can be constructed via the scheme

$$\begin{aligned} m^{(n+1)}(h)^3 &= C_1 h - \int_0^h (h-z) \frac{\varphi^{(n)}(z)}{m^{(n)}(z)} dz , & m^{(0)}(h) &= (C_1 h)^{1/3} ; \\ \varphi^{(n+1)}(h) &= C_2 h - \int_0^h \frac{h-z}{m^{(n)}(z)} dz , & \varphi^{(0)}(h) &= C_2 h , \end{aligned} \quad (2.42)$$

where $m \sim m^{(n)}$, $\varphi \sim \varphi^{(n)}$ to $n+1$ terms; $n = 0, 1, \dots$. The above construction produces a formal expansion of $m(h)$ in ascending powers of h . The first three terms are evaluated in Appendix A.3.2; the result reads

$$m(h) = (C_1 h)^{1/3} - \frac{3}{40} \frac{C_2}{C_1} h^2 + \frac{27}{700} C_1^{-4/3} h^{8/3} + \mathcal{O}(h^{11/3}) \quad h \downarrow 0 . \quad (2.43)$$

Note the powers of h entering (2.43), i.e., $1/3$ (leading order), 2 (first correction) and $8/3$, in comparison to the powers $1/3, 1, 5/3$ appearing in (2.32).

In the present setting of self-similarity, we have $h = h(\eta)$ and $m(h(\eta)) = h'(\eta)$ where $\eta = xt^{-1/5}$ [28]. By integration and inversion of (2.43), we find an expansion of $m(h(\eta))$ in the vicinity of the facet edge, as $\bar{\eta} = \eta - \eta_{f,1} \downarrow 0$:

$$m(h(\eta)) = \left(\frac{2}{3}\right)^{1/2} C_1^{1/2} \bar{\eta}^{1/2} - \frac{8}{315} C_2 \bar{\eta}^3 + \frac{8}{945} \bar{\eta}^4 + \mathcal{O}(\bar{\eta}^{11/2}) . \quad (2.44)$$

Note the absence of the powers 1, 3/2, 2, 5/2; cf. equation (A5) in [28]. Likewise, by symmetry we can write an expansion for $m(h)$ as $h \uparrow 1$. The above procedure suggests expanding the slope in integer powers of $\bar{\eta}^{1/2}$ [28].

Remark 4. Integral equation (2.37) can result from integrating the slope ODE $m[m(m^3)_{hh}]_{hh} = 1$ under the conditions $m \rightarrow 0$ and $\varphi \rightarrow 0$ as $h \downarrow 0$ and $h \uparrow 1$. Our technique exemplifies the passage to the continuum limit *via the integral equation* so that these conditions emerge directly from the difference scheme.

Remark 5. It is tempting to extend the results of Proposition 2 to the time-dependent setting (without self-similarity), where $m_j(t) \rightarrow m(h, t)$. The emergent pair of integral relations for $m(h, t)$ and the continuum flux, $\varphi(h, t)$, is

$$\begin{aligned} m(h, t)^3 &= C_1(t)h - \int_0^h (h-z) \frac{\varphi(z, t)}{m(z, t)} dz , \\ \varphi(h, t) &= C_2(t)h - \int_0^h (h-z) \partial_t [m(z, t)^{-1}] dz, \quad 0 < h < 1, \quad t > 0, \end{aligned} \quad (2.45)$$

provided the integrals converge; $C_1(t)$, $C_2(t)$ are subject to the vanishing of m and φ as $h \uparrow 1$. In principle, it may not be legitimate to iterate (2.45) as above (under self-similarity) in order to obtain an expansion for $m(h, t)$ near a facet edge, unless t is sufficiently large. By differentiation of (2.45), we obtain the familiar PDE $\partial_t m = -m^2 \partial_h^2 (m \partial_h^2 m^3)$ [28, 62].

Remark 6. By (2.45), the slope is $m(h(x, t), t) = \mathcal{O}((x - x_f(t))^{1/2})$ as $x \rightarrow x_f(t)$ (position of a facet edge) for sufficiently long times, consistent with the hypothesis of

local equilibrium invoked in earlier continuum theories, e.g., in [62]. Further iterations are suggestive of the nature of the expansion for $m(h, t)$ in the vicinity of large facet edges. To compute coefficients of the expansion, it is algebraically convenient to make the substitution $m(h, t) = \sum_{n=1}^{\infty} A_n(t)(x - x_f(t))^{n/2}$ into the PDE for $m(h, t)$; then, the values $A_2 = A_3 = A_4 = A_5 = 0$ are recovered by dominant balance [28].

2.3.2.2 ADL kinetics

Next, we focus on fourth-order scheme (2.13), which is also the subject of [4]. By the similarity solution $m_j(t) = (4t + K)^{-1/4} M_j$, proved in [4], and $\psi_j = M_j^3$, the related difference equations read

$$\psi_{j+2} - 4\psi_{j+1} + 6\psi_j - 4\psi_{j-1} + \psi_{j-2} = f_j = \epsilon^4 \psi_j^{-1/3}, \quad (2.46a)$$

for $j = 0, 1, \dots, N - 1$, along with the conditions

$$\psi_{-1} = 0 = \psi_N, \quad \psi_0 - 2\psi_{-1} + \psi_{-2} = 0 = \psi_{N-1} - 2\psi_N + \psi_{N+1}; \quad (2.46b)$$

recall that $\varphi_j = -(\psi_{j+1} - 2\psi_j + \psi_{j-1})$ is the j th-terrace adatom flux. There are at least two routes to studying (2.46): either split it into two second-order schemes by using φ_j as an auxiliary variable, or leave the fourth-order scheme intact and use only ψ_j . We choose the latter way here.

Proposition 3. (A continuum limit in ADL kinetics) *In the limit $\epsilon \downarrow 0$, discrete scheme (2.46) reduces to the integral equation*

$$\psi(h) = m(h)^3 = C_1 h - C_3 h^3 + \frac{1}{6} \int_0^h \frac{(h-z)^3}{m(z)} dz, \quad 0 < h < 1; \quad (2.47)$$

thus, $\lim_{h \downarrow 0} m(h) = 0 = \lim_{h \downarrow 0} \varphi(h)$ (φ : flux). The constants C_1, C_3 are subject to respective conditions at $h = 1$: $\lim_{h \uparrow 1} m(h) = 0 = \lim_{h \uparrow 1} \varphi(h)$. By (2.47), (a sufficiently differentiable) $m(h)$ satisfies $m(m^3)_{hhhh} = 1$; cf. [4].

By our usual practice, we assume that the integral in (2.47) converges and a solution exists in some appropriate sense.

Proof. We treat the f_j in (2.46) as a given forcing term and solve for ψ_j using (2.20) and (2.21), with recourse to a generating polynomial $\Psi(s)$; see Appendix A.2.3 for details. After some algebra, the variables ψ_j are found to be

$$\begin{aligned} \psi_j = & \frac{1}{6} \left[(\psi_1 - 2\psi_0)j^2(j+3) + 2(\psi_0 + \psi_1)j + 6\psi_0 \right. \\ & \left. + \epsilon^4 \sum_{p=0}^{j-2} (j-p-1)(j-p)(j-p+1)\psi_p^{-1/3} \right], \quad j = 0, \dots, N-1, \end{aligned} \quad (2.48)$$

where

$$\psi_1 - 2\psi_0 = \frac{-NF(1) + F'(1)}{N+1}, \quad (2.49a)$$

$$\begin{aligned} 2(N+1)(\psi_1 + \psi_0) = & N(2N-1)F(1) + (2N^2 - 5N + 2)F'(1) \\ & - 3(N-1)F''(1) + F'''(1), \end{aligned} \quad (2.49b)$$

$$\psi_0 = \frac{N(2N+1)F(1) + N(2N-5)F'(1) - 3(N-1)F''(1) + F'''(1)}{6(N+1)}. \quad (2.49c)$$

Recall $F(s) = \sum_{j=0}^{N-1} f_j s^j$. The prime in (2.49) denotes the derivative in s .

Now let $N \rightarrow \infty$, and $\epsilon \downarrow 0$ with $(N+1)\epsilon = 1$. By formulas (2.49), we find

$$\frac{\psi_1 - 2\psi_0}{\epsilon^3} \xrightarrow{\epsilon \downarrow 0} - \int_0^1 \frac{1-z}{m(z)} dz, \quad (2.50a)$$

$$\frac{\psi_0 + \psi_1}{\epsilon} \xrightarrow{\epsilon \downarrow 0} \frac{1}{2} \int_0^1 \frac{1-z - (1-z)^3}{m(z)} dz, \quad (2.50b)$$

$$\psi_0 = \mathcal{O}(\epsilon) \rightarrow 0. \quad (2.50c)$$

For fixed height $h = (j+1)\epsilon$ (with $j \rightarrow \infty$), we let $\psi_j \rightarrow \psi(h)$, thus reducing sum equation (2.48) to integral equation (2.47) with

$$C_1 := \lim_{\epsilon \downarrow 0} \frac{\psi_0 + \psi_1}{3\epsilon} = \frac{1}{6} \int_0^1 \frac{1-z - (1-z)^3}{m(z)} dz, \quad (2.51a)$$

$$C_3 := -\lim_{\epsilon \downarrow 0} \frac{\psi_1 - 2\psi_0}{6\epsilon^3} = \frac{1}{6} \int_0^1 \frac{1-z}{m(z)} dz, \quad (2.51b)$$

and neglect of ψ_0 . The resulting continuum-scale slope $m(h)$ vanishes as $h \downarrow 0$. In addition, $\varphi_j \rightarrow \varphi(h)$ with $\lim_{h \downarrow 0} \varphi(h) = 0$, as verified directly by (2.47). Equations (2.51) imply that the slope and flux also vanish at the other end point, as $h \uparrow 1$. The differentiation of (2.47) furnishes the ODE $m(m^3)_{hhhh} = 1$ where $\varphi(h) = -(m^3)_{hh}$. \square

Corollary 3. *The constants C_1, C_3 entering (2.47) are positive. Further, the large-scale flux, $\varphi(h) = -(m^3)_{hh}$, is positive for $0 < h < 1$.*

Corollary 3 declares the concavity of $\psi(h) = m(h)^3$ proved by AKW [4].

In the spirit of Sections 2.3.1 and 2.3.2.1, a formal expansion for the slope near facet edges can plausibly be derived by iterations of (2.47). The ensuing slope behavior is $m(h) = (C_1 h)^{1/3} + \mathcal{O}(h^{7/3})$ as $h \downarrow 0$; so, the leading-order term is compatible with local equilibrium. Hence, with $\eta = xt^{-1/4}$, we have (cf. (2.44))

$$m(h(\eta)) = \left(\frac{2}{3}\right)^{1/2} C_1^{1/2} \bar{\eta}^{1/2} + \mathcal{O}(\bar{\eta}^{7/2}) \quad \text{as } \bar{\eta} \rightarrow 0; \quad \bar{\eta} = t^{-1/4}(x - x_f(t)). \quad (2.52)$$

Further details of these computations are left to the interested reader.

Remark 7. The derivation can be extended to the full time dependent setting, where $m_j(t) \rightarrow m(h, t)$. The integral relation consistent with step laws is

$$m(h, t)^3 = C_1(t)h - C_3(t)h^3 + \frac{1}{6} \int_0^h (h-z)^3 \partial_t [m(z, t)^{-1}] dz, \quad (2.53)$$

where $0 < h < 1$ and $t > 0$. The PDE reads $\partial_t m = -m^2 \partial_h^4 m^3$ [4].

Chapter 3: Evaporation-condensation in radial geometry

Radial geometry captures essence of island models. In particular, the radial geometry is the simplest model that encapsulates the role of the curvature of the crystal surface. To capture with minimal complexity the main elements that may cause close agreement of discrete and continuum-scale dynamics, we focus on an ad hoc yet physically plausible evaporation model that is rich enough to include step curvature, elastic-dipole step-step repulsions [61, 78], and a terrace-width-dependent discrete step mobility. The main mass transport process of evaporation-condensation kinetics is exchange of adatoms between steps and the surrounding vapor. In this kinetics, the step velocity is proportional to the chemical potential and surface diffusion is assumed to be absent, so adatoms on terrace are assumed to be small in number or even if they exist, they don't affect the step motion.

In principle, evaporation coexists with, but is simpler to study than, surface diffusion. In the latter process, adatoms diffuse on terraces and on step edges, and attach or detach at steps from or to terraces [53, 84]. There have been works on the radially symmetric surface diffusion models [62, 71]; however, due to its complexity, the results are limited to numerical simulation. We are not aware if this simplified model has a concrete physical application. Nonetheless, the model serves as a reference case in the study of realistic, more complicated microscopic theories. In fact, our hybrid scheme approach has been applied to terrace diffusion in [76]. We also discuss how our model results from the

simplification of a step scheme that includes desorption, surface diffusion, and a negative (“inverse”) Ehrlich-Schwoebel (ES) effect [17, 21, 80, 91], by which adatoms on terraces attach/detach at down-steps with a kinetic rate that is larger than the rate for up-steps. At the macroscale, our model reduces to a description of generic appeal: The flow of the continuum-scale height is expressed as the variation of a familiar singular surface free energy, which we consider as given [40, 97]. Outside the facet, this entails to a second-order parabolic PDE proposed by Spohn [97]. We treat the facet as a free boundary. One choice is to apply “natural boundary conditions” from the subgradient formalism which is intimately connected to continuum thermodynamics [55].

At the level of steps, the step velocity is proportional to the step chemical potential, the variation of a total step free energy, which we also consider as given; the respective coefficient, or discrete mobility, is chosen linear in the width of the *upper* terrace, giving rise to a forward difference scheme and stable step dynamics in the radial setting. We propose two step flow models, called M1 and M2, each of which formally reduces to Spohn’s PDE away from the facet. In both models, the step velocity is driven by the step chemical potential, the variation of the total step free energy. In M1 the step mobility is simply proportional to the upper-terrace width; whereas in M2 the mobility is modified by an extra *discrete geometry-induced* factor. Our numerics under conical initial data indicate that the discrete slopes become self similar at long time.

Our main findings are:

- (i) discrete slopes by M1 are in agreement with predictions of the subgradient theory;
- (ii) discrete slopes by M2 deviate from results of the subgradient formalism; and
- (iii) the above discrepancy is eliminated by introduction of a *jump* at the facet edge of a (properly defined) continuum flux function, which replaces the natural boundary

condition that this flux be continuous.

The modification of the natural boundary condition in (iii) aims to account for the facet microstructure: The discontinuity is expressed in terms of the extra, discrete geometric factor of step mobility evaluated for a pair of extremal steps at times of *top-step collapses*; data for this factor is extracted from discrete simulations. In the special case with non-interacting steps in M2, we verify that this factor has a value close to an exact result from the convergence of the discrete scheme.

These results indicate that, depending on step kinetics, facets may be incorporated into a continuum theory by adjusting a coefficient in a known (natural) boundary condition of the subgradient formalism. This finding essentially justifies the use of this formalism as our starting point. For nonzero step-step interactions, the natural boundary conditions include continuity of *height*, *slope* and the *flux* entering the conservation form of the PDE outside the facet. Retaining these variables, we point out that adjusting the flux at the facet edge in correspondence to collapses of atomic layers suffices to yield continuum predictions in agreement with discrete simulations.

We numerically show that this connection depends critically on the step kinetics (particularly the step velocity law); for example, the subgradient theory is in agreement with the step flow in the context of M1.

3.1 Formulation

In this section we introduce the geometry of the problem and the governing equations (ODEs) of step motion. A key element of our modeling is the use of step mobilities that give rise to discrete dynamics prohibiting step crossing even for zero step interactions in M1 and M2.

3.1.1 Geometry

The geometry is shown in Figure 2.1. At the macroscale, the crystal surface is described by a continuous height profile, $h(r, t)$, with respect to a fixed (xy -) plane of reference.

The (circular) facet has zero-slope orientation, height $h_f(t)$ and radius $r_f(t)$. We expect that $\dot{h}_f(t)$ is nonpositive and $\dot{r}_f(t)$ is nonnegative, i.e., the facet loses height and expands, as in the surface diffusion case [62].

At the microscale, this configuration consists of concentric circular, descending steps of constant atomic height, a . The i th step has radius $r_i(t)$, where initially (at $t = 0$) r_i is nonzero for $0 \leq i \leq N$ with $N \gg 1$; by convention, $r_i(t) \equiv 0$ if $i < 0$ and $i > N$, for all $t \geq 0$. We take N to be large yet finite, so that the structure can be considered as semi-infinite for all practical purposes (but not in sections 3.3.2 and 4.2). Steps are expected to shrink and collapse on top of the facet; only steps with $n \leq i \leq N$ are present at times $t_n \leq t < t_{n+1}$, where t_n is the collapse time of the n th step of the initial configuration; by convention, set $r_n(t) \equiv 0$ if $t \geq t_n$ ($n \geq 0$). Thus, i in nonzero r_i is a variable index enumerating steps of the initial configuration that remain on the structure. We assume that $r_{i+1}(0) > r_i(0)$ for all i ; then, $r_{i+1}(t) > r_i(t)$ for all later times (see section 3.3). Accordingly, the discrete slopes defined by

$$\mathcal{M}_i = \frac{a}{r_{i+1} - r_i} \tag{3.1}$$

are positive ($\mathcal{M}_i > 0$) and bounded, $\mathcal{M}_i \leq \mathcal{O}(1)$. Near the top step, $r_{i+1} - r_i$ can be much larger than a and, thus, \mathcal{M}_i is small (as we verify numerically).

Let $h_{\text{top}}(t)$ denote the height of the top layer at time t (see Figure 2.1). Because of step collapses on top of the facet, $h_{\text{top}}(t)$ must decay; evidently, $0 < h_{\text{top}} - h_f = \mathcal{O}(a) \downarrow 0$ in the macroscopic limit. The everywhere-continuous surface height, $h(r, t)$, is the

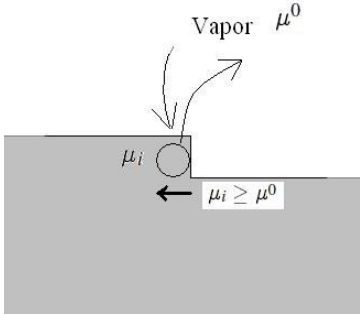


Figure 3.1:

continuum limit of the discrete (piecewise constant) height $h_d(r, t)$ which satisfies

$$h_{\text{top}}(t) - h_d(r, t) = (i - n)a , \quad (3.2)$$

for $r_{i-1} < r < r_i$ and $t_{n-1} \leq t < t_n$. In the continuum limit, where $a \downarrow 0$ and $ia = \mathcal{O}(1)$,

we assert that

$$ia \rightarrow h_f(0) - h(r, t) . \quad (3.3)$$

The right-hand side is used as a continuum Lagrangian variable in chapter 4.

3.1.2 Discrete equations of motion

In our mass transport process, evaporation-condensation, atoms are exchanged between step edges and the surrounding vapor. We neglect diffusion along step edges [53]; and leave out material deposition from above. Hence, the surface is expected to relax only by lowering its energy. Furthermore, we adapt entropic and elastic-dipole *nearest-neighbor* step interactions [53, 61, 78].

We start with a step velocity law of the form

$$\frac{dr_i}{dt} = \dot{r}_i = -\nu_i(\mu_i - \mu^0) , \quad i = 0, 1 \dots, N , \quad (3.4)$$

which captures the effect of adatoms being exchanged between concentric circular step edges and the surrounding vapor; $N \gg 1$. In (5.3), $r_i(t)$ is the i th-step radius, ν_i is a (positive) discrete mobility (specified below), μ^0 is the constant chemical potential of the surrounding vapor, and μ_i is the step chemical potential; this μ_i incorporates step curvature (stiffness) and elastic-dipole step-step interactions [53], and depends on (r_{i-1}, r_i, r_{i+1}) (see section 3.1). We then obtain a large system of ordinary differential equations (ODEs) for the step radii. This system describes successive annihilations of the top (extremal) layers of an axisymmetric structure; each collapse time t_n is defined as the earliest time at which $r_n(t) = 0$ ($n \geq 0$). We take $r_i(t) \equiv 0$ if $i \leq n$ and $t \geq t_n$. Because of these annihilations, the surface height is expected to decrease with time. For definiteness, set $\mu^0 = 0$ in (5.3).

A few comments on the physical origin of (5.3) are in order. The guiding principle is that atoms on step edges move from higher to lower chemical potential (see, Figure 3.1). For example, when the top circular step is small enough, its chemical potential (μ_i) is dominated by the step line tension and tends to become large; thus, atoms leave the step edge and this in turn retreats (and shrinks). This behavior is consistent with (5.3).

The associated step mobility reads

$$\nu_i = \nu \mathcal{G}_i \frac{r_i - r_{i-1}}{a}; \quad \mathcal{G}_i = \mathcal{G}_i(t) = \begin{cases} 1 & \text{for M1} \\ \frac{r_i + r_{i-1}}{2r_i} & \text{for M2} \end{cases}, \quad (3.5)$$

where a is the step height and ν is a positive constant ($\nu > 0$). The geometric factor \mathcal{G}_i in M2 can be derived as a special limit of the BCF model.

The quantity \mathcal{G}_i forms a crucial geometric factor. Note that step velocity law (5.3) for M2 reduces to the one for M1 away from the facet because $r_{i+1} - r_i \ll r_i, r_{i+1}$. This condition breaks down near the facet.

We assume that $r_{i+1}(0) > r_i(0)$ for all i ; then, $r_{i+1}(t) > r_i(t)$ for all later times (see section 3.3). Accordingly, the discrete slopes defined by

$$\mathcal{M}_i = \frac{a}{r_{i+1} - r_i} \quad (3.6)$$

are positive ($\mathcal{M}_i > 0$) and bounded, $\mathcal{M}_i \leq \mathcal{O}(1)$. Near the top step, $r_{i+1} - r_i$ can be much larger than a and, thus, \mathcal{M}_i is small (as we verify numerically).

Next, we address the specifics of M1 and M2. The (radial) velocity of the i th step stems from (5.3) and (5.4):

$$\dot{r}_i = -\nu \mathcal{G}_i \frac{r_i - r_{i-1}}{a} \mu_i ; \quad \mathcal{G}_i = \begin{cases} 1 & \text{for M1} \\ \frac{r_i + r_{i-1}}{2r_i} & \text{for M2} \end{cases} , \quad (3.7)$$

for $n \leq i \leq N$ and any $n \geq 0$, where ν has units of length/energy/time; recall that $r_{i-1}(t) \equiv 0$ if $i \leq n$, $t_{n-1} \leq t < t_n$. We claim that in M2 the above formula for \mathcal{G}_i is compatible with the radial geometry; for a derivation of \mathcal{G}_i from the BCF model with desorption and negative ES barrier, see Appendix B.

Note in passing that, in the limit $a \downarrow 0$ with $r_i - r_{i-1} = \mathcal{O}(a)$, $\mathcal{G}_i \rightarrow 1$ and ODEs (3.7) become $\partial_t h = -\nu \mu$, where μ is the macroscopic limit of μ_i . This outcome is in agreement with Spohn's evaporation model [97]; see section 3.2 for details.

To determine μ_i , we first describe the total step free energy, E^a , which accounts for step line tension as well as entropic and elastic-dipole step repulsive interactions:

$$E^a(t) = \sum_{i=n}^N 2\pi r_i(t) [g_1 a + \mathcal{V}^a(r_i(t), r_{i+1}(t))] , \quad (3.8)$$

where the pairwise interaction energy between steps of radii r and ρ is [49]

$$2\pi r \mathcal{V}^a(r, \rho) := 2\pi \check{g}_3 \frac{r\rho}{\rho + r} \left(\frac{a}{\rho - r} \right)^2 . \quad (3.9)$$

In (3.8) and (3.9), $g_1 a$ is the step line tension (energy/length) and \check{g}_3 expresses the strength of step-step repulsion per unit length of a step; for later algebraic convenience, replace \check{g}_3 by the (macroscopic) parameter [62]

$$g_3 = \frac{3}{2} \frac{\check{g}_3}{a} . \quad (3.10)$$

The step chemical potential is defined through the variational formula [64]

$$\sum_i a \oint_{L_i} \mu_i v_i ds = \Omega \dot{E}^a(t) , \quad (3.11)$$

where L_i is the i -th step curve and v_i is the step velocity. Relation (3.11) implies

$$\begin{aligned} \mu_i &= \frac{\Omega}{a} \frac{1}{2\pi r_i} \frac{\partial E^a}{\partial r_i} \\ &= \frac{\Omega g_1}{r_i} + \frac{\Omega}{r_i a} \frac{\partial \{r_i [\mathcal{V}^a(r_i, r_{i+1}) + \mathcal{V}^a(r_i, r_{i-1})]\}}{\partial r_i} \\ &= \frac{\Omega g_1}{r_i} + \frac{2}{3} \Omega \frac{g_3 a^2}{r_i} \left\{ \psi(r_i, r_{i+1}) - \psi(r_{i-1}, r_i) + \right. \\ &\quad \left. \frac{1}{r_i^2} [\phi(r_i, r_{i+1}) + \phi(r_{i-1}, r_i)] \right\} , \end{aligned} \quad (3.12)$$

where Ω is the atomic volume, $\Omega \approx a^3$, and

$$\psi(r, \rho) = \frac{2r\rho}{\rho + r} \frac{1}{(\rho - r)^3} , \quad (3.13)$$

$$\phi(r, \rho) = \left(\frac{\rho r}{\rho + r} \right)^2 \frac{1}{(\rho - r)^2} . \quad (3.14)$$

Accordingly, we obtain the step velocity law

$$\begin{aligned} \dot{r}_i &= -\frac{\Omega \nu g_1}{r_i} \frac{r_i - r_{i-1}}{a} \mathcal{G}_i \left\{ 1 + \frac{2ga^2}{3} \left[\psi(r_i, r_{i+1}) \right. \right. \\ &\quad \left. \left. - \psi(r_{i-1}, r_i) + \frac{\phi(r_i, r_{i+1}) + \phi(r_{i-1}, r_i)}{r_i^2} \right] \right\} , \quad g = \frac{g_3}{g_1} , \end{aligned} \quad (3.15)$$

where $n \leq i \leq N$ for $t_{n-1} < t < t_n$ and $r_{N+1}(t) \equiv 0$; \mathcal{G}_i is defined in (3.7). The parameter g is the relative strength of step line tension and step-step repulsion.

Equation (3.15) can be non-dimensionalized by use of the variables $\tilde{r}_i = r_i/a$ and

$\tilde{t} = (\nu g_1 \Omega / a^2) t$; or, alternatively, via units with $a = 1 = \nu g_1$. We follow this route in

sections 3.3 and 3.4.5–3.5.3. In sections 3.2–3.4.4, we retain the dimensional variables so as to indicate transparently the passage to the continuum limit.

3.2 Formal continuum limit outside facet

In this section, we review the derivation of PDEs for the surface height and slope profiles away from the facet on the basis of the step velocity law (3.15). Our computations are formal, primarily invoking notions of pointwise convergence (with the exception of (3.21) for μ); similar, yet more detailed, heuristic derivations are presented in [62, 64] as parts of the (technically more involved) case with surface diffusion in 2D, where the step velocity is the difference of adatom fluxes each of which is expressed in terms of differences of step chemical potentials of neighboring terraces. We emphasize that the derived continuum laws are valid only for $r > r_f(t)$. The a priori unknown facet position, $r_f(t)$, should be determined from solving a free boundary problem (see section 3.4).

Consider $N \gg i \gg n \gg 1$ with $ia = \mathcal{O}(1)$, in view of (3.3). We assume that the discrete slopes, M_i , are kept fixed; cf. (3.6). On each terrace, $r_{i-1} < r < r_i$, we have $h_d(r, t) = \text{const.}$. A continuum height function $h(r, t)$, slope function $m(r, t)$, chemical potential $\mu(r, t)$ are assumed to exist as a continuum limit of ai , M_i , μ_i respectively as $a \rightarrow 0$, $r_{i+1} - r_i \rightarrow 0$. For this assumption to be valid, it is necessary that $r_{i+1} - r_i \ll r_i$ (*cond.1*). When this condition is not met, the “continuum” equations are subject to influences from the discrete equations, which makes the theory no longer fully macroscopic. A discussion on the influence of the geometric factor of extreme steps at the continuum scale is provided in 3.4.3.

Here, we take the continuum limit under the assumption of (*cond.1*). As $r \uparrow r_i(t)$, the

differentiation of $h_d(r, t)$ with respect to time yields

$$\dot{r}_i \rightarrow \partial_t h(r, t)/m(r, t)|_{r=r_i(t)} \quad \text{as } a \rightarrow 0, \quad (3.16)$$

where $m(r, t) = -\partial_r h(r, t)$ and $r > r_f(t)$. Equation (3.16) reveals the limit of the left-hand side of (3.15).

On the other hand, the discrete mobility, $\nu_i = \nu \mathcal{G}_i(r_i - r_{i-1})/a$, approaches

$$\nu_i \rightarrow \nu/m(r, t)|_{r=r_i(t)}, \quad r > r_f(t). \quad (3.17)$$

for both M1 and M2. Thus, if $\mu_i(t) \rightarrow \mu(r, t)$, the continuum-scale chemical potential, (3.16) and (3.17) yield

$$\partial_t h(r, t) = -\nu \mu(r, t) \quad r > r_f(t). \quad (3.18)$$

There are at least two routes to obtaining a formula for μ . One way is to directly take the limit of (3.12) under the condition $\mathcal{O}(a) = r_i - r_{i-1} \ll r_i$ for large i . For this purpose, the right-hand side of (3.12) is expressed in terms of discrete slopes, M_i , with the main substitution

$$r_{i\pm 1} \sim r \pm \frac{a}{m(r, t)}, \quad r = r_i.$$

The algebraic manipulations of this procedure are detailed in [62] (see also [49]). The resulting formula reads [62]

$$\mu(r, t) = \frac{\Omega g_1}{r} + \Omega g_3 \frac{1}{r} \frac{\partial}{\partial r} (r m^2), \quad r > r_f(t). \quad (3.19)$$

Alternatively, by (3.8) and (3.11) one can write $\mu(r, t)$ as the first variation of the continuum limit of $E^{\text{st}}(t; a)$. In view of the coarea formula

$\sum_i a \oint_{L_i} \cdot ds \rightarrow \int |\nabla h| \cdot dA$ [64], this limit is the well-known surface free energy [40]

$$E^{\text{st}} \xrightarrow{a \rightarrow 0} E(h) = \iint \left(g_1 |\nabla h| + \frac{g_3}{3} |\nabla h|^3 \right) dA, \quad (3.20)$$

where $dA = dx dy$ and integration is carried out on the crystal reference (“basal”) plane. The free energy density $\gamma(|\nabla h|) \equiv g_1|\nabla h| + (g_3/3)|\nabla h|^3$ is manifestly singular at the zero slope surface orientation, $\nabla h = 0$, which defines the facet. Now, μ is obtained through [62, 64]

$$\langle \mu, \partial_t h \rangle = \Omega \dot{E} \Rightarrow \mu(r, t) \equiv \Omega \frac{\delta E}{\delta h}, \quad r > r_f(t), \quad (3.21)$$

where $\langle \mu, \varphi \rangle = \iint \mu(x, y) \varphi(x, y) dA$ denotes the usual L^2 -inner product, and $\delta E / \delta h$ is the variational derivative of $E(h)$. Equation (3.21) is consistent with continuum thermodynamics and is valid outside the facet. The use of (3.20) and integration by parts lead to (3.19).

Equations (3.18) and (3.19) yield a PDE for the height,

$$\partial_t h = -\nu \Omega g_1 \operatorname{div} \boldsymbol{\xi}, \quad r > r_f(t), \quad (3.22)$$

where the radial vector $\boldsymbol{\xi}$ is

$$\boldsymbol{\xi} = \xi e_r, \quad \xi(r, t) = 1 + gm(r, t)^2, \quad (3.23)$$

and e_r is the unit radial vector. The PDE for the positive slope, $m = -\partial_r h > 0$, outside the facet is

$$\partial_t m = -\nu \Omega g_1 \left\{ r^{-2} - g \partial_r \left[r^{-1} \partial_r (rm^2) \right] \right\}. \quad (3.24)$$

It is worthwhile noting that (3.22) has the form of a mass conservation statement, where $\boldsymbol{\xi}$ plays the role of a vector-valued flux associated with $\partial_t h$.

We emphasize that both M1 and M2 reduce to the same PDE (3.22) outside the facet; however, as we will see in the next section, the boundary conditions for (3.22) must be adjusted to M1 and M2 distinctively for the continuum solution to be in agreement with the step motion.

3.3 Existence of unique discrete solution

In this section, we prove that, in contrast to diffusion limited (DL) kinetics [26], steps do *not* collide in M1 and M2 even for zero step interactions. We give separate proofs for $g = 0$ and $g > 0$. For $g = 0$, our proof is uniform in the initial number, N , of steps whereas this uniformity is lost for $g > 0$. Thus, for $g = 0$ we can consider a semi-infinite surface structure.

3.3.1 Case with zero step interactions, $g = 0$

The absence of step collisions can be loosely explained by inspection of (3.15) for $g = 0$. Suppose two steps tend to coalesce at some time; then, the innermost step moves faster whereas the other step is slowed down (because of the governing backward scheme), and step collision is thus avoided. Note that the assumed backward scheme is deemed natural in our setting, given that the preferred direction of motion of each step (with a minus sign in (3.7)) is *towards* the origin.

The main result of this subsection is

Theorem 1. *Let $N \in \mathbb{N}$ be the initial number of steps and $I = \{0, 1, \dots, N\}$. Consider $\mathbf{r}(t) = (r_0(t), r_1(t), \dots, r_N(t))$ and $\mathbf{f}(\mathbf{r}) = (f_0(\mathbf{r}), f_1(\mathbf{r}), \dots, f_N(\mathbf{r}))$ where*

$$f_i(\mathbf{r}) = \begin{cases} -\mathcal{G}_i \frac{r_i - r_{i-1}}{r_i} & r_i \neq 0 \\ 0 & r_i = 0 \end{cases}, \quad (3.25)$$

and $r_{-1}(t) \equiv 0$ in the definition of f_0 ; the factor \mathcal{G}_i is defined in (3.7).

Then, there exists a unique global solution to the initial value problem (IVP)

$$\dot{\mathbf{r}} = \mathbf{f}(\mathbf{r}), \quad \mathbf{r}(0) = \mathbf{r}^{in}, \quad \mathbf{r}^{in} \in W = \{\mathbf{x} \in \mathbb{R}^N \mid 0 < x_0 < \dots < x_N\} \quad (3.26)$$

in the domain $\Omega = \{\mathbf{x} = (x_i)_{i \in I} \mid x_i \neq 0, i \in I\}$. Furthermore, this solution stays in W for

$t \in [0, t_0)$ and in $W_i = \{\mathbf{x} \in \mathbb{R}^N | 0 = x_0 = \dots = x_i, x_{i+1} < \dots < x_N\}$ for $t \in [t_i, t_{i+1})$, where t_i is the time when r_i reaches 0; here, $0 < t_0 < t_1 < \dots < t_N < \infty$. $r_i(t)$ is continuous for all t and smooth on (t_{j-1}, t_j) for $j = 0, \dots, N$ (here, take $t_{-1} = 0$).

Proof. It suffices to give a proof for M1, i.e., if $\mathcal{G}_i = 1$ for all i . Because in M2 the factor \mathcal{G}_i is bounded for all i , the proof for M2 is almost identical; hence, we omit it.

First, we prove the existence of a unique local solution to problem (3.26). Observe that each f_i is smooth on W with $\nabla f_i = (0, \dots, 0, \frac{1}{r_i}, -\frac{r_{i-1}}{r_i^2}, 0, \dots, 0)$. So, for every $\mathbf{r} \in W$, let $0 < \delta < \min_{i \in I} \{r_i\}$. Then, for any $\mathbf{y} \in B^N(\mathbf{r}, \delta)$ we have

$$|\nabla f_i(\mathbf{y})|^2 = \frac{1}{y_i^2} + \frac{y_{i-1}^2}{y_i^4} \leq \left(\frac{1}{r_i - \delta} \right)^2 + \frac{(r_{i-1} + \delta)^2}{(r_{i+1} - \delta)^4} < \infty \quad (3.27)$$

for each i . Hence, \mathbf{f} is locally Lipschitz; by the Picard-Lindelöf theorem [41], IVP (3.26) has a unique local solution in Ω . This local solution is smooth since \mathbf{f} is smooth.

Let $\mathbf{r}^{in} \in W$ and suppose that $[0, T)$ is a maximal interval on which the problem $\dot{\mathbf{r}} = \mathbf{f}(\mathbf{r}), \mathbf{r}(0) = \mathbf{r}^{in}$ has a solution in W . Since $r_0(t) = r_0^{in} - t$, we establish an upper bound for T :

$$T \leq r_0^{in} < \infty. \quad (3.28)$$

We will show that $\mathbf{r}(t)$ approaches ∂W as $t \uparrow T$. Suppose by contradiction that $\mathbf{r}(t)$ does not approach ∂W as $t \uparrow T$. Then, in particular, we have $\min_i \inf_{t \in [0, T)} r_i(t) > 0$ and \mathbf{f} is uniformly bounded on the image $\mathbf{r}([0, T))$. Thus, $\mathbf{r}(t)$ is Cauchy-continuous. Therefore, the (classical) solution can be extended to $[0, T + b)$ by a standard theorem in the theory of ODE [14] that states that an extension of the solution exists at T if $\lim_{t \uparrow T} \mathbf{r}(t)$ exists in W . This assertion contradicts the maximality of T . We thus conclude that $\mathbf{r}(t)$ approaches ∂W as $t \uparrow T$.

Now, partition ∂W into $V_1 = \{\mathbf{x} \in \mathbb{R}^N | \exists i \in I \setminus \{0\} \text{ such that } x_i = x_{i-1}\}$ and

$V_2 = \partial W \setminus V_1$. Suppose by contradiction that $\mathbf{r}(T) \in V_1$. Let $\{r_j\}_{j \in J}$ be a set consisting of all components of \mathbf{r} such that $r_j(T) = r_{j-1}(T)$. In particular, J is not empty. So let $j_0 \in J$ be the smallest index. Then, given any $\epsilon > 0$, there exists some interval $(T - c, T)$ on which $\dot{r}_{j_0} = -\frac{r_{j_0} - r_{j_0-1}}{r_{j_0}} > -\epsilon$. By taking $\epsilon = \sup_{[0, T)} |\dot{r}_{j_0-1}|$, we see that $\frac{d}{dt}(r_{j_0} - r_{j_0-1}) = \dot{r}_{j_0} - \dot{r}_{j_0-1} > -\epsilon + \epsilon = 0$ on $(T - c, T)$. Hence, $\lim_{t \uparrow T} [r_{j_0}(t) - r_{j_0-1}(t)] \neq 0$ and j_0 cannot be in J . By this contradiction, we conclude that (3.26) has a unique global solution whose trajectory meets the subset $\{r_0 = 0\} \setminus V_1$ of a hyperplane $\{r_0 = 0\}$ at some finite time T . Define $t_0 := T$; by the definition of f_0 , $r_0(t) \equiv 0$ for $t \in [t_0, \infty)$. Next, proceed as in the above argument with the dimension of the solution reduced by 1. Repeat this procedure until $\mathbf{r} = 0$. \square

Remark 2. In the above proof, t_n are the step collapse times. For $g = 0$ and conical initial data (i.e., $r_i(0)$ linear with i), we will obtain explicit solutions for the top two steps of ODEs (3.26), with indices $i = n, n + 1$ and $t \in (t_{n-1}, t_n)$. For this special case, the explicit solution indicates that steps do not collide, as verified through our numerics (section 3.5).

Remark 3. A consequence of Theorem 1 is that the discrete slope \mathcal{M}_i is positive and bounded for any i and N ; the step mobility ν_i is also positive.

Remark 4. The proof of Theorem 1 holds as $N \rightarrow \infty$ (for semi-infinite structures).

Corollary 1. *If the continuum limit of the solution to IVP (3.26) exists, this limit yields a monotone continuum-scale height for all time $t > 0$ provided the height profile is strictly monotone at $t = 0$.*

In fact, we will verify the last statement for the case of conical initial data through an exact closed-form solution of the evolution PDE for the slope (see section 3.4.5).

3.3.2 Case with repulsive step interactions, $g > 0$

For positive g , the proof for the existence of a unique solution to ODE system (3.15) and the non-crossing property of steps for such a solution is in the spirit of the proof for $g = 0$. However, for $g > 0$, $\dot{\mathbf{r}}(t)$ becomes unbounded as $r_j \rightarrow r_{j-1}$ for some j in the step interaction terms of μ_i . Hence, the proof that we provide below holds only when N is finite.

The core result of this subsection is

Theorem 2. *Let $N \in \mathbb{N}$ be the initial number of steps and $I = \{0, 1, \dots, N\}$. Consider $\mathbf{r}(t) = (r_0(t), r_1(t), \dots, r_N(t))$ and $\mathbf{f}(\mathbf{r}) = (f_0(\mathbf{r}), f_1(\mathbf{r}), \dots, f_N(\mathbf{r}))$ where*

$$f_i(\mathbf{r}) = -\mathcal{G}_i \frac{r_i - r_{i-1}}{r_i} \left\{ 1 + \frac{2g}{3} \left[\psi(r_i, r_{i+1}) - \psi(r_{i-1}, r_i) + \frac{\phi(r_i, r_{i+1}) + \phi(r_{i-1}, r_i)}{r_i^2} \right] \right\} \quad \text{if } r_i \neq 0, \quad (3.29a)$$

$$f_i(\mathbf{r}) = 0 \quad \text{if } r_i = 0. \quad (3.29b)$$

Here, ψ and ϕ are defined by (3.13) and (3.14), respectively; $r_{-1}(t) \equiv 0$ in the definition of f_0 while $r_{N+1}(t) \equiv 0$ in the definition of f_N ; and \mathcal{G}_i is defined in (3.7).

Then, there exists a unique global solution to the IVP

$$\dot{\mathbf{r}} = \mathbf{f}(\mathbf{r}), \quad \mathbf{r}(0) = \mathbf{r}^{in}, \quad \mathbf{r}^{in} \in W = \{\mathbf{x} \in \mathbb{R}^N \mid 0 < x_0 < \dots < x_N\} \quad (3.30)$$

in the domain $\Omega = \{\mathbf{x} = (x_i)_{i \in I} \mid x_i \neq 0, i \in I\}$. Furthermore, this solution stays in W for $t \in [0, t_0)$ and in $W_i = \{\mathbf{x} \in \mathbb{R}^N \mid 0 = x_0 = \dots = x_i, x_{i+1} < \dots < x_N\}$ for $t \in [t_i, t_{i+1})$, where t_i is the time when r_i reaches 0. Here, $0 < t_0 < t_1 < \dots < t_N < \infty$; and $r_i(t)$ is continuous for all t and is smooth on (t_{j-1}, t_j) for $j = 0, \dots, N$.

Proof. Again, we only provide a proof for M1, where $\mathcal{G}_i = 1$; the proof for M2 is very similar and thus omitted.

In the spirit of the proof for $g = 0$, we first prove the existence of a unique local solution to problem (3.30). Observe that each f_i is smooth on W . For each vector $\mathbf{r} \in W$, let $0 < \delta < \min_{i \in I} \{r_i, (r_i - r_{i-1})/4\}$. Then, by recourse to ODEs (3.15), for all $\mathbf{y} \in B^N(\mathbf{r}, \delta)$ we note the following bound in regard to partial derivatives of f_i :

$$\left| \frac{\partial}{\partial y_i} \left(\frac{y_i - y_{i-1}}{y_i} \psi(y_i, y_{i+1}) \right) \right|^2 = \left| \frac{2y_i y_{i+1}}{y_i(y_i + y_{i+1})} \frac{1}{(y_{i+1} - y_i)^3} - \left(1 - \frac{y_{i-1}}{y_i}\right) \right. \\ \left. \frac{2y_i y_{i+1}}{(y_i + y_{i+1})^2} \frac{1}{(y_{i+1} - y_i)^3} + 3 \left(1 - \frac{y_{i-1}}{y_i}\right) \frac{2y_i y_{i+1}}{y_i + y_{i+1}} \frac{1}{(y_{i+1} - y_i)^4} \right|^2 \leq K(\delta), \quad (3.31)$$

where $K(\delta) = \mathcal{O}(1/\delta^3)$ for small δ . In (3.31), we used an inverse triangle inequality, $|y_i - y_{i-1}| \geq |r_i - r_{i-1}| - |y_i - r_i| - |y_{i+1} - r_{i+1}| \geq 2\delta$ in order to obtain a bound for each term; for example, the first term in the right-hand side is bounded by

$\frac{(r_i + \delta)(r_{i+1} + \delta)}{(r_i - \delta)(r_i + r_{i+1} - 2\delta)} \frac{1}{4\delta^3}$. We omit the details on the rest of partial derivatives for f_i , since the procedure is similar to the one for (3.31). Thus, every $|\nabla f_i|$ is bounded from above.

Therefore, \mathbf{f} is locally Lipschitz; by the Picard-Lindelöf theorem [41], we assert the existence of a unique local solution to problem (3.30).

Now, as before, let $\mathbf{r}^{in} \in W$ and $[0, T)$ be a maximal interval on which the problem

$$\dot{\mathbf{r}} = \mathbf{f}(\mathbf{r}), \quad \mathbf{r}(0) = \mathbf{r}^{in} \quad (3.32)$$

has a (classical) solution in W . Notice that on W , $\dot{r}_0(t) < \dot{r}_0^{(0)}(t)$ where $r_0^{(0)}(t)$ denotes the first component of the solution for IVP (3.26) with (3.25). Thus,

$r_0(t) < r_0^{(0)}(t) = r_0^{in} - t$ and we obtain an upper bound for T :

$$T \leq r_0^{in} < \infty. \quad (3.33)$$

By neglecting the negative terms in (3.29) for each i , we obtain the inequality

$$\dot{r}_i(t) \leq \frac{4g}{3} \frac{1}{(r_i - r_{i-1})^2}. \quad (3.34)$$

We now show that $\mathbf{r}(t)$ approaches ∂W as $t \uparrow T$. Suppose by contradiction that this statement is false. Then, $r_i \not\rightarrow r_{i-1}$ and the right-hand side of (3.34) is clearly bounded above on $[0, T)$. Hence, $\mathbf{f}(\mathbf{r})$ is uniformly bounded on the image $\mathbf{r}([0, T))$ and, by recourse to the argument given in the proof for Theorem 1, we conclude that $\mathbf{r}(t)$ approaches ∂W as $t \uparrow T$.

As in the proof of Theorem 1, now partition ∂W into V_1 and $V_2 = \partial W \setminus V_1$. Next, we prove that $\mathbf{r}(t) \rightarrow V_2$ as $t \rightarrow T$. Let $\{r_j\}_{j \in J}$ be a set consisting components of \mathbf{r} such that $r_j(T) = r_{j-1}(T)$. Suppose by contradiction that \mathbf{r} reaches V_1 at time T ; this implies that the set J is nonempty. If, for some $j \in J$, \dot{r}_j grows unbounded in the positive direction near time T yet \dot{r}_{j-1} is bounded above, then $\dot{r}_j - \dot{r}_{j-1} > 0$ on some interval $(T - c, T)$, which contradicts the definitions of T and J . Thus, the desired result follows: \mathbf{r} does not reach V_1 by time T .

Because J is nonempty, there exists the smallest index $j_0 \in J$ and the largest index $j_* \in J$ such that the sequence $j_0, j_0 + 1, \dots, j_* - 1, j_*$ is contained in J . Since $j_0 - 1 \notin J$, we have that $r_{j_0-1} - r_{j_0-2} \not\rightarrow 0$ and $\psi(r_{j_0-2}, r_{j_0-1})$ is bounded. Thus, the only positive term in $f_{j_0-1}(\mathbf{r})$ is bounded near time T , so $\dot{r}_{j_0-1} = f_{j_0-1}(\mathbf{r})$ is bounded from above in some interval $(T - \tilde{c}, T)$. On the other hand, $j_* + 1 \notin J$ implies that

$\psi(r_{j_*}, r_{j_*+1}), \phi(r_{j_*}, r_{j_*+1})$ are both bounded. Also, since $j_* \in J$, we deduce that $\phi(r_{j_*-1}, r_{j_*})$ grows as $(r_{j_*} - r_{j_*-1})^{-2}$ whereas $\psi(r_{j_*-1}, r_{j_*})$ grows as $(r_{j_*} - r_{j_*-1})^{-3}$.

Thus, $\dot{r}_{j_*}(t)$ must grow unbounded in the positive direction as $t \rightarrow T$.

Hence, the properties that r_{j_0-1} is bounded and r_{j_*} is unbounded warrant that there exists some $j \in J$ for which \dot{r}_j grows unbounded above for times near T yet \dot{r}_{j-1} is bounded above. We conclude that IVP (3.30) has a unique global solution $\mathbf{r}(t)$ that ends when the trajectory meets the subset $\{r_0 = 0\} \setminus V_1$ of the hyperplane $\{r_0 = 0\}$ at some

finite time T . Define $t_0 := T$; by definition (3.29) of f_0 , $r_0(t) \equiv 0$ for $t \in [t_0, \infty)$. Now proceed as above with a new IVP in which the dimension of solution is reduced by 1. Repeat this procedure until $\mathbf{r} = 0$. □

Remark 5. The above proof relies on the fact that J is a finite set and there exists the largest index in J (i.e., J is bounded); in particular, it is necessary that N be finite. Thus, we may not use our proof for $g > 0$ in order to assert positivity of the discrete slope for a semi-infinite structure (as $N \rightarrow \infty$).

Remark 6. For $g > 0$, one can state a result analogous to Corollary 1.

3.4 Subgradient formalism and free-boundary conditions

In this section, we start with the subgradient formalism in order to extract the natural boundary conditions at the facet edge; these conditions form our starting point for the comparison of continuum solutions to step simulations. Our numerical simulations (section 3.5) indicate that the natural boundary conditions yield a continuum slope in agreement with predictions of M1 but *not* M2. In anticipation of this discrepancy, in section 3.4.3 we propose a set of modified boundary conditions by incorporating the discrete geometric factor on top of the facet into one of the conditions in terms of a jump of the flux (see section 3.5 for numerical studies of this replacement). In section 3.4.4, we prescribe linear initial data. In section 3.4.5, we analytically solve the free-boundary problems for $g = 0$ (non-interacting steps) to single out differences between the two continuum solutions, without and with a flux jump.

3.4.1 Subgradient formalism

A guiding principle in the analysis of PDE (3.22) with (3.23) is that the height profile evolves by the most rapid decrease of the free energy, $E(h)$. Qualitatively speaking, this principle is consistent with step motion law (3.7) in view of (3.12); clearly, the trajectory of $(r_0(t), r_1(t), \dots, r_N(t))$ is driven by the decrease of the total step free energy, $E^a(t)$. At the moment, we lack a more precise energy-based connection of the subgradient theory with steps.¹

By the extended gradient formalism, the evolution law for h is stated as [55]

$$\partial_t h(r, t) = -\nu\Omega g_1 \operatorname{div}\boldsymbol{\xi}(r, t) \quad \text{for all } r \geq 0, \quad (3.35)$$

where $\operatorname{div}\boldsymbol{\xi}$ is proportional to $\delta E/\delta h$ outside the facet, $|\boldsymbol{\xi}| \leq 1$ on the facet, and $\boldsymbol{\xi} = \xi e_r$. The flux $\boldsymbol{\xi}$ is uniquely determined from (3.35) under the assumption of sufficient regularity. Physically, (3.35) expresses global mass conservation for the height, h , if $\boldsymbol{\xi}$ is interpreted as a mass flux comprising atoms exchanged with the vapor. Some elements of the subgradient theory are reviewed in section 1.6.1.

3.4.2 Natural boundary conditions

Next, we write down explicit boundary conditions for (3.22) with (3.23). Note that four (three) conditions are needed, since the PDE for h is of second (first) order for $g > 0$ ($g = 0$), and $r_f(t)$ and $h_f(t)$ are parts of the solution. If $r < r_f(t)$ then $h = h_f(t)$. By continuity of the height, $h(\cdot, t)$, we write

$$h_f(t) = h(r, t) \quad \text{as } r \downarrow r_f(t). \quad (3.36)$$

¹To the best of our knowledge, so far such a connection has been established rigorously for a 1D finite step train connecting semi-infinite facets in ADL kinetics [4, 5].

This condition is natural on physical grounds but is also inferred from the functional space for solutions to (3.35) (see section 1.6.1). Equation (3.35) on the facet reads $\dot{h}_f = -\nu\Omega g_1 r^{-1} \partial_r(r\xi)$, by which $\nu\Omega g_1 \xi(r, t) = -(r/2)\dot{h}_f + C(t)/r$ if $r < r_f(t)$; set $C(t) \equiv 0$ so that $\xi(\cdot, t)$ be bounded. Thus, continuity of $\xi(\cdot, t)$ entails

$$-\frac{r_f(t)}{2} \dot{h}_f = \nu\Omega g_1 [1 + gm(r, t)^2] \quad \text{as } r \downarrow r_f(t) . \quad (3.37)$$

For large r , the solution must be compatible with the prescribed initial data:

$$h(r, t) \sim h(r, 0); \text{ or } m(r, t) \sim -\partial_r h(r, 0) \quad \text{as } r \rightarrow \infty , \quad (3.38)$$

which is a “far field” condition.

For $g > 0$, one more condition must be imposed. Recall that $|\xi| \leq 1$ on the facet, $\xi = 1 + gm^2 > 1$ outside the facet, and ξ is continuous. Thus, the slope is continuous:

$$\lim_{r \downarrow r_f(t)} m(r, t) = 0 . \quad (3.39)$$

Equations (3.36)–(3.39) form the set of natural boundary conditions for PDE (3.22) outside the facet. In view of (3.39), the differentiation of (3.36) with respect to t can be used to replace (3.36) and (3.37) by a single condition via elimination of \dot{h}_f .

3.4.3 Alternate condition: flux jump at facet edge

Next, we modify condition (3.37) by introducing an ad hoc jump of the flux $\xi(\cdot, t)$. Our goal is to describe the effect on the macroscopic limit of individual steps collapsing on top of the facet by retaining the variables (height, slope, flux) of the natural boundary conditions.

Physically, the main idea can be outlined as follows. In the continuum limit, t_n is treated as the continuous time, t [71]. A reasonable boundary condition that captures the events

of collapsing top layers must express via some effective averaging in time the mass exchange between top (annihilated) steps and vapor in the time intervals $[t_n, t_{n+1}]$. We propose an ad hoc possible remedy for the underlying averaging process: an, in principle time-dependent, jump of the flux $\xi(\cdot, t)$. In the case with self similarity of slopes, which we focus on, this jump is expressed by a time-independent factor due to a scaling property of t_n with large n . More generally, it is hoped that this approach can be applied to full time-dependent settings, without restriction to self similarity.

For the step dynamics of M2, in particular, we specify the jump in terms of values of $\mathcal{G}_i(t)$ for pairs of extremal steps at $t = t_n$. This factor encapsulates, in a simple geometric form, information about the facet microstructure. At the moment, this choice is essentially empirical (see Remarks 8 and 9): the only firm justification that we can provide is the observed agreement of the ensuing continuum slope with step simulations for M2 (section 3.5).

Our proposal is to keep evolution law (3.35) for $0 \leq r < r_f(t)$ and $r > r_f(t)$, along with height continuity and (for $g > 0$) slope continuity; but replace (3.37) by the generalized condition

$$-\frac{r_f(t)}{2}\dot{h}_f = \nu\Omega g_1 \tilde{\mathcal{G}}(t; g)[1 + gm(r, t)^2] \quad \text{as } r \downarrow r_f(t) , \quad (3.40)$$

where $\tilde{\mathcal{G}}(t; g)$ is allowed to differ from unity; we henceforth suppress the g -dependence of $\tilde{\mathcal{G}}$. The function $\tilde{\mathcal{G}}(t)$ should be compatible with the vanishing of individual, atomic layers on top of the facet. In particular, for M2 we propose the definition

$$\tilde{\mathcal{G}}(t) \equiv \mathcal{G}_i(t_n)|_{i=n+2} = \frac{r_{n+2}(t_n) + r_{n+1}(t_n)}{2r_{n+2}(t_n)} \quad (3.41)$$

for $t_n \leq t < t_{n+1}$, accounting for the two extremal steps; recall that $r_n(t_n) = 0$.

Remark 7. In section 3.5.2, we numerically test (3.40) and (3.41). First, for M1 we

show that, for large t , the replacement of $\tilde{\mathcal{G}}(t)$ by unity produces continuum slopes in excellent agreement with our step simulations. For M2, we demonstrate that, if n (and t) is large: (i) (3.41) yields $\tilde{\mathcal{G}}(t; g) \sim \mathfrak{c}(g)$ where \mathfrak{c} is a constant computed from data for t_n ; and (ii) the resulting continuum slopes follow closely step simulations. In the subgradient formalism, $\mathfrak{c} = 1$.

Remark 8. Notably, some other choices which are almost as simple as (3.41) fail to yield equally satisfying numerical results for $g > 0$. For example, suppose we set $\tilde{\mathcal{G}}(t) \equiv \mathcal{G}_{n+2+k}(t_n)$ for $k + 1 \in \mathbb{N}$ and $t_n \leq t < t_{n+1}$, viewing the jump as a function of k for every fixed n . We numerically observe that the value $k = 0$ is best for agreement of the continuum prediction with step simulations for M2; in fact, the factor $\tilde{\mathcal{G}}$ is found to be monotonically increasing with k in this scenario.

Remark 9. Especially for non-interacting steps, $g = 0$, we can claim that the continuum theory consistent with M2 has a flux jump yet does *not* require input from discrete simulations. Suppose we employ (3.41) in this case; then, we find that $\tilde{\mathcal{G}}(t)$ becomes approximately equal to 0.766 for large n ; see Appendix C for related computations. This value produces a continuum slope in agreement with discrete simulations (see section 3.5.1.2). On the other hand, by interpreting the facet height as shock, we can evaluate the flux jump from a Rankine-Hugoniot condition; then, we find $\tilde{\mathcal{G}}(t) = 3/4$ (section 4.1), which also yields a continuum slope in excellent agreement with step simulations (section 3.5.1.2). This observation indicates the empirical nature of (3.41). A detailed discussion on the shock picture is provided in chapter 4.

Remark 10. An emerging question is whether our generalized boundary condition (3.40) for the flux should require input from discrete simulation data, as suggested by (3.41) within a full (t_n -independent) continuum framework for interacting

steps. We find that numerically computed $\tilde{\mathcal{G}}(t)$ of interacting steps does not change much in value from $\tilde{\mathcal{G}}(t)$ of non-interacting steps. Specifically, we see that for $g = 0.1$, $\tilde{\mathcal{G}}(t) = 0.764$ and for $g = 1$, $\tilde{\mathcal{G}}(t) = 0.762$. These value again produce a continuum slope in agreement with discrete simulations (see section 3.5.2.2). This observation indicates that the value of $\tilde{\mathcal{G}}(t)$ is not sensitive to the value of $g \geq 0$ and perhaps independent of the value of g . In Part II of this thesis, we see that this conjecture is true at least in the continuum limit.

3.4.4 Initial data

In the remainder of this article, we consider an initial conical profile of unit slope.

Hence, we impose the initial height profile

$$h(r, 0) \equiv h_0(r) = \begin{cases} h_{f0} , & r < r_{f0} , \\ h_{f0} - (r - r_{f0}) , & r > r_{f0} , \end{cases} \quad (3.42)$$

where $r_{f0} = r_f(0)$ and $h_{f0} = h_f(0)$. This profile corresponds to the initial step train

$$r_i(0) = r_{f0} + ia \quad i = 0, 1, \dots, N , \quad (3.43)$$

where the top layer is located at height h_{f0} .

3.4.5 Exactly solved case: zero step interaction ($g = 0$)

In this subsection, we analytically solve the free-boundary problems of sections 3.4.1 and 3.4.3 in the absence of step-step interaction. In this case, the continuity of slope,

condition (3.39), is *not* applicable. First, we restrict attention to a continuous flux, for

$\tilde{\mathcal{G}}(t) = 1$; the resulting formula for $m(r, t)$ exhibits self-similar behavior. Second, we

extend our computation to $\tilde{\mathcal{G}}(t) \neq 1$. Detailed derivations are presented in Appendix D.

In the remainder of this section, we employ units with $\nu\Omega g_1 = 1 = a$.

For $g = 0$, PDE (3.22) reduces to

$$\partial_t h = -\frac{1}{r} \quad r > r_f(t) , \quad (3.44)$$

which leads to the solution

$$h(r, t) = h_0(r) - \frac{t}{r} \quad r > r_f(t) ; \quad h(r, t) = h_f(t) \quad r < r_f(t) . \quad (3.45)$$

Hence, the slope profile is

$$m(r, t) = 1 - \frac{t}{r^2} \quad r > r_f(t) ; \quad m(r, t) = 0 \quad r < r_f(t) . \quad (3.46)$$

It remains to compute the facet radius, $r_f(t)$, by applying initial data (3.42). The height continuity, $h_f(t) = h_{f0} + r_{f0} - r_f - t/r_f$, along with generalized condition (3.40) on $\xi(\cdot, t)$ yield an ODE for $r_f(t)$. We now distinguish two cases for the flux ξ .

3.4.5.1 Continuous flux ξ

In the special case without flux jump, $\tilde{\mathcal{G}}(t) \equiv 1$, $r_f(t)$ is computed in simple closed form for all $t \geq 0$ (see Appendix D); in particular,

$$r_f(t) \sim \sqrt{3t} \quad \text{as } t \rightarrow \infty . \quad (3.47)$$

Accordingly, we compute the facet height:

$$h_f(t) \sim h_{f0} + r_{f0} - \frac{4}{\sqrt{3}}\sqrt{t} \quad \text{as } t \rightarrow \infty . \quad (3.48)$$

The slope has the form $m(r, t) = \mathbf{m}(\eta)$ with $\eta = r/\sqrt{t}$, where $\eta \sim \text{const.}$ at the facet edge for large t . By (3.46) and (3.47), note that

$$m(r, t) \rightarrow m_f := \mathbf{m}(\sqrt{3}) = 2/3 \quad \text{as } r \downarrow r_f(t), \quad t \rightarrow \infty . \quad (3.49)$$

3.4.5.2 Discontinuous flux ξ

A similar procedure is applied for $\tilde{\mathcal{G}}(t) = \mathbf{c} \neq 1$; we find an exact expression for $t = T(r_f)$, yet r_f is no longer computable in simple closed form (see Appendix D). By this computation, we find

$$r_f(t) \sim \sqrt{(4\mathbf{c} - 1)t}, \quad (3.50)$$

$$h_f(t) \sim h_{f0} + r_{f0} - \frac{4\mathbf{c}}{\sqrt{4\mathbf{c} - 1}} \sqrt{t} \quad \text{as } t \rightarrow \infty, \quad (3.51)$$

where $\mathbf{c} > 1/2$. The height and slope profiles are computed from (3.45); evidently, $m(r, t) = \mathbf{m}(\eta)$ where $\eta \sim \text{const.}$ at the facet edge as $t \rightarrow \infty$. Note that

$$m(r, t) \rightarrow m_f = 1 - \frac{1}{4\mathbf{c} - 1} \quad \text{as } r \downarrow r_f(t), \quad t \rightarrow \infty; \quad (3.52)$$

in particular, $m_f = 1/2$ if $\mathbf{c} = 3/4$ (see Remark 9 and section 4.1).

3.5 Numerical simulations

In this section, we provide numerical simulations to compare the discrete dynamics for M1 and M2 (without and with a geometry-induced step mobility) to continuum theories (with and without natural boundary conditions). The cases with $g = 0$ and $g > 0$ are presented separately since for $g = 0$ we invoke *exact* continuum solutions; while for $g > 0$, in the context of M2, we make use of numerically computed discrete data (collapse times t_n) in our modified boundary condition for the flux ξ . Especially for $g > 0$, we solve numerically PDE (3.24) for the slope profile by *assuming* self-similarity. In part of our numerics, we use as a starting point an approximate solution for the continuum slope that we extract heuristically via boundary layer theory if $0 < g \ll 1$ [62]. We apply units with $\nu\Omega g_1 = 1 = a$.

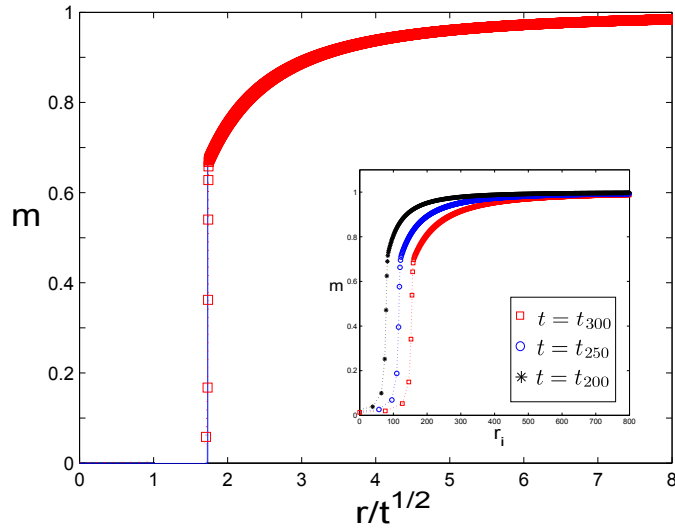


Figure 3.2: Continuum slope $m(r, t)$ (solid line) and discrete slopes $\mathcal{M}_i(t)$ (symbols) as functions of r/\sqrt{t} (where $r = r_i$) in the context of M1 for $g = 0$ and initial cone of unit slope with $N = 9 \times 10^3$ steps. The slope $m(r, t)$ is computed from (3.46) with natural boundary conditions; and $\mathcal{M}_i(t)$ are obtained at $t = t_n$ by numerically solving (3.15) with $\mathcal{G}_i(t) \equiv 1$. The vertical line indicates the facet position, $\eta_f = r_f(t)/\sqrt{t} \simeq \sqrt{3}$. Inset: Respective simulation data for \mathcal{M}_i versus r_i at collapse times $t = t_n$ ($n = 200, 250, 300$), indicating self-similar behavior of $\mathcal{M}_i(t)$ for $n \gg 1$; the simulation data collapse to the graph of main figure.

3.5.1 Numerics for $g=0$

Next, we solve (3.15) for $g = 0$ under initial data (3.43) and compute the corresponding slopes $\mathcal{M}_i = 1/(r_{i+1} - r_i)$. In Appendix C, we derive exact solutions for the two top-step positions for validation of our numerics. We consider separately M1, where $\mathcal{G}_i(t) \equiv 1$ for an idealized step mobility (Appendix C.1); and M2, for a geometry-induced step mobility (Appendix C.2).

3.5.1.1 Non-geometric step mobility (M1)

In regard to the continuum slope, we invoke the natural boundary conditions (with a continuous flux ξ). In Figure 3.2, we plot simulation data for \mathcal{M}_i versus r_i at different times $t = t_n$, and observe that the data collapse to a single graph if r_i is scaled by \sqrt{t} . Figure 3.2 also shows that the numerically computed $\mathcal{M}_i(t)$ follow closely the predicted $m(r, t)$; in particular, the step simulations verify the predicted slope discontinuity at the facet edge where $m \rightarrow 2/3$ as $r \downarrow r_f$ by (3.49).

The self-similar behavior of the slope profile implies a scaling law for the step collapse times, t_n , for $n \gg 1$. We now give a heuristic argument (in the context of M1) for this scaling by combining the facet height drop due to step collapses with the natural boundary conditions.² Requiring that the facet height decrease by multiples of the step size, $a = 1$, we impose the relation $h_f(t_{n-1}) - h_f(t_n) = 1$ [49, 71], which we replace by $-(t_n - t_{n-1})\dot{h}_f \sim 1$ assuming $(t_n - t_{n-1})|\ddot{h}_f| \ll |\dot{h}_f|$. By (3.37) and (3.39), we obtain that, for large t , $\delta t(t) \sim \frac{1}{2} r_f(t)$ where $\delta t(t) = t_n - t_{n-1}$ is the continuum version of the step-collapse time difference and $t_n = t \gg 1$. From (3.47) we obtain $\delta t(t) \sim \sqrt{3t}/2$, by which $t_n \sim (3/16)n^2$. This scaling law including the prefactor of $3/16$ is verified by our numerics; see Figure 3.3 where the collapse times t_n are plotted versus n . This observation provides additional evidence that, for $g = 0$, the natural boundary conditions are consistent with step flow in M1.

3.5.1.2 Geometry-induced step mobility (M2)

Now set $g = 0$ and $\mathcal{G}_i = (r_i + r_{i-1})/(2r_i)$ in (3.15) for the discrete dynamics. At the continuum scale, we invoke the slope from generalized boundary condition (3.40) with

²For M2, a similar argument can be sketched but we do not pursue it here.

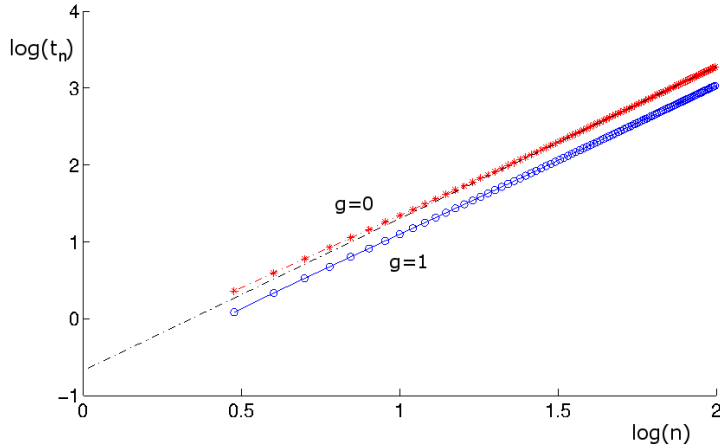


Figure 3.3: Log-log plot of step collapse times t_n versus n for $g = 0$ (asterisks) and $g = 1$ (circles) in the context of M1, numerically computed from (3.15) for $\mathcal{G}_i(t) \equiv 1$ and initial cone of unit slope with $N = 400$ steps. The dot-dashed (straight) line indicates the numerically computed large- n asymptotic behavior of t_n for $g = 0$. The scaling law $t_n \sim cn^\beta$ is verified for $n \gg 1$ with $\beta \approx 2$ for $g = 0, 1$. For $g = 0$, we graphically find $c = 0.1879 \approx 3/16$, in agreement with the analytical prediction via natural boundary conditions.

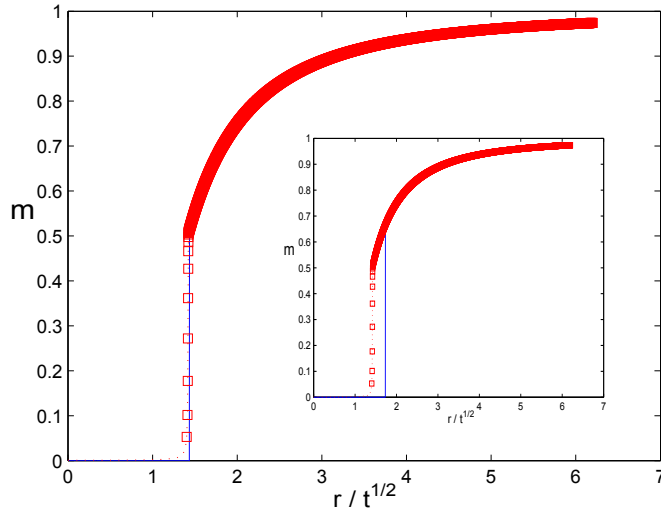


Figure 3.4: Continuum slope $m(r, t)$ (solid line) and discrete slopes $\mathcal{M}_i(t)$ (symbols) as functions of r/\sqrt{t} in the context of M2 for long times ($n \gg 1$), $g = 0$, and an initial cone of unit slope with $N = 15 \times 10^3$ steps. The discrete slopes $\mathcal{M}_i(t)$ are determined from numerically solving at $t = t_n$ ODEs (3.15) with $\mathcal{G}_i = (r_i + r_{i-1})/(2r_i)$. In the main figure, the slope $m(r, t)$ is computed from (3.46) under jump condition (3.40) with (3.41) using an exact result for step collapse times (Appendix C.2). Inset: The same step simulation data for \mathcal{M}_i in comparison to exact continuum slope (3.46) under natural boundary conditions.

$\tilde{\mathcal{G}}(t) = \mathfrak{c} \neq 1$. We consider two cases for \mathfrak{c} . First, we use the value of \mathfrak{c} ($\mathfrak{c} \simeq 0.766$) extracted from formula (3.41) combined with exact solutions for the two top-step ODEs, as shown in Appendix C.2. Alternatively, we use $\mathfrak{c} = 3/4$ which we compute analytically by interpreting the facet height as shock and applying a Rankine-Hugoniot condition corresponding to a particular hyperbolic conservation law; see section 4.1.

Figures 3.4 and 3.5 show the comparison of continuum solutions to step simulations in the above two cases; the produced continuum slopes are practically indistinguishable, as expected. In particular, our step simulations predict that the slope at the facet edge

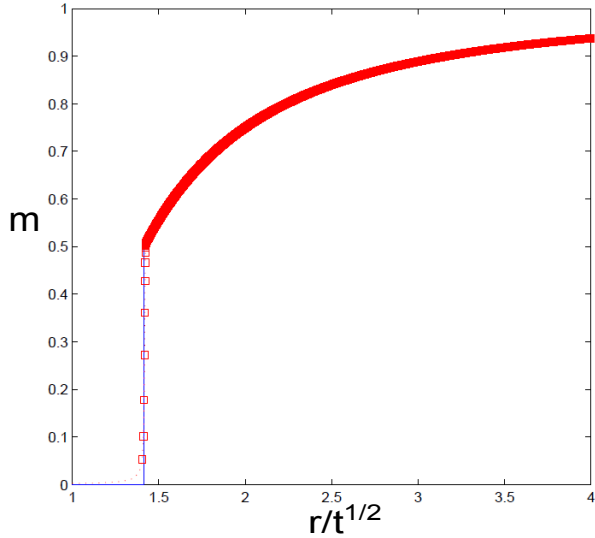


Figure 3.5: Continuum slope $m(r, t)$ (solid line) and discrete slopes $\mathcal{M}_i(t)$ (symbols) as functions of r/\sqrt{t} in the context of M2 for long times ($n \gg 1$), $g = 0$, and an initial cone of unit slope with $N = 15 \times 10^3$ steps. The continuum slope $m(r, t)$ is now computed from (3.46) under jump condition (3.40) with $\tilde{\mathcal{G}}(t) = 3/4$ on the basis of a Rankine-Hugoniot condition for a hyperbolic conservation law (section 4.1). The discrete slopes $\mathcal{M}_i(t)$ are determined from numerically solving at $t = t_n$ ODEs (3.15) with $\mathcal{G}_i = (r_i + r_{i-1})/(2r_i)$, as in Figure 3.4.

approaches approximately the value $1/2$ as $r \downarrow r_f$, consistent with (3.52) for $\mathfrak{c} = 3/4$.

Note that the continuum theory under natural boundary conditions *fails* to produce a slope consistent with step flow (see inset of Figure 3.4).

3.5.2 Numerics for $g > 0$

In this subsection, we study PDE (3.24) via numerics for $g > 0$ by assuming that the continuum slope is self similar at long time. We are motivated by: (i) the exact solution of section 3.4.5, where we found that $m(r, t) = \mathbf{m}(\eta)$ with $\eta = r/\sqrt{t}$ and $r_f(t) = \mathcal{O}(\sqrt{t})$

for $t \gg 1$; and (ii) our step simulations for $\mathcal{M}_i(t)$. Accordingly, we formally reduce the evolution PDE for $m(r, t)$ to an ODE for $\mathbf{m}(\eta)$; solve this ODE numerically for $g > 0$ under a boundary condition with a flux jump; and compare the continuum predictions to step simulations for $n \gg 1$.

First, we provide some numerical evidence that the discrete slopes have an apparently self-similar structure for large enough time: In Figure 3.6 (inset), we plot the discrete slopes, $\mathcal{M}_i(t)$, versus r_i for $g = 1$ at different collapse times, $t = t_n$, in the context of M1. We observe the data collapse once r_i is scaled with \sqrt{t} , which indicates self similarity of $\mathcal{M}_i(t)$. This observation is also made for other values of g and for M2 via step simulations.

Next, we introduce similarity variables by writing $m(r, t) \sim t^\omega \mathbf{m}(\eta)$ for $\eta = rt^{-\lambda}$ and large t ; the real exponents λ and ω are yet to be determined. By substitution into PDE (3.24) for $g > 0$, elimination of t from the coefficients yields $(\omega, \lambda) = (0, 1/2)$, which is consistent with the discrete simulations. In particular, the value $\lambda = 1/2$ implies the facet radius growth $r_f(t) = \mathcal{O}(\sqrt{t})$; in this regime, the facet height should decay with $-\dot{h}_f(t) = \mathcal{O}(t^{-1/2})$. By condition (3.40), the factor $\tilde{\mathcal{G}}(t)$ should become time independent; thus, we set $\tilde{\mathcal{G}}(t) = \mathbf{c} = \text{const.}$

We proceed to describe the free-boundary problem for $\mathbf{m}(\eta)$ in detail. PDE (3.24) away for the facet is converted to the ODE

$$-\frac{1}{2}\eta\mathbf{m}'(\eta) = -\eta^{-2} + g[\eta^{-1}(\eta\mathbf{m}^2)']' \quad \eta > \eta_f := r_f(t)/\sqrt{t}; \quad (3.53)$$

here, η_f is unknown and the prime denotes differentiation with respect to η . Now we turn attention to boundary conditions for (3.53) by resorting to (3.36) and (3.38)–(3.40)

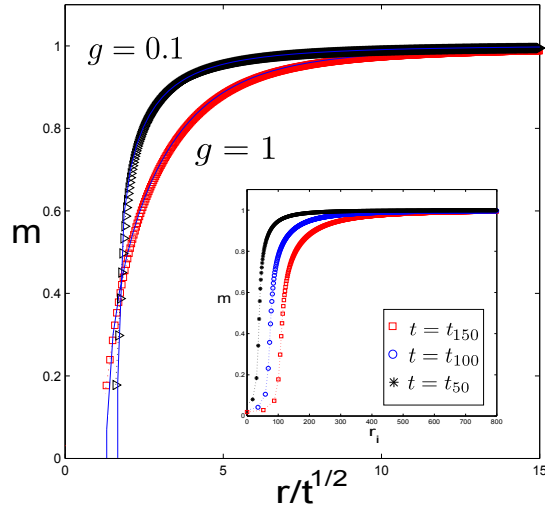


Figure 3.6: Continuum slope $m(r, t)$ (solid line) and discrete slopes $\mathcal{M}_i(t)$ (symbols) for M1 as functions of r/\sqrt{t} for initial cone of unit slope with $N = 9 \times 10^3$ steps; $g = 0.1$ (triangles) and $g = 1$ (squares). The slope $m(r, t)$ is computed from numerically solving (3.53)–(3.56) with $\mathbf{c} = 1$ ($\check{\mathbf{c}} = 1$) stemming from natural boundary conditions; and $\mathcal{M}_i(t)$ are determined from (3.15) with $\mathcal{G}_i(t) = 1$. Inset: Discrete slopes \mathcal{M}_i versus position $r = r_i$ at distinct collapse times $t = t_n$ ($n = 50, 100, 150$) for $g = 0.1$; the simulation data collapse to the graph of main figure.

with $\tilde{\mathcal{G}}(t) = \mathbf{c}$. By elimination of \dot{h}_f , we find that $\mathbf{m}(\eta)$ satisfies

$$g(\eta \mathbf{m}^2)' = \check{\mathbf{c}} \quad \eta \downarrow \eta_f, \quad (3.54)$$

$$\mathbf{m}(\eta) \rightarrow 1 \quad \eta \rightarrow \infty, \quad (3.55)$$

$$\mathbf{m}(\eta) = 0 \quad \eta \downarrow \eta_f; \quad \check{\mathbf{c}} := 2\mathbf{c} - 1. \quad (3.56)$$

Note that there are three boundary conditions for a second-order ODE because η_f forms part of the solution. We have not been able to analytically integrate out (3.53)–(3.56); hence, we proceed to find a solution numerically. We assume (but do not prove) that the self-similar slope is positive, $\mathbf{m}(\eta) > 0$ if $\eta > \eta_f$.

To solve the (free) boundary value problem of (3.53)–(3.56), we first apply a transformation of (η, \mathbf{m}) that (i) maps (η_f, ∞) to a finite interval, and (ii) renders linear the highest-order derivative in ODE (3.53) [26, 28]. Simply apply a simple translation, $s = \eta - \eta_f$. This maps (η_f, E) to $(0, \check{E} = E - \eta_f)$ where E ($E \gg \eta_f$) is a large number (which replaces infinity). In addition, we convert ODE (3.53) to a system of first-order ODEs for the variables $Y_1(s) = \mathbf{m}^2(\eta)$ and $Y_2(s) = (\mathbf{m}^2)'(\eta)$, $s \in (0, \check{E})$:

$$\begin{aligned} Y_1'(s) &= Y_2(s), \\ Y_2'(s) &= \frac{1}{g} \left[(s + \eta_f)^{-2} - \frac{1}{4}(s + \eta_f)Y_1^{-1/2}Y_2 \right] + (s + \eta_f)^{-2}Y_1 - (s + \eta_f)^{-1}Y_2, \end{aligned}$$

along with boundary conditions at $s = 0$ (facet edge) and $s = \check{E}$, obtained from (3.54)–(3.56); in particular, $Y_1(\check{E}) = 1$. It is of interest to seek the power series

expansion³

$$\mathbf{m}(\eta) = Y_1(s)^{1/2} \sim \sum_{l=1}^k c_l s^{l/2} =: S_k(s), \quad (3.57)$$

which satisfies condition (3.56). By (3.54), we compute $c_1^2 = (g\eta_f/\check{c})^{-1}$. The remaining coefficients, $c_l = c_l(\eta_f, g, \check{c})$ for $l = 2, \dots, k$, are found via dominant balance in (3.53). In Appendix F, we tabulate the coefficients c_l for $1 \leq l \leq 13$ ($k = 13$).

In our numerics for $\mathbf{m}(\eta)$, we apply an iterative algorithm (e.g., the `bvp4c` Matlab routine [44]) based on a suitable initial guess for $Y_1(s)$ that aims to satisfy $Y_1(\check{E}) = 1$. In this vein, we can make use of (3.57) as we evaluate $Y_1(s)$ at a fixed point s_0 near 0 in terms of η_f ; then we choose $k = 13$. A satisfactory approximate initial guess for $Y_1(s)$ for $0 < g < 1$, which apparently causes our numerical scheme to converge to a reasonable slope profile, is constructed through boundary layer theory [45, 62]; see section 3.5.3 for related formulas.

3.5.2.1 Numerics for M1

In Figure 3.6, we plot the discrete slopes \mathcal{M}_i for M1 and the continuum slope m under natural boundary conditions versus r/\sqrt{t} for the values $g = 0.1$ and 1. Our numerical comparison shows that step flow is consistent with the predictions of the extended-gradient formalism.

In particular, we verify that the facet size decreases with $g = g_3/g_1$ at fixed time t .

Physically, this effect can be attributed to the tendency of steps to cover a larger part of the surface if their repulsion (g_3) increases or their self-energy (line tension, g_1)

³Expansion (3.57) is only postulated. This expansion is consistent with the structure of the evolution PDE. A similar expansion is derived formally in [65] by direct reduction of discrete schemes to an integral equation for m and subsequent iteration for the setting of evaporation dynamics of a 1D step train connecting two semi-infinite facets. We do not pursue a rigorous justification for (3.57).

decreases; as a result, in principle any microscale event on top of the facet, i.e., collapse of a step, is expected to have a more pronounced effect on the macroscopic profile as g becomes smaller (see, e.g., [71] for a model of DL kinetics).

We now derive a scaling law for the step collapse times, t_n , by combining the natural boundary conditions with the discrete facet height drop (see section 3.5.1.1). By $\delta t(t) \sim \frac{1}{2} r_f(t)$, where $\delta t(t) = t_n - t_{n-1}$ and $t_n = t \gg 1$. we find $t_n - t_{n-1} \sim C(g)\sqrt{t}$; thus, $t_n \sim C^2 n^2/4$ for $n \gg 1$ (cf. Figure 3.3 for $g = 1$). This $C(g)$ should decrease with g since stronger step repulsions cause steps to shrink faster on top of the facet [71]; this monotone behavior is verified by our numerics.

3.5.2.2 Numerics for M2

In Figures 3.7 and 3.8, we compare step simulations for M2 to predictions of continuum theories for distinct values of g ($g = 0.1$ and 1). Evidently, the generated discrete slopes are in agreement with the macroscopic slope coming from a flux jump, condition (3.40) with (3.41), where the requisite t_n are computed from simulations. By contrast, the continuum slope stemming from natural boundary conditions (including flux continuity) deviates from step simulation data (see inset of Figure 3.7).

3.5.3 Approximation by boundary layer theory

In this subsection, we formally construct an approximate solution to the free-boundary problem described by PDE (3.24) with conditions (3.36) and (3.38)–(3.40) if $0 < g \ll 1$. The assumption of self similarity is not necessary in principle. The main observation is that by setting $g = 0$ in the evolution PDE (3.24) it is impossible to obey the continuity of slope, (3.39). So, we split the domain outside the facet into two regions: an “outer”

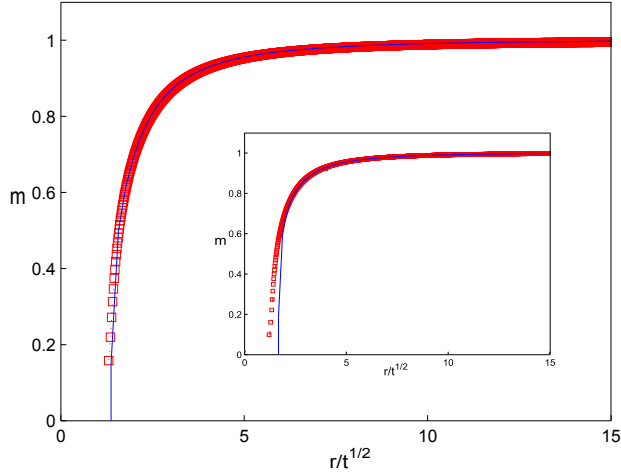


Figure 3.7: Continuum slope $m(r, t)$ (solid line) and discrete slopes \mathcal{M}_i (symbols) for M2 as functions of r/\sqrt{t} for long times, $g = 0.1$, and initial cone of unit slope with $N = 7 \times 10^3$ steps. The discrete slopes $\mathcal{M}_i(t)$ are determined from numerically solving ODEs (3.15) with $\mathcal{G}_i = (r_i + r_{i-1})/(2r_i)$. Main figure: The continuum-scale slope, $m(r, t)$, is computed from numerically solving (3.53)–(3.56) with \check{c} from (3.41), accounting for flux jump. Inset: With the same step simulation data, the continuum-scale slope $m(r, t)$ is computed from flux continuity, for $\check{c} = 1$.

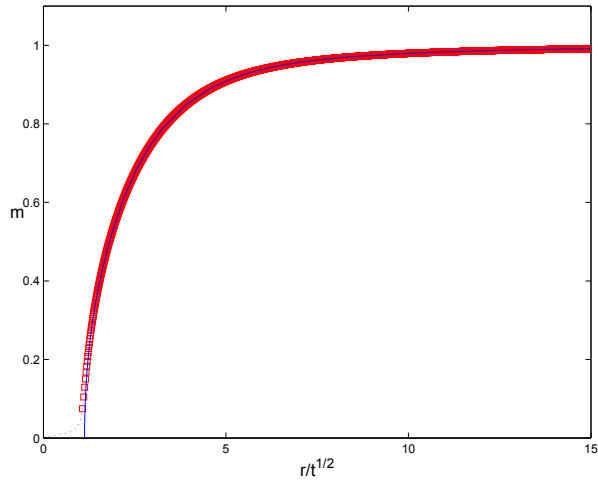


Figure 3.8: Continuum slope $m(r, t)$ (solid line) and discrete slopes \mathcal{M}_i (symbols) for M2 as functions of r/\sqrt{t} for long times, $g = 1$, and initial cone of unit slope with $N = 10^4$ steps. The discrete slopes $\mathcal{M}_i(t)$ are determined from ODEs (3.15) with $\mathcal{G}_i = (r_i + r_{i-1})/(2r_i)$. The continuum-scale slope, $m(r, t)$, is computed from numerically solving (3.53)–(3.56) with \tilde{c} from (3.41), accounting for a flux jump at the facet edge.

region, in which the step self-energy (line tension) dominates over the step interaction energy; and the “inner” region (boundary layer), in which the step interaction energy is significant [62]. The width of the boundary layer should scale with a positive power of g . Inside the boundary layer, the slope m varies smoothly from its zero value ($m = 0$) at the facet edge to the behavior predicted for $g = 0$ in the outer region; cf. (3.46). In general, the outer solution should be compatible with the continuity of height, flux jump, and far field condition. Hence, we only need to compute the inner solution by imposing zero slope at the facet edge. Here, we provide only the final formulas; details of our boundary layer analysis are given in Appendix E.

We start by defining the inner variable

$$\zeta = \frac{r - r_f(t)}{g^\alpha w(t)},$$

where $g^\alpha w(t)$ measures the (a priori unknown) width of the boundary layer, α is a positive exponent (to be determined), and $r_f(t) = r_f(t; g = 0)$ denotes the facet radius for $g = 0$; $\zeta = \mathcal{O}(1)$ inside the layer. After some algebra, we find (see Appendix E)

$$\alpha = 1, \quad w(t) = \dot{r}_f(t)^{-1} \left[1 - \frac{t}{r_f(t)^2} \right], \quad (3.58)$$

where formulas for $r_f(t)$ are provided in section 3.4.5 and Appendix D. A composite formula for the slope away from the facet reads

$$m(r, t) \sim 1 - \frac{t}{r^2} + a_0(t)[f_0(\zeta) - 1] \quad r > r_f(t), \quad a_0(t) = 1 - \frac{t}{r_f(t)^2}, \quad (3.59)$$

which encompasses both outer and inner solutions. The function $a_0(t)$ is the limiting value of the outer slope at the facet edge; while $f_0(\zeta)$ for the inner solution satisfies

$$f_0(\zeta) = 1 - e^{-\zeta/2} e^{-f_0(\zeta)} \quad \zeta > 0. \quad (3.60)$$

Note that $1 - f_0(\zeta)$ decays exponentially as $\zeta \rightarrow \infty$; thus, (3.59) properly reduces to the continuum solution for $g = 0$ outside the boundary layer. Formulas (3.58) and (3.59) can be simplified for $t \gg 1$ by use of asymptotic formula (3.47), under flux continuity; or, more generally, formula (3.50) that includes a flux jump.

Chapter 4: Shock-wave formalism

In this chapter, we discuss the interpretation of the facet height as a shock wave. We will use this perspective to show a convergence of discrete schemes with collapsing layers in special cases with no step interaction. Our starting point is to view the continuum step position, R , as a function of height and time. We point out that the flux (ξ) continuity, which is consistent with step flow in M1, can be read as a certain Rankine-Hugoniot type condition for general $g \geq 0$. Our discussion becomes more concrete for non-interacting steps ($g = 0$): We present a family of hyperbolic conservation laws and identify the shock accordingly.

In particular, we consider M1 and M2 as discretization of respective weak formulations for distinct conservation laws. In fact, we prove that the discrete solution of each model converges to the entropy solution of a conservation law; this limit must be the above shock wave. In this context, the boundary condition for the flux ξ is viewed as a Rankine-Hugoniot-type condition from the corresponding weak formulation; R is *zero* on the one side of the shock, as implied by the initial data for step radii. In this vein, we exactly evaluate the jump of ξ for M2.

This is not the first time when facets are connected to shocks; see [27, 28, 34–36, 99] where PDE solutions are recognized as shocks; however, we adapt the shock notion with a different perspective: to link this picture to step schemes. We are able to establish indirectly a connection of the subgradient theory to schemes for non-interacting steps.

At the moment, we are not able to use this analysis for nonzero step interactions.

4.1 Facet height as shock

Consider PDE (3.22) away from the facet. Using Lagrangian variables [27, 28], we view the step radius, R , as a function of height h and time t . Let $\chi = h_f(0) - h$, which measures the height relative to the initial surface structure in the (physical) domain with $h < h_f(t)$; and set $R = R(\chi, t)$ in this domain. By the level set motion law $\partial_t R = \partial_t h/m$ where $m = (\partial_\chi R)^{-1}$, PDE (3.22) reads

$$\partial_t(R^2) + 2\Omega\nu g_1 \partial_\chi \left[R \left(1 + g(\partial_\chi R)^{-2} \right) \right] = 0 \quad \chi > \chi_f(t) := h_f(0) - h_f(t), \quad (4.1)$$

assuming monotone increasing $R(\cdot, t)$. It should be stressed that this PDE holds and is consistent with step flow away from the facet; and in principle breaks down as χ approaches χ_f from above because of discrete effects.

Suppose a continuum theory that is consistent with steps is formulated everywhere.

Intuitively, in our models such a theory would have to be compatible with an extension of the domain of $R(\cdot, t)$ via $R(\chi, t) \equiv 0$ for $\chi < \chi_f$; $R(\cdot, t)$ would acquire a jump at $\chi = \chi_f$. We expect this property to emerge from the discrete schemes since the initial data and solutions of ODEs for M1 and M2, where step radii are set to zero after their collapse times, appear consistent with this prescription. A difficulty is that this jump in principle cannot be derived from existing fully continuum principles. We view this speculated discontinuity, and any related jump of functions of R , as a shock-like wave in (χ, t) ; the shock speed is $\dot{\chi}_f(t) = -\dot{h}_f(t)$, the speed of the facet, which decays with time. It is now tempting to claim that the boundary condition for the flux $\xi(r, t)$ at the facet edge corresponds to a Rankine-Hugoniot-type condition for the shock speed. Specifically, for M1 we write PDE (4.1) as the conservation statement $\partial_t \varrho + \partial_\chi \mathfrak{J} = 0$ with “density”

$\varrho = \pi R^2$ (step area) and associated “flux” $\mathfrak{J} = (2\pi R)\nu\Omega g_1[1 + g(\partial_\chi R)^{-2}]$ for $\chi > \chi_f$; and define $\varrho = \pi R^2 \equiv 0$ and $\mathfrak{J} \equiv 0$ for $\chi < \chi_f$. Then, ξ -continuity, equation (3.37), is equivalent to $\dot{\chi}_f = [\mathfrak{J}]/[\varrho]$ at $\chi = \chi_f(t)$, where $[\varrho]$ denotes the jump of ϱ ; the strength of the shock is proportional to the facet area, which grows with time.¹

These considerations become more concrete for $g = 0$, as shown in section 4.2. In this case, for smooth $R(\chi, t)$ we can generate a family of hyperbolic conservation laws via multiplication of (4.1) by $R^{\varsigma-1}$ with $\varsigma > 0$:

$$\partial_t(R^{\varsigma+1}) + \Omega\nu g_1 \left(\frac{\varsigma+1}{\varsigma} \right) \partial_\chi(R^\varsigma) = 0 \quad \chi > \chi_f(t). \quad (4.2)$$

The definition of the facet height as shock follows naturally: Extend $R(\chi, t)$ to all real χ by replacing (4.2) by its weak formulation, assuming initial data with $R(\chi, 0) \equiv 0$ for $\chi < \chi_f(0) = 0$. In other words, we artificially extend the evolution PDE to the vapor ($h > h_f$) by stating that no steps exist there. It turns out that, among all possible weak solutions of (4.2) compatible with the given initial data [57], step flow is consistent with a shock wave with $R \equiv 0$ for $\chi < \chi_f(t)$; in particular, the continuum limit of M1 (M2) corresponds to (4.2) with $\varsigma = 1$ ($\varsigma = 2$). The shock-wave strength is $r_f(t)^{\varsigma+1}$. The precise statement regarding convergence is deferred to section 4.2.

In particular, we write the Rankine-Hugoniot condition as

$$-\dot{h}_f(t) = \Omega\nu g_1 \left(\frac{\varsigma+1}{\varsigma} \right) r_f(t)^{-1}. \quad (4.3)$$

The corresponding weak solution, $u(\chi, t) = R(\chi, t)^{\varsigma+1}$, satisfies an entropy condition; thus, it is the unique entropy solution to (4.2) [57]. In particular, for $\varsigma = 1$, (4.3) is precisely the continuity of ξ in the subgradient formulation with $g = 0$. Furthermore, for

¹The jump of $R(\cdot, t)$, which is present in M1 and M2, should not be confused with the jump of ξ , which is introduced for M2 and vanishes in M1. The shock-like wave refers to the former jump.

$\varsigma = 2$, (4.3) produces a discontinuous flux ξ at the facet edge; a comparison to condition (3.40) entails $\tilde{\mathcal{G}}(t) = 3/4$. Our simulations (Figures 3.2 and 3.5) indicate that step flow is consistent with the above shock-wave interpretation.

4.2 Convergence of discrete schemes for $g = 0$

Next, we show that for $g = 0$ and linear initial data for the step radii, r_i , the solution to each of M1 and M2 is the entropy solution of (4.2) with $\varsigma = 1$ and 2, respectively. In the remainder of this section, we adopt the standard formalism of difference schemes for conservation laws [58, 59], assuming that the reader has some familiarity with numerical methods. We apply units with $\Omega\nu g_1 = 1$; the step height a is the mesh size (with $a \rightarrow 0$). In this section and Appendix 4.3, the surface structure is assumed to be finite (i.e., it is contained in a bounded region) so that a compactness theorem can be invoked. In particular, we restrict the domain of (4.3) to $\chi \leq h_f(0)$. We note in passing that solving (4.3) does not require any condition at this boundary since we use characteristics. Consider ODEs (3.15) with $g = 0$ (and replace i by j). We extend the discrete dynamics to all integer j , by extending the initial data for r_j to 0 for $j < 0$. The ODEs for both M1 and M2 are recast to the conservative form

$$\dot{U}_j = -\frac{1}{a}[F(U(t); j) - F(U(t); j - 1)] , \quad (4.4)$$

where $U_j(t) = U^a(\chi_j, t)$ is the discrete solution variable, which equals r_j^2 for M1 and r_j^3 for M2, with $\chi_j = ja$ (mesh in \mathbb{R}), $\chi_N = Na = h_f(0)$; and $U = U^a$ denotes the a -dependent, infinite-dimensional vector with components U_j . (The fact that the finite surface structure ends at $\chi = h_f(0)$ does not alter the solution of (7.4) because the ODE

for U_j depends only on U_i for $i \leq j$.) The numerical flux F is defined by

$$F(U(t); j) = \begin{cases} cU_j(t)^{\mathfrak{b}} & U_j > 0, \\ 0 & U_j \leq 0, \end{cases} \quad (4.5)$$

where $0 < \mathfrak{b} \leq 1$ and c is a positive constant; $(\mathfrak{b}, c) = (1/2, 2)$ for M1 and

$(\mathfrak{b}, c) = (2/3, 3/2)$ for M2. In the following analysis, set $c = 1$ without loss of generality.

F is Hölder-continuous with exponent \mathfrak{b} . It is also useful to define $\chi_{j \pm 1/2} = (j \pm 1/2)a$.

One of our goals is to show that the solution to (4.4) with (4.5) and $\mathfrak{b} = \varsigma/(\varsigma + 1)$

converges to a weak solution of conservation law (4.2). Specifically, we aim to prove that,

as $a \rightarrow 0$, $U^a(t)$ converge (weakly) to $u(\chi, t) = R(\chi, t)^{\varsigma+1}$ that is the entropy solution to

(4.2). Equation (4.4) with (4.5) is amenable to known methods for the convergence of

conservative difference schemes [59]. The numerical flux, F , is “consistent” with the

respective conservation law if we extend the definition of “consistency” in [59] to include

Hölder-continuous functions with exponents in $(0, 1]$.

We can show that for M1 and M2 there exists a convergent sequence in $\{U^a\}$ as $a \rightarrow 0$

(see Lemma 1 in Appendix 4.3). Based on this property, our core result is

Proposition 1. *Let $U(t) = U^a(t)$ be a solution of numerical scheme (4.4) with flux*

(4.5) and initial data that is compactly supported and monotone increasing within its

support. Then, $U^a(t)$ converges to the unique entropy solution $u(\chi, t)$ of the conservation

law $\partial_t u + \partial_\chi f(u) = 0$ with flux

$$f(u) = \begin{cases} u^{\mathfrak{b}}(t) & u > 0, \\ 0 & u \leq 0, \end{cases} \quad (4.6)$$

and initial data $u(\chi, 0)$ compatible with the discrete initial data.

The proof of Proposition 1 is technical but uses standard techniques [59]; it is therefore deferred to the next section 4.3.

In the statement of Proposition 1, the term “compatible” is used to mean that the initial discrete data stems from the cell average of the continuum-scale data [59]. The linear initial data for $r_j(t)$ and $h(r, t)$ of section 3.4.4 satisfy this property: By setting $u(\chi, t) = R(\chi, t)^{\zeta+1}$ (by the notation of section 4.1) and $\beta = \zeta + 1$, we have

$$\int_{\chi_{j-1/2}}^{\chi_{j+1/2}} u(\chi, 0) \, d\chi = \int_{\chi_{j-1/2}}^{\chi_{j+1/2}} \chi^\beta \, d\chi = \frac{\chi^{\beta+1}}{\beta+1} \Big|_{\chi_{j-1/2}}^{\chi_{j+1/2}} = a[\chi_j^\beta + \mathcal{O}(a)].$$

Note that the proof of convergence followed here does not seem applicable to the case with nonzero step interactions ($g > 0$). Difficulties include the definition of numerical flux, apparent unboundedness of the step chemical potential, and the effect of finite N . The case with nonzero g is the subject of work in progress.

4.3 Proof of convergence of step schemes for $g = 0$

In this section, we provide a proof of Proposition 1 by invoking the formalism of the Lax-Wendroff theorem [58]. For ease of notation, we suppress dependencies that are not explicitly used, i.e., let $U^a(t) = (U_j(t))_{j \in \{i \in \mathbb{Z} | i \leq N\}}$ and $F_j(t) = F(U^a(t); j)$ (where \mathbb{Z} : the set of integers). Below, $\|u - U^a\|_{\mathcal{X}}$ means the error, by the metric of space \mathcal{X} , in the approximation of $u(\chi, t)$ by the piecewise constant function with values $U_j(t)$ for $\chi \in (\chi_{j-1/2}, \chi_{j+1/2})$; also, φ_z means $\partial_z \varphi$ for $z = \chi, t$. We use the notions of total variation (TV) and TV-stability, defined in [59].

Before we proceed to the main proof of Proposition 1, it is advisable to address the sense by which solutions of our discrete schemes may converge.

Lemma 1. *For a compactly supported initial condition (i.e., a finite height profile) that*

is monotone increasing within its support, the discrete dynamics for M1 and M2 are TV diminishing with time. In particular, the U^a is TV-stable.

Proof. From section 3.3, if the initial data is monotone increasing in j , the dynamical system preserves the step ordering; in fact, steps do not collide. Therefore, for a class of dynamics with appropriate initial conditions including linear $r_j(0)$, $\dot{U}_j(t) \leq 0$ and $U_j(t)$ is always non-increasing with respect to time for all j . This fact together with the monotonicity of $\{U_j\}$ implies $TV(U(t)) \leq TV(U(0)) < \infty$ (by telescoping). \square

As a consequence, the family $\{U^a(t)\}$ is L^1 -compact for any $a \rightarrow 0$, $t \in [0, T]$ and fixed T [59]. Thus, there exists a L^1 -convergent sequence in $\{U^a\}$, which we denote by (U^a) with a slight abuse of notation, for each of M1 and M2 ($\mathfrak{b} = 1/2, 2/3$). Without proof, we claim that this property is true for $0 < \mathfrak{b} \leq 1$ in (4.5), and use it in the proof of Proposition 1. We improve the above convergence result by showing that all convergent sequences approach the same entropy solution of a specific (\mathfrak{b} -dependent) conservation law.

Proof of Proposition 1. First, we show that every convergent sequence in $\{U^a(t)\}$ L^1 -converges to a weak solution of conservation law (4.2). Our proof is similar to the ones for the Lax-Wendroff theorem [58, 59], except for the fact that, for M1 and M2, we proved above (not simply assume) existence of convergent sequences in $\{U^a\}$. Fix $T \in [0, \infty)$ and consider a sequence in $\{U^a\}$ that converges to some $u \in L^1((-\infty, h_f(0)] \times [0, T])$. With a slight abuse of notation, we denote elements of this sequence by U^a , with components $U_j^a = U_j$. Let $\varphi \in C_0^\infty((-\infty, h_f(0)] \times [0, T])$ be a test

function. We assert that

$$\begin{aligned}
a \int_0^T \sum_j \varphi_t(\chi_j, t) U_j dt &- a \sum_j \varphi(\chi_j, 0) U_j(0) = -a \int_0^T \sum_j \varphi(\chi_j, t) \dot{U}_j(t) dt \\
&= a \int_0^T \sum_j \frac{1}{a} \varphi(\chi_j, t) [F_j(t) - F_{j-1}(t)] dt \\
&= -a \int_0^T \sum_j \frac{\varphi(\chi_{j+1}, t) - \varphi(\chi_j, t)}{a} F_j(t) dt, \tag{4.7}
\end{aligned}$$

via summation by parts; boundary terms vanish since φ is compactly supported. The leftmost-hand side (top line) of (4.7) converges to

$$\int_0^T \int_{-\infty}^{\infty} \varphi_t(\chi, t) u(\chi, t) d\chi dt - \int_{-\infty}^{\infty} \varphi(\chi, 0) u(\chi, 0) d\chi,$$

in view of boundedness of φ (and φ_t). Below, we show that the right-hand side (bottom line) of (4.7) converges to

$$-\int_0^T \int_{-\infty}^{\infty} \varphi_\chi(\chi, t) f(u(\chi, t)) d\chi dt:$$

$$\begin{aligned}
&\int_0^T \left[\int_{-\infty}^{\infty} \varphi_\chi(\chi, t) f(u(\chi, t)) d\chi - a \sum_j \frac{\varphi(\chi_{j+1}) - \varphi(\chi_j)}{a} F_j(t) \right] dt \\
&= \sum_j \int_0^T \int_{\chi_j}^{\chi_{j+1}} \left[\varphi_\chi(\chi, t) f(u(\chi, t)) - \frac{\varphi(\chi_{j+1}) - \varphi(\chi_j)}{a} F_j(t) \right] d\chi dt; \tag{4.8}
\end{aligned}$$

the terms on the right-hand side are re-arranged to yield

$$\begin{aligned}
&\sum_j \int_0^T \int_{\chi_j}^{\chi_{j+1}} \varphi_\chi [f(u(\chi, t)) - F_j(t)] d\chi dt \\
&+ \sum_j \int_0^T \int_{\chi_j}^{\chi_{j+1}} \left[\varphi_\chi(\chi, t) - \frac{\varphi(\chi_{j+1}) - \varphi(\chi_j)}{a} \right] F_j(t) d\chi dt, \tag{4.9}
\end{aligned}$$

recalling that f coincides with F . Since F_j is bounded in $\text{supp}(\varphi)$, the second term in (4.9) converges to 0. The first term is bounded by

$$\begin{aligned}
&\|\partial_\chi \phi\|_{L^\infty} \sum_j \int_0^T \int_{\chi_j}^{\chi_{j+1}} |f(u(\chi, t)) - F_j(t)| d\chi dt \\
&\leq C \int_0^T \|u - U^a\|_{L^{\mathfrak{b}}_\chi} dt \leq \tilde{C} \|u - U^a\|_{L^1(\mathbb{R} \times [0, T])}, \tag{4.10}
\end{aligned}$$

where \tilde{C} is a constant depending on the Hölder exponent, \mathfrak{b} , of F ; also, the embedding $L^{\mathfrak{b}} \subset L^1$ on a compact set was used. Because $\|u - U^a\|_{L^1} \rightarrow 0$, we conclude that u is a weak solution of (4.2) with $\mathfrak{b} = \varsigma/(\varsigma + 1)$.

Next, we show that $\{U^a\}$ satisfies a (semi-discrete) entropy condition [59]. Let $\eta(\cdot) \in C^\infty((-\infty, h_f(0)])$ be any convex function² and $\psi(\cdot)$ be its entropy flux function, i.e., $\psi'(u) = \eta'(u)f'(u)$ [59], where the prime denotes differentiation in u and $f' \in L^1((-\infty, h_f(0)))$ is interpreted as a weak derivative. Accordingly, we have

$$\begin{aligned} -\frac{1}{a} [\psi(U_j) - \psi(U_{j-1})] &= -\frac{1}{a} \int_{U_{j-1}}^{U_j} \psi'(u) \, du = -\frac{1}{a} \int_{U_{j-1}}^{U_j} \eta'(u) f'(u) \, du \\ &\geq -\frac{\eta'(U_j)}{a} \int_{U_{j-1}}^{U_j} f'(u) \, du = \eta'(U_j) \dot{U}_j(t) = \partial_t \eta(U_j) . \end{aligned} \quad (4.11)$$

The application of a procedure similar to the one applied to show the weak convergence of the solution leads to the entropy inequality $\partial_t \eta(u) + \partial_x \psi(u) \leq 0$ in the weak sense [59]. Because all convergent sequences in the family $\{U^a\}$ approach the same limit, we conclude that $\{U^a\}$ weakly converges to the entropy solution. \square

It is worthwhile noting that the *finite* support of the initial data does not affect our proof, because each discrete scheme is backward in j for $g = 0$. This property ceases to hold for $g > 0$.

²This function $\eta(u)$ should not be confused with the similarity variable $\eta = r/\sqrt{t}$ of section 3.5.

PART II: Analysis

Chapter 5: Introduction (Part II)

We shall discuss two singular degenerate parabolic PDEs corresponding to different physical problems (see, Part I chapter 3 for their physical origin). In radial coordinates, we write the main equations for a function $h(r, t)$ for $r \geq 0, t > 0$:

$$h_t - \frac{1}{r} \partial_r \left[r \left(\frac{h_r}{|h_r|} + g|h_r|h_r \right) \right] = 0, \quad (5.1)$$

$$h_t - \frac{1}{2r^2} \partial_r \left(r^2 \frac{h_r}{|h_r|} \right) - \frac{g}{r} \partial_r (r|h_r|h_r) = 0, \quad (5.2)$$

where the parameter $g \geq 0$ controls the strength of dissipation in the equations and h_r is the partial derivative with respect to the radial component. As in Part I, we will refer to the models corresponding to (5.1) and (5.2) as M1 and M2, respectively. Physically speaking, $h(r, t)$ is a height function of a radially symmetric crystal structure on a reference plane (see, Ch.3 for details). Both of these PDEs are characterized by the strong diffusivity effect on facets (where the solution has zero slope).

In the extreme case of $g = 0$, we will see that the lack of dissipation allows for a special and simpler treatment of the problem: In such case, both of these PDEs (5.1) and (5.2) can be formulated as gradient flow equations with respect to the radial coordinates in certain dimensions. In particular, they can be considered as a total variation (TV) flow in respective dimensions. Furthermore, equation (5.1) can be considered as a generalization of a TV flow even in the presence of dissipation ($g > 0$). The

well-posedness of the TV flow is widely known and it can be shown via an application of the theory of monotone operators [2]. However, this convenient setting is not available for equation (5.2) with $g > 0$ due to its lack of a divergence form. Hence the main objective of Part II of this thesis is to develop a theory that provides the well-posedness for the solution of (5.2) with $g > 0$. Our study of the model M2 with $g > 0$ will be guided by the results for M2 with $g = 0$ as well as M1 with $g > 0$.

It is important to note that (5.1) and (5.2) are equivalent when h is smooth and $h_r \neq 0$. The difference between the two equations becomes apparent in the behavior of the surface near the facets (flat regions corresponding to intervals in which $h_r = 0$) on which $h_r/|h_r|$ is not well-defined and both equations (5.1) and (5.2) develop a singularity. Before we continue with our analysis, we recall from Part I the origin of equations (5.1) and (5.2). Our starting point is the discrete equations:

$$\frac{dr_i}{dt} = \dot{r}_i = -\nu_i(\mu_i - \mu^0), \quad i = 0, 1, \dots, N, \quad (5.3)$$

where the discrete mobility ν_i depends on the choice of models M1 and M2:

$$\nu_i = \nu \mathcal{G}_i \frac{r_i - r_{i-1}}{a}; \quad \mathcal{G}_i = \mathcal{G}_i(t) = \begin{cases} 1 & \text{for M1} \\ \frac{r_i + r_{i-1}}{2r_i} & \text{for M2} \end{cases}, \quad (5.4)$$

where a is the step size of discretization and we will set $\nu = 1$ for simplicity. \mathcal{G}_i is what we call a geometric factor in the mobility and the derivation of this factor is provided in Appendix B. Note that (5.3) for M1 and M2 reduce to the same equation in the continuum limit away from the facet where $r_{i+1} - r_i \ll r_i, r_{i+1}$. This condition breaks down near the facet and the description of continuum limits of M1 and M2 become ambiguous.

In Part I, we predicted distinct near-facet behaviors for the continuum limits of discrete models M1 and M2. The choice of (5.1) and (5.2) is phenomenological yet they are motivated by the study of step noninteracting case via the shock formulation (see, Ch.4). Our choice is the result of the expectation that the discrete mobility does not influence the continuum limit of the dissipation term near the facet at which the dissipation vanishes.

Our ultimate goal is to understand the connection between the ODEs (5.3) and PDEs (5.1) and (5.2); however our current presentation is incomplete for the reason that we do not directly compare the discrete structure with the continuum limit (aside from the noninteracting case in chapter 4). Nevertheless, we will conclude Part II of this thesis with what we consider to be a “reasonable” continuum theory that is conjectured to be compatible with the underlying discrete structure. This is already an improvement over the previously available method of applying subgradient formulation, which was shown to be unsuitable in the study of M2 (see, chapter 3 and [49, 50, 71]). Furthermore, it is our hope that the following discussion provides an intuition for the determination factor of the continuum limit depending on the discrete schemes.

Now, we go back to the discussion on (5.2) with $g \neq 0$. Recall from the earlier discussion in this section that this case cannot be written in a divergence form. Instead, by rewriting (5.2) as

$$\partial_t h = \frac{1}{r^2} \partial_r \left[r^2 \left(\frac{1}{2} \frac{h_r}{|h_r|} + g |h_r| h_r \right) \right] - \frac{g}{r} |h_r| h_r, \quad (5.5)$$

it becomes evident that the right-hand side of equation (5) has two terms of very different nature: one is in a gradient form whereas the other one is of Hamilton-Jacobi

type. Thus, the analysis of equation (5) calls for a theory capable of handling the non-local nature of the evolution of facet as well as a Hamilton-Jacobi term with a spatial dependence, which breaks certain symmetries. To this end, we employ the theory of proper viscosity solution, which was first applied to problems of this type by Y. Giga, M.-H. Giga, and N. Požér [31]. This new approach combines the traditional theory of viscosity solution and gradient flow.

Roughly speaking, the main idea of this theory is to capture the speed of facet through the energy by introducing “test facets” and test functions that represent those test facets. Note that the classic descriptions of viscosity solutions are local; in contrast, the solution in the present context is anticipated to have a nonlocal behavior by cause of the strong singularity at the facet.

Our theory differs from [31] in many technical aspects: Most significantly, we adopt a non-periodic setting to be consistent with our physical motivation (see, chapter 3). Our diffusion term also contains a spatial dependence, which poses some additional difficulty in analysis. The effect of these modifications is not trivial and requires a careful examination. The addition of a diffusion term has some regularizing effect; nonetheless, it does not prevent the facet formations.

Equations (5.1)-(5.2) are supplemented by the following initial and boundary conditions.

$$\left\{ \begin{array}{l} h|_{t=0} = h_0(r) = -\gamma r, \quad r \geq 0 \\ h_r(0, t) = 0 \quad t \in (0, \infty) \\ \lim_{r \rightarrow \infty} h(r, t) = \lim_{r \rightarrow \infty} h_0, \quad t \geq 0. \end{array} \right. \quad (5.6)$$

Since our main interest is the near-facet behavior of $h(r, t)$, the choice of boundary conditions at a large $r > 0$ is not crucial for our purposes and they are chosen to fit our

mathematical convenience.

The rest of the thesis is organized as follows: In section 5.1, we describe the solutions of (5.1) with $g \geq 0$ and (5.2) with $g = 0$. In section 5.2, the main results of Part II are stated. In chapter 6, some preliminary definitions are introduced leading up to a definition of viscosity solutions for equation (5.2). In chapter 7, we prove that sub-/super-solutions satisfy a comparison principle, which immediately yields uniqueness of viscosity solutions. In chapter 8, we prove the existence of viscosity solutions for a category of initial conditions.

In the rest of the introduction we will briefly review the theory of TV flow and motivate our main results.

5.1 The gradient flow approach

In this brief section, we handle the cases for which the theory of the TV flow is directly applicable. In order to extend the analysis beyond facets, we employ the subgradient theory.

5.1.1 Case of M1, $g \geq 0$

First, we observe that equation (5.1) is the radially symmetric version of the following equation in \mathbf{R}^2 :

$$h_t - \operatorname{div} \left(\frac{\nabla h}{|\nabla h|} + g|\nabla h|\nabla h \right) = 0. \quad (5.7)$$

Consider the following energies defined on $L^2(\mathbf{R}^2)$:

$$E_0^1(\phi) = \begin{cases} \int_{\Omega} |\nabla \phi| & \text{if } \phi \in BV(\Omega) \cap L^2(\Omega) \\ +\infty & \text{otherwise} \end{cases} \quad (5.8)$$

and

$$E_g^1(\phi) = \begin{cases} \int_{\Omega} |\nabla \phi| + \frac{g}{3} |\nabla \phi|^3 & \text{if } \phi \in BV(\Omega) \cap L^2(\Omega), \nabla \phi \in L^3(\Omega, \mathbf{R}^2) \\ +\infty & \text{otherwise} \end{cases} . \quad (5.9)$$

There is an extensive theory available to analyze the gradient flow with respect to equation since (5.8) is exactly the energy for the TV flow [2, 3, 24, 25, 33]. Similarly, the following well-posedness theorem is available for the solution of the gradient flow with respect to the energy (5.9)

Theorem 3. *Let Ω be a bounded piecewise smooth open subset of \mathbf{R}^2 . Define*

$E_g^1 : L^2(\Omega) \rightarrow (-\infty, \infty]$ as (5.9). Then E_g^1 is convex, proper, and lower semi-continuous (l.s.c.) For each $u_0 \in L^2(\Omega)$ there exists a unique function $u \in C([0, \infty), L^2(\Omega))$ with $u' \in L^\infty([0, \infty); L^2(\Omega))$ such that $u(0) = u_0$, $u(t) \in W^{1,3}(\Omega)$ for each $t > 0$ and u is a solution of (5.7) in the following sense:

$$u'(t) + \partial E_g^1(u(t)) \ni 0, \quad \text{for a.e. } t \geq 0. \quad (5.10)$$

Furthermore, we can obtain further regularity for u . First recall that for an energy E , $\mathcal{D}(E)$ denote the domain of E and means $\mathcal{D}(E) = \{f \in L^2(\Omega) | E(f) < \infty\}$. Then the duality theorem [1, Theorem 2.15] with the energy (5.9) yields:

Proposition 2. *Recall that $\operatorname{div}(\cdot) = \frac{1}{r} \partial_r(r \cdot)$ for radially symmetric functions in \mathbf{R}^2 .*

Suppose that $u \in \mathcal{D}(E_g^1) \subset BV(\Omega) \cap W^{1,3}(\Omega)$ is radially symmetric. Then $v \in \partial E_g^1(u)$ if

and only if

$$v = \operatorname{div} (z + g|\nabla u|\nabla u) \in L^2(\Omega) \quad (5.11)$$

for some $z \in L^\infty(\Omega, \mathbf{R}^n)$ and $\operatorname{div} \xi \in L^2(\Omega)$ where $\xi = z + g|\nabla u|\nabla u$, and $z(x) = \frac{\nabla u}{|\nabla u|}$ for a.e. x such that $|\nabla u(x)| \neq 0$.

This proposition provides the notion of curvature extended by the well-defined z everywhere including the facet. This is a crucial element in the next chapter in defining what is called a *nonlocal curvature*.

5.1.2 Case of M2, $g = 0$

The theory of TV flow can be also applied to analyze the case M2 with $g = 0$. Indeed, in this case, (5.2) is the radial symmetric version of

$$h_t - \frac{1}{2} \operatorname{div} \left(\frac{\nabla h}{|\nabla h|} \right) = 0 \quad (5.12)$$

in a bounded open subset Ω of \mathbf{R}^3 and $\operatorname{div}(\cdot) = \frac{1}{r^2} \partial_r(r^2 \cdot)$. Solution to this equation can thus be considered using the same theory as before, with the energy:

$$E_0^2(\phi) = \begin{cases} \int_{\Omega} |\nabla \phi| & \text{if } \phi \in BV(\Omega) \cap L^2(\Omega) \\ +\infty & \text{otherwise} \end{cases} \quad (5.13)$$

Remark 11. (i)(5.2) also can be interpreted as a gradient flow with respect to a weighted energy and norm in \mathbf{R}^2 [30].(ii) The embedding of the problem into \mathbf{R}^3 does not bear any physical significance.

5.2 Case of M2, $g > 0$

The last topic of this chapter is the model M2 with $g > 0$. This is of course the most interesting case as it is physically important (see, chapter 3) but cannot be handled

directly with the existing results.

Motivated by the case of M2 with $g = 0$, we view equation (5) as an extension of a 3D TV flow with addition of Hamilton-Jacobi term. We wish to investigate what properties of TV flow carry out after this addition. In particular, we notice that this additional term *does not* prevent the strong diffusivity effect—it may smooth out the edge of facets but will not prevent facets from forming. On the other hand, the convenient divergence structure is lost by this addition of dissipation and we may no longer apply existing theories to (5) when $g > 0$.

Our main result in Part II is the existence and uniqueness of a proper viscosity solution for equation (5.2) with $g > 0$. To that end, we will rewrite (5.2) while separating two situations:

- On the facet, we view (5.2) as the radially symmetric version of

$$h_t - \frac{1}{2} \operatorname{div} \left(\frac{\nabla h}{|\nabla h|} + 2g|\nabla h|\nabla h \right) + g \frac{|\nabla h|\nabla h}{|x|} = 0 \quad \text{in } \mathbf{R}^3 \quad (5.14)$$

- Outside the facet, we interpret (5.2) as

$$h_t - \operatorname{div} \left(\frac{\nabla h}{|\nabla h|} + g|\nabla h|\nabla h \right) = 0 \quad \text{in } \mathbf{R}^2. \quad (5.15)$$

The purpose of (5.15) is to simplify our proofs. We reiterate that since $\frac{h_r}{|h_r|}$ is not singular away from the facet, we expect the solution away from the facet to be independent of the form of the equation and equations (5.2), (5), (5.14), (5.15) are equivalent in such region.

Here, we state our main result in Part II:

Theorem 4. *Suppose that $u_0(r) \in C([0, \infty))$ satisfies the far field condition (5.6). Then there exists a unique proper viscosity solution $u(r, t)$ (see, Definition 5) to (5.2) with an*

initial data $u_0(r)$.

As usual, the uniqueness will follow from a comparison principle, which is interesting in itself:

Theorem 5. (*Comparison Principle*) *Let u, v be a proper sub- and super-solution of (5.2) respectively (see, Definition 5). If $u(\cdot, 0) \leq v(\cdot, 0)$ on $[0, \infty)$ then $u(\cdot, t) \leq v(\cdot, t)$ for all $0 \leq t < T$.*

Finally, the following corollary states that the formula for facet motion is unaffected by the addition of the step-interaction (g term). In particular, we conjecture that this extra term does not change the facet motion formula that we obtained as a limit (in a weak sense) of the discrete behavior in chapter 4 remains valid for the step interacting cases:

Corollary 2. *Consider proper viscosity solutions of equations (5.1) and (5.2) at time $t \geq 0$ with initial/boundary conditions (5.6). Suppose that $h_f(t)$ is the height of a facet of the solution whose radial coordinate is given by the interval $[R_+(t), R_-(t)] \subset [0, \infty)$.*

Then the formula for the facet speed is independent of the parameter $g \geq 0$ and it is given by

$$(h_f)_t = -2 \frac{R_- - R_+}{R_-^2 - R_+^2} \quad \text{for M1} \quad (5.16)$$

and

$$(h_f)_t = -3 \frac{R_-^2 - R_+^2}{R_-^3 - R_+^3} \quad \text{for M2} \quad (5.17)$$

Remark 12. In order to be consistent with Par I, we note that equation (5.16) and (5.17) must be written as $(h_f)_t = -3\nu \frac{R_-^2 - R_+^2}{R_-^3 - R_+^3}$ and $(h_f)_t = -2\nu \frac{R_- - R_+}{R_-^2 - R_+^2}$ where $\nu > 0$ is a material parameter (for the specifics of $\nu > 0$, see equations (3.37) and (3.40)) that is

common in M1 and M2. Since the value of ν does not affect our analysis, we set $\nu = 1$ throughout Part II.

For the rest of this thesis, we will analyze (5.2) with $g > 0$.

Chapter 6: Proper viscosity solutions: definitions

In this chapter, we first introduce a notion of viscosity solution for (5.2). We will treat (5.2) as an extension of TV flow in \mathbf{R}^3 in an axisymmetric setting. To this end, we define parabolic domains of spatial radius $R > 0$ in \mathbf{R} , \mathbf{R}^2 , \mathbf{R}^3 : $Q = [0, R) \times (0, T)$, $Q_2 = B_R^2(0) \times (0, T)$, $Q_3 = B_R^3(0) \times (0, T)$ for $T > 0$. Here, $B_R^d(0)$ denotes a ball of radius R in \mathbf{R}^d centered at 0. We closely follow the footsteps of Y. Giga, M.-H. Giga, and N. Pozer who introduced the theory of proper viscosity solutions in the periodic setting [31]; however, we need to carefully address a more physically plausible geometry that is compatible with modelling in chapter 3. With this goal, we incorporate nonperiodic geometry, which requires an extra care and poses additional challenges. We also note that the theory of viscosity solution presented here applies to the simple cases of (5.1) with $g \geq 0$ and (5.2) with $g = 0$. Moreover, it is evident from the following definitions that the viscosity solutions coincide with the solutions of the TV flow for these simple cases.

Definition 1. (*Support function*) Let Ω_{\pm} be a pair of open sets such that $\overline{\Omega}_+ \subset \Omega_- \subset \mathbf{R}$ and $\psi \in Lip(\mathbf{R})$. We say that ψ is a support function of a pair (Ω_-, Ω_+) if

$$\psi(x) \begin{cases} > 0 & \text{in } \Omega_+ \\ = 0 & \text{on } D := \overline{\Omega}_- \setminus \Omega_+ \\ < 0 & \text{in } \overline{\Omega}_-^c \end{cases} \quad (6.1)$$

Definition 2. (*Test pair*) Let (Ω_-, Ω_+) be a pair of bounded open sets in \mathbf{R} with $\overline{\Omega}_+ \subset \Omega_-$. Then we say that (Ω_-, Ω_+) is a test pair. Here, Ω_+ may be \emptyset .

In what follows, we build functions that represent the test pairs.

Definition 3. (*Admissible faceted test function*) Let $f \in \text{Lip}([0, R])$ be a support function of a test pair (Ω_-, Ω_+) and $\hat{x} \in \overline{\Omega}_- \setminus \Omega_+$. The function $\phi(x, t) = f(x) + g(t)$, where $g \in C^1([\hat{t} - \tau, \hat{t} + \tau])$ for some $\tau > 0$ and $\hat{t} \in (0, T)$, is called an admissible faceted test function at $(\hat{x}, \hat{t}) \in [0, R] \times (0, T)$ with pair (Ω_-, Ω_+) . The pair (Ω_-, Ω_+) is called the pair associated with ϕ at (\hat{x}, \hat{t}) .

An admissible faceted test function represents a facet of a graph through the notion of general position:

Definition 4. (*General position*) We say that an admissible faceted test function ϕ at $(\hat{x}, \hat{t}) \in Q$ with pair (Ω_-, Ω_+) is in general position of radius $\eta > 0$ with respect to $h : [0, R] \times [0, T] \rightarrow \mathbf{R}$ at (\hat{x}, \hat{t}) if for all $a \in [0, \eta]$, we have $\hat{x} + \eta \in \Omega_- \setminus \Omega_+$ and if there exists $\tau > 0$ such that

$$h(x - a, t) - h(\hat{x}, \hat{t}) \leq \phi(x, t) - \phi(\hat{x}, \hat{t}) \quad \text{for all } x \in [0, R], t \in [\hat{t} - \tau, \hat{t} + \tau]. \quad (6.2)$$

If such an $\eta > 0$ exists, we simply say that ϕ is in general position with respect to h at (\hat{x}, \hat{t}) .

Finally, we define proper sub-/super-solutions.

Definition 5. (*Proper sub-solution*). An upper semi-continuous function

$u : [0, R] \times [0, T] \rightarrow \mathbf{R}$ is a proper viscosity subsolution of (5.2) if the following holds:

1. (*Conventional test*). If $\phi \in C_{r,t}^{2,1}(U)$ in a neighborhood $U \subset [0, R] \times [0, T]$ of a point $(\hat{r}, \hat{t}) \in (0, R) \times (0, T)$ is a test function such that $u - \phi$ has a local maximum at

(\hat{r}, \hat{t}) and $|\partial_r \phi|(\hat{r}, \hat{t}) \neq 0$, then

$$\phi_t(\hat{r}, \hat{t}) - k(\hat{r}, \partial_r \phi(\hat{r}, \hat{t}), \partial_r^2 \phi(\hat{r}, \hat{t})) \leq 0, \quad (6.3)$$

where $k(r, p, X) = \frac{1}{r} \text{sign}(p) + \frac{g}{r} p |p| + 2g |p| X$ for $r, p, X \in \mathbf{R}$ so that

$$\begin{aligned} k(r, \partial_r \phi, \partial_r^2 \phi) &= \frac{1}{r} \frac{\partial}{\partial r} \left(r \frac{\partial_r \phi}{|\partial_r \phi|} \right) + \frac{g}{r} \partial_r (r \partial_r \phi |\partial_r \phi|) \\ &= \frac{1}{r} \text{sign}(\partial_r \phi) + \frac{g}{r} \partial_r \phi |\partial_r \phi| + 2g \partial_r^2 \phi |\partial_r \phi| \end{aligned} \quad (6.4)$$

2. (Neumann boundary condition).

Let $U \subset [0, R] \times [0, T]$ be a neighborhood of a point $(0, \hat{t})$. If $\phi \in C_{r,t}^{2,1}(U)$ is a test function such that $u - \phi$ has a local maximum at $(0, \hat{t})$ then it satisfies

$$\min \left\{ \lim_{r \rightarrow 0^+} [\phi_t(r, \hat{t}) - k(r, \partial_r \phi(r, \hat{t}), \partial_r^2 \phi(r, \hat{t}))], -\partial_r \phi(0, \hat{t}) \right\} \leq 0. \quad (6.5)$$

3. (Faceted test) If $\phi : [0, R] \rightarrow \mathbf{R}$ is an admissible faceted test function such that ϕ is in general position of radius $\eta > 0$ with respect to u at a point $(\hat{x}, \hat{t}) \in [0, R] \times [0, T)$, then

$$\phi_t(\hat{x}, \hat{t}) + 3 \frac{R_-^2 - R_+^2}{R_-^3 - R_+^3} \leq 0, \quad (6.6)$$

where (Ω_-, Ω_+) is a test pair associated with ϕ at (\hat{x}, \hat{t}) and $\hat{D} = [R_+, R_-]$ is the closed connected component of $D = \bar{\Omega}_- \setminus \Omega_+$ such that $\hat{x} \in \hat{D}$.

4. (Far field condition) There exists some $\gamma \in \mathbf{R}$, $A, B, C > 0$, and $\ell < 0$, such that for all $t \geq 0$ and large enough $r > 0$, u satisfies

$$|u(r, t) - (\gamma + \ell r)| \leq C e^{-Ar+Bt}. \quad (6.7)$$

A proper super-solution can be defined similarly. A function is called a proper viscosity solution if it is both proper sub-solution and proper super-solution at the same time.

Remark 13. For a disk shaped facet, the solution of this problem has a facet speed $(h_f(t))_t = -\frac{3}{R_-}$. This differs from the M1-facet speed $(h_f)_t = -\frac{2}{R_-}$ by a multiplicative factor of $\mathcal{G} := 3/2$. For $g = 0$, this factor is in agreement with the results from chapter 4, in which the convergence of the underlying discrete schemes to the respective solutions of M1 and M2 were proven. Notably, the factor \mathcal{G} derived here is *independent* of the value of $g \geq 0$; this is consistent with the numerical prediction from the chapter 3, in which the estimates for \mathcal{G} did not appear to change significantly with respect to the values of g (see, (3.37), (3.40), remarks 9 and 10).

Remark 14. For the sake of proving the comparison principle, it is convenient to replace u by a radially symmetric function $\tilde{u}(x, t) = u(|x|, t)$, $x \in \mathbf{R}^2$, when examining condition 1 (conventional test) and write (6.3) as a gradient flow. Then condition 1 is replaced with the following condition 1R:

Definition 6. 1R. (Revised conventional test) If $\tilde{\phi} \in C_{x,t}^{2,1}(U)$ is a radial function in a neighborhood $U \subset B_R(0) \times [0, T)$, where $B_R(0)$ is a ball of radius R centered at 0 in \mathbf{R}^2 , of a point (\hat{x}, \hat{t}) such that $\tilde{u} - \tilde{\phi}$ has a local maximum at (\hat{x}, \hat{t}) and $|\nabla \tilde{\phi}|(\hat{x}, \hat{t}) \neq 0$, then

$$\tilde{\phi}_t(\hat{x}, \hat{t}) - k(\nabla \tilde{\phi}(\hat{x}, \hat{t}), \nabla^2 \tilde{\phi}(\hat{x}, \hat{t})) \leq 0 \quad (6.8)$$

where $k(p, X) = \frac{1}{|p|} \text{trace} X \left(I - \frac{p \otimes p}{|p|^2} \right) + g \text{trace} X \left(|p| + \frac{p \otimes p}{|p|} \right)$ so that (6.8) reads

$$\tilde{\phi}_t(\hat{x}, \hat{t}) - \text{div} \left(\frac{\nabla \tilde{\phi}}{|\nabla \tilde{\phi}|} + g |\nabla \tilde{\phi}| \nabla \tilde{\phi} \right) \leq 0 \quad (6.9)$$

Note that k no longer has an explicit spatial dependence. This property will be convenient in the proof of the comparison principle in chapter 7. From here on, we drop tilde and denote \tilde{u} also by u for the sake of ease of notation.

Remark 15. Since $\phi \in C_{r,t}^{2,1}(U)$, it turns out that

$\lim_{r \rightarrow 0^+} [\phi_t(r, \hat{t}) - k(r, \partial_r \phi(r, \hat{t}), \partial_r^2 \phi(r, \hat{t}))] \leq 0$ if and only if $-\partial_r \phi(0, \hat{t}) \leq 0$. Therefore,

it suffices to check $-\partial_r\phi(0, \hat{t}) \leq 0$ in order to verify the condition (6.5). Furthermore, if we define

$$G(r, \tau, p, X) = \begin{cases} \tau - k(r, p, X) & \text{if } r \neq 0 \\ -p & \text{if } r = 0 \end{cases} \quad (6.10)$$

then the conventional test and the Neumann boundary condition can be combined into one criterion:

Let $\phi \in C_{r,t}^{2,1}(U)$ in a neighborhood $U \subset [0, R] \times [0, T]$ of a point $(\hat{r}, \hat{t}) \in [0, R] \times (0, T)$ be a test function. Suppose that $u - \phi$ has a local maximum at (\hat{r}, \hat{t}) and (i) $|\partial_r\phi|(\hat{r}, \hat{t}) \neq 0$, and (ii) if $\hat{r} = 0$, $\lim_{r \rightarrow 0} |\partial_r\phi|(r, \hat{t}) \neq 0$. Then

$$\underline{G}(\hat{r}, \phi_t(\hat{r}, \hat{t}), \partial_r\phi(\hat{r}, \hat{t}), \partial_r^2\phi(\hat{r}, \hat{t})) \leq 0, \quad (6.11)$$

where \underline{G} is a lower semicontinuous envelop of G [19].

Finally, we reconcile our definition of proper viscosity solutions with the one introduced in [31].

Lemma 2. *Definition 5 of proper viscosity solution is equivalent to [31, Definition 3.3] of proper viscosity solution for (5.2).*

We caution the readers that the setting in [31] is periodic and Lemma 2 truly makes sense only if we change our domain to a simpler periodic domain; however, such a change does not make any sense for the physical setting that we want to describe.

In the rest of this section, we will state a series of definitions from [31] leading up to the notion of proper viscosity solution and prove Lemma 2. In [31], the gradient flow approach (see, chapter 5) is extended to equations of non-divergence type. The optimization approach as in the analysis of TV flows is used to find a vector z that

replaces $\nabla h/|\nabla h|$ while minimizing $\|\operatorname{div} z\|_{L^2}$. Since the gradient flow theory cannot be applied to (5.2), such a vector z is used in the context of the viscosity solution in order to approximate the facet speed; it is natural to seek a viscosity solution to a generalization of the TV model because of possible occurrences of discontinuities in BV functions and the merit of viscosity solutions to allow discontinuous functions. To this end, we introduce Cahn-Hoffman vector field in an attempt to extend the solution to (5.2) across the facets [2, 31]:

Definition 7. Let (Ω_-, Ω_+) be a test pair. We say that a vector field $z \in [L^\infty(D)]^3$ such that $\operatorname{div}(z) \in L^2(D)$ for $D = \bar{\Omega}_- \setminus \Omega_+$ is a Cahn-Hoffman vector field in D if z satisfies

$$|z| \leq 1 \text{ a.e. in } D \tag{6.12}$$

as well as the boundary condition:

$$z \cdot \nu_{\partial\Omega_\pm} = -1 \text{ on } \partial\Omega_\pm \tag{6.13}$$

almost everywhere.

Definition 8. Let (Ω_-, Ω_+) be a test pair. Let w_0 be a solution of the variational problem:

$$\min \mathcal{S}, \quad \mathcal{S} = \left\{ \int_D |w|^2 dx \mid w = \operatorname{div} z \text{ and } z \text{ is a Cahn-Hoffman vector field in } D \right\}. \tag{6.14}$$

Then we call w_0 the nonlocal curvature of (Ω_-, Ω_+) and we denote it by $\Lambda(\Omega_-, \Omega_+)$.

Note that it is convex and the set of Cahn-Hoffman vector fields is closed in $L^2(D)$. So if $\mathcal{S} \neq \emptyset$, then at least one minimizer of \mathcal{S} exists.

The non-locality of w_0 is evident from the definition because the choice of w_0 depends on both Ω_- and Ω_+ . Before we proceed to show the uniqueness of the minimizer w_0 , we first recall a few definitions: the total variational energy on $L^2(B_R(0))$ is defined as

$$E(\psi) = \begin{cases} \int_{B_R(0)} |\nabla \psi| & \text{if } \psi \in BV(B_R(0)) \cap L^2(B_R(0)) \\ +\infty & \text{otherwise} \end{cases} \quad (6.15)$$

and the effective domain of E is $\mathcal{D}(E) = \{\phi \in L^2(B_R(0)) \mid E(\phi) < \infty\}$ and the domain of ∂E is $\mathcal{D}(\partial E) = \{\phi \in L^2(B_R(0)) \mid \partial E(\phi) \neq \emptyset\}$.

Also recall the following property of the TV flow [1]:

Lemma 3. *Given $\psi \in Lip(\Omega)$, $w \in -\partial E(\psi)$ if and only if there exists $z \in L^\infty(\Omega)$, $\text{div}(z) \in L^2(\Omega)$ such that*

$$\text{div} z = w \quad \text{and} \quad z \in \partial W(\nabla \psi) \quad \text{a.e. on } \Omega, \quad (6.16)$$

where $W(p) = |p|$.

We also introduce the following lemma in the interest of establishing a connection between support functions and Cahn-Hoffman vector fields later [31, Proposition 2.8].

Lemma 4. *Suppose that $u \in Lip(B_R(0))$ is a radially symmetric function and define $G_t = \{x \in B_R(0) : u(x) > t\}$. Suppose that $z \in L^\infty(B_R(0))$, $\text{div}(z) \in L^2(B_R(0))$ such that $z \in \partial W(\nabla u)$ a.e. on $B_R(0)$. Then $z \cdot \nu_{\partial G_0} = -1$.*

Now we return to showing that the variational problem (6.14) has a *unique* solution.

The following proposition ensures the existence of support functions and of

Cahn-Hoffman vector fields:

Proposition 3. *Let (Ω_-, Ω_+) be a test pair.*

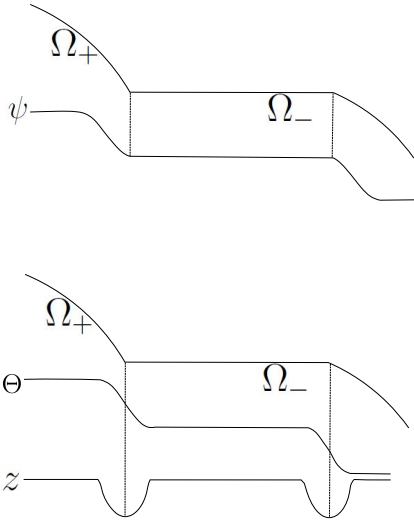


Figure 6.1: $\Theta := -\theta(d_{\Omega_-}) + \theta(d_{\Omega_+})$

- (a) There exists a support function ψ of (Ω_-, Ω_+) .
- (b) There exists a Cahn-Hoffman vector field z in $D = \overline{\Omega_-} \setminus \Omega_+$. Consequently, there exists a solution w_0 of the variational problem.
- (c) In fact, $w_0 = -\partial^0 E(\psi)(x)$ a.e. on D for any support function ψ of (Ω_-, Ω_+) such that $\psi \in \mathcal{D}(\partial E)$. Thus, (6.14) has a unique solution.

Proofs of Proposition 3 (a)-(c) can be found in [31]. Here, we give a proof for our simpler case for the sake of completeness.

Proof. (a) It is clear from the smoothness of $\Omega_- = B_{R_-}$ and $\Omega_+ = B_{R_+}$ that a support function ψ of (Ω_-, Ω_+) exists; however, for the sake of completeness, we will explicitly construct such a ψ .

Define a signed distance function $d_E(x)$ as

$$d_E(x) = \begin{cases} \text{dist}(x, E) & \text{if } x \in \overline{E^c} \\ -\text{dist}(x, E^c) & \text{if } x \in E \end{cases} \quad (6.17)$$

For $\delta_0 = \text{dist}(\partial\Omega_-, \partial\Omega_+) > 0$, define $\theta(\sigma)$ to be a smooth function on \mathbf{R} satisfying as

$$0 \leq |\theta'| \leq 1, \quad \theta(\sigma) = \begin{cases} \sigma & \text{for } |\sigma| \leq \delta_0/2 \\ \frac{3}{4}\delta_0 \text{ sign } \sigma & \text{for } |\sigma| \geq \delta_0 \end{cases} . \quad (6.18)$$

Define

$$\psi(x) = \begin{cases} -\theta(d_{\Omega_+}) & \text{in } \Omega_+ \\ 0 & \text{in } D \\ -\theta(d_{\Omega_-}) & \text{in } (\overline{\Omega_-})^c \end{cases} . \quad (6.19)$$

Clearly, ψ is a support function of (Ω_-, Ω_+) . Furthermore, ψ is Lipschitz because

$d_E \in C^2$ for $E = \Omega_-, (\Omega_+)^c$.

(b) Using the smooth function θ from part (a), define

$z = -\nabla(\theta(d_{\Omega_-}) + \theta(d_{\Omega_+})) = -\theta'(d_{\Omega_-})\nabla d_{\Omega_-}(x) - \theta'(d_{\Omega_+})\nabla d_{\Omega_+}(x)$. Then $|z| \leq 1$ and

$z \cdot \nu_{\Omega_-} = -\theta'(d_{\Omega_-})\nabla d_{\Omega_-}(x) \cdot \nu_{\Omega_-} = -1$. Similarly, $z \cdot \nu_{\Omega_+} = -1$. Therefore, z satisfies

the boundary conditions of Cahn-Hoffman vector field. In particular, \mathcal{S} is non-empty

and there exists at least one minimizer w_0 of \mathcal{S} .

(c) Let w_0 be a solution of the variational problem (6.14). Then there exists a

Cahn-Hoffman vector field z_0 in D such that $w_0 = \text{div} z_0$ in D . Let ψ be an arbitrary

support function of (Ω_-, Ω_+) such that $\psi \in \mathcal{D}(\partial E)$. Then by Lemma 3, there exists

$z_\psi \in L^\infty(\text{int}D)$ such that $\text{div} z_\psi = w \in L^2(\text{int}D)$ and $z_\psi \in \partial W(\nabla\psi)$. Consequently, z_ψ is

a Cahn-Hoffman vector field in D due to Lemma 4.

Define

$$\bar{z} = \begin{cases} z_0 & \text{on } D, \\ z_\psi & \text{on } D^c \end{cases}. \quad (6.20)$$

Then by definition of $\partial^0 E(\psi)$,

$$\|\operatorname{div}(z_\psi)\|_{L^2(B_R(0))} \leq \|\operatorname{div}(\bar{z})\|_{L^2(B_R(0))}. \quad (6.21)$$

Thus,

$$\|\operatorname{div}(z_\psi)\|_{L^2(D)} \leq \|\operatorname{div}(z_0)\|_{L^2(D)}. \quad (6.22)$$

By the uniqueness of the minimizer, we have $w_0 = \operatorname{div} z_\psi$ a.e. on D .

□

Hence, the non-local curvature $\Lambda(\Omega_-, \Omega_+)$ is well defined as a result of Proposition 3.

Finally, we compute an explicit formula for $\Lambda(\Omega_-, \Omega_+)$ in the radial case, i.e.

$$\Omega_- = B_{R_-}(0), \quad \Omega_+ = B_{R_+}(0):$$

Lemma 5. *For $\Omega_- = B_{R_-}(0)$, $\Omega_+ = B_{R_+}(0) \subset \mathbf{R}^3$ and $D = \bar{\Omega}_- \setminus \Omega_+$, the nonlocal curvature is given by*

$$\Lambda(\Omega_-, \Omega_+) = -3 \frac{R_-^2 - R_+^2}{R_-^3 - R_+^3}. \quad (6.23)$$

Proof. Construct a Cahn-Hoffman vector field z so that $w := \operatorname{div} z$ is a constant. Denote

$b := \Lambda(\Omega_-, \Omega_+) = -3 \frac{R_-^2 - R_+^2}{R_-^3 - R_+^3}$. z is a radially symmetric solution of the Poisson equation

with Neumann boundary data:

$$\begin{cases} \Delta \phi = b & \text{in } D, \\ \nabla \phi \cdot \nu = \pm 1 & \text{on } |x| = R_\pm. \end{cases} \quad (6.24)$$

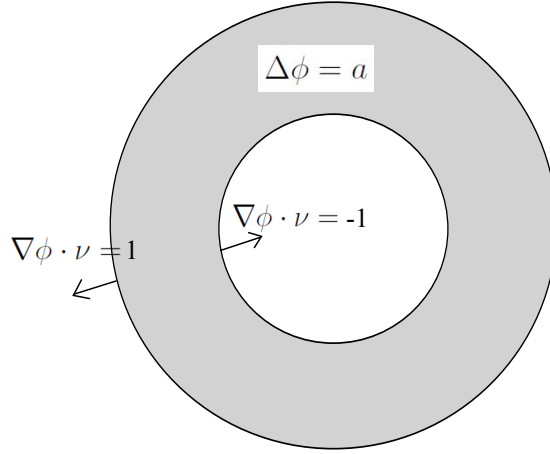


Figure 6.2: The shaded region is $D = \bar{\Omega}_- \setminus \Omega_+$

Then a usual theory of the Poisson equation implies that $\phi(x) = -a|x|^{-1} + \frac{b}{6}|x|^2$ for $x \in \mathbf{R}^3$, $a = (R_+R_-)^2 \frac{R_- - R_+}{R_-^3 - R_+^3}$. Then $z = \nabla\phi = (a|x|^{-2} + \frac{b}{3}|x|) \frac{x}{|x|}$ is a Cahn-Hoffman vector field.

Finally, since a Euler-Lagrangian equation of the minimization problem (6.14) is $\nabla(\operatorname{div}z) = 0$ where z is a Cahn-Hoffman vector field, a constant $w = b$ is a minimizer of S . □

Corollary 3. *Let D' be a connected component of D . Then in a radial setting, every connected component of D is a torus, say, $\hat{D} = \bar{B}_{R_-}(0) \setminus B_{R_+}(0) \subset \mathbf{R}^3$. Thus,*

$$\Lambda(\Omega_-, \Omega_+)|_{\hat{D}} = -3 \frac{R_-^2 - R_+^2}{R_-^3 - R_+^3}.$$

Proof. Cahn-Hoffman vector fields are defined on each connected component of D .

Thus, (d) follows from the following Lemma 5. □

Due to Lemma 5, we may rewrite condition 2 (faceted test) in the definition of

sub-/super-solution by the following condition 2R:

Definition 9. *2R. (Revised faceted test) If $\phi : B_{\mathbf{R}}^2(0) \rightarrow \mathbf{R}$ is an admissible faceted test function such that ϕ is in general position of radius $\eta > 0$ with respect to u at a point $(\hat{x}, \hat{t}) \in Q_2$, then*

$$\phi_t(\hat{x}, \hat{t}) - \Lambda(\Omega_-, \Omega_+) \leq 0, \quad (6.25)$$

where $(\Omega_- = B_{R_-}^2(0), \Omega_+ = B_{R_+}^2(0))$ is the test pair associated with ϕ at (\hat{x}, \hat{t}) .

Chapter 7: Comparison Principle

In this chapter, we prove the following comparison principle, which implies in particular the uniqueness of the solution. The main arguments in this chapter closely follow the method developed by [31]; however, our distinct boundary conditions require a careful examination and extra steps.

Theorem 6. (*Comparison Principle*) *Let u and v be a proper sub- and super-solution of (5.2) respectively. If $u(\cdot, 0) \leq v(\cdot, 0)$ on $[0, \infty)$ then $u(\cdot, t) \leq v(\cdot, t)$ on $[0, \infty)$ for all $0 \leq t < T$.*

Proof. Let γ_u, ℓ_u and γ_v, ℓ_v denote the constants from the far-field conditions associated with u and v , respectively. The initial condition $u(\cdot, 0) \leq v(\cdot, 0)$ implies that $\ell_u \leq \ell_v$ and in addition, if $\ell_u = \ell_v$, then $\gamma_u \leq \gamma_v$ must be satisfied. Let $\delta > 0$. Note that the formulas for k (equation (6.4)) together with (6.3) and the facet speed (6.6) do not depend on the value of v itself. Therefore, if v is a super-solution, then so is $v_\delta = v + \delta$ and v_δ satisfies the far-field condition in which γ_v is replaced by $\gamma_v + \delta$. So we may assume that for a large enough $R_\delta > 0$, $u(r, t) \leq v_\delta(r, t)$. On the other hand, if $u(r, t) \leq v_\delta(r, t)$ everywhere for all $\delta > 0$, then by passing to the limit $\delta \rightarrow 0$, we obtain $u(r, t) \leq v(r, t)$ everywhere. Therefore, in what follows, we replace v by v_δ and show that $u(\cdot, t) \leq v(\cdot, t)$ in $B_R(0)$ for some large $R > 0$ under the assumption that $u(\cdot, t) \leq v(\cdot, t)$ on $[R, \infty)$ for all $t \in [0, T]$.

Our argument is based on a type of doubling of variable argument. For positive

constants ϵ, σ, γ and $\xi \in \mathbf{R}$, set functions

$$w(x, y, t, s) = u(x, t) - v(y, s). \quad (7.1)$$

$$S(t, s; \sigma, \gamma) = \frac{|t - s|^2}{2\sigma} + \frac{\gamma}{T - t} + \frac{\gamma}{T - s} \quad (7.2)$$

$$\Psi_\xi(x, t, y, s; \epsilon, \sigma, \gamma) = \frac{|x - y - \xi|^2}{2\epsilon} + S(t, s; \sigma, \gamma) \quad (7.3)$$

For each ξ , define

$$\Phi_\xi(x, t, y, s; \epsilon, \sigma, \gamma) := w(x, t, y, s) - \Psi_\xi(x, t, y, s; \epsilon, \sigma, \gamma). \quad (7.4)$$

In what follows, we will analyze the maxima of Φ_ξ .

Suppose that the comparison principle does not hold, i.e.,

$$m_0 := \sup_{(x,t) \in \bar{Q}} [u(x, t) - v(x, t)] > 0. \quad (7.5)$$

The following proposition from [29, Proposition 7.1] yields some useful bounds that is uniform in ξ for small ξ .

Proposition 4. *Set $M := \max_{\bar{Q} \times \bar{Q}} w \geq m_0$, $m'_0 := \frac{7}{8}m_0$, $\kappa(\epsilon) := \frac{1}{2}(\epsilon(m_0 - m'_0))^{1/2}$.*

There exist positive constants ϵ_0, σ_0 and γ_0 such that for any $\epsilon \in (0, \epsilon_0)$, $\sigma \in (0, \sigma_0)$,

$\gamma \in (0, \gamma_0)$ and $\xi \in \mathbf{R}$ such that $|\xi| \leq \kappa(\epsilon)$ the following is true:

If $(x_\xi, t_\xi, y_\xi, s_\xi) \in \arg \max_{\bar{Q} \times \bar{Q}} \Phi_\xi(\cdot; \epsilon, \sigma, \gamma)$ then

(i) $(x_\xi, t_\xi, y_\xi, s_\xi) \in Q \times Q$.

(ii) $|t_\xi - s_\xi| \leq (M\sigma)^{1/2}$, $|x_\xi - y_\xi - \xi| \leq (M\epsilon)^{1/2}$,

(iii) $\sup \Phi_\xi > m'_0$.

We consider the following two cases:

- Case I: For all ϵ, σ, γ and $|\xi| < \kappa(\epsilon)$, all the points of maximum lie on the space diagonals, i.e.

$$\arg \max_{\bar{Q} \times \bar{Q}} \Phi_\xi \subset \{(x, t, y, s) \in \bar{Q} \times \bar{Q} : x - y = \xi\}. \quad (7.6)$$

- Case II: There exists $\epsilon, \sigma, \gamma > 0$, such that $|\xi| < \kappa(\epsilon)$ and

$$(x, t, y, s) \in \arg \max_{\bar{Q} \times \bar{Q}} \Phi_\xi \text{ such that } x - y \neq \xi.$$

The separation of case I and case II makes the role of ξ clear: For case I, $\nabla \Psi_\xi = 0$ at $(\hat{x}_\xi, \hat{t}_\xi, \hat{y}_\xi, \hat{s}_\xi)$ for all ξ small enough, which provides some room to construct a facet around $\hat{x}_0 = \hat{y}_0$ ($\xi = 0$).

For case II, $\nabla \Psi_\xi \neq 0$ at $(\hat{x}_\xi, \hat{t}_\xi, \hat{y}_\xi, \hat{s}_\xi)$ so one may treat Ψ_ξ as a conventional test function.

7.1 Case I

Let us fix $\epsilon \in (0, \epsilon_0)$, $\sigma \in (0, \sigma_0)$, $\gamma \in (0, \gamma_0)$ such that (7.6) holds for all ξ , $|\xi| \leq \kappa(\epsilon)$. To simplify the notation, we set $r := \frac{1}{3}\kappa(\epsilon)$. We also do not explicitly state the dependence of the following formulas on the fixed ϵ, σ and γ . Let us define

$$\ell(\xi) = \sup_{\bar{Q} \times \bar{Q}} \Phi_\xi. \quad (7.7)$$

The first step is the application of the following constancy lemma [29, Lemma 7.5] to show that $\ell(\xi)$ is constant for $|\xi| \leq \lambda$.

Lemma 6. (*Constancy lemma*). *Let K be a compact set in \mathbf{R}^N for some $N > 1$ and let θ be a real-valued upper semi-continuous function on K . Let ϕ be a C^2 function on \mathbf{R}^d with $1 \leq d < N$. Let G be a bounded domain in \mathbf{R}^d . For each $\xi \in G$ assume that there is a maximizer $(r_\xi, \rho_\xi) \in K \subset (\mathbf{R}^d, \mathbf{R}^{N-d})$ of*

$$\Theta_\xi(r, \rho) = \theta(r, \rho) - \phi(r - \xi) \quad (7.8)$$

over K such that $\nabla\phi(r_\xi - \xi)$. Then

$$\theta_\phi(\xi) = \sup \{\Theta_\xi(r, \rho) : (r, \rho) \in K\} \quad (7.9)$$

is constant on G .

We apply the constancy lemma with the following parameters:

$$\begin{aligned} N = 4, \quad d = 1, \quad \rho = (y, t, s) \in [0, R] \times [0, T] \times [0, T], \quad G = B_{2\lambda}(0), \\ \theta(r, \rho) = w(r + y, t, y, s) - S(t, s), \quad \phi(r) = \frac{|r|^2}{2\epsilon} + \delta, \\ K = \{(x - y, y, t, s) : (x, y) \in [0, R]^2, (t, s) \in [0, T]^2\}. \end{aligned}$$

Here, K can be treated as a compact subset of $\mathbf{R} \times \mathbf{R} \times [0, T]^2$.

Corollary 4. *We infer that $\ell(\xi) = \theta_\phi(\xi)$ is constant for $|\xi| \leq \lambda$.*

The following lemma is a direct consequence of the consistency lemma and it forms a bases for the construction of ordered facets:

Lemma 7. *Let $(\hat{x}, \hat{t}, \hat{x}, \hat{s}) \in \operatorname{argmax} \Phi_0$. Then*

$$u(x, t) - v(y, s) - S(t, s) \leq u(\hat{x}, \hat{t}) - v(\hat{x}, \hat{s}) - S(\hat{t}, \hat{s}) \quad (7.10)$$

for all $s, t \in (0, T)$ and $x, y \in [0, R]^2$ such that $|x - y| \leq \lambda := \kappa(\epsilon)/2$.

Proof. Note that $\hat{y} = \hat{x}$ because $\max \Phi_0$ occurs on the diagonal. For $|x - y| \leq \kappa(\epsilon)$, by

the constancy of ℓ , we have

$$u(x, t) - v(y, s) - S(t, s) = \Phi_{x-y}(x, t, y, s) \quad (7.11)$$

$$\leq \ell(x - y) = \ell(0) \quad (7.12)$$

$$= u(\hat{x}, \hat{t}) - v(\hat{x}, \hat{s}) - S(\hat{t}, \hat{s}). \quad (7.13)$$

Lemma 7 provides room to construct ordered facets, whose support functions will play the role of admissible test functions for u and v . □

To this end, fix $(\hat{x}, \hat{t}, \hat{x}, \hat{s}) \in \operatorname{argmax} \Phi_0$ and set

$$\alpha := u(\hat{x}, \hat{t}), \quad \beta := v(\hat{x}, \hat{s}) \quad (7.14)$$

and define the closed sets

$$U := \{u(\cdot, \hat{t}) \geq \alpha\} \quad V = \{v(\cdot, \hat{s}) \leq \beta\}. \quad (7.15)$$

Now, we introduce the generalized neighborhood. For a given set $A \subset \mathbf{R}$, we define

$$A^\rho = \begin{cases} A + \overline{B}_\rho(0), & \rho > 0, \\ A, & \rho = 0, \\ \{x \in A : \overline{B}_{|\rho|}(x) \subset A\}, & \rho < 0. \end{cases} \quad (7.16)$$

Replace A^ρ by $A^\rho \cap [0, R]$ while still denoting A^ρ . Since $r = \frac{\kappa(\epsilon)}{3}$, we have the following inequality as a consequence of Corollary 4

Corollary 5.

$$u(x, t) \leq \alpha + S(t, \hat{s}) - S(\hat{t}, \hat{s}) \quad \text{for } x \in V^{3r}, t \in (0, T), \quad (7.17)$$

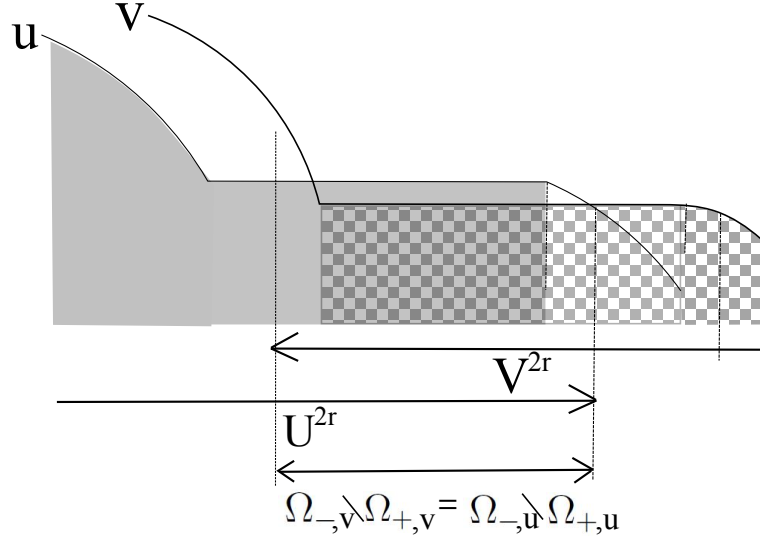


Figure 7.1: In this simple example, u, v are monotone. In such a case, $D = \Omega_{-,u} \setminus \Omega_{+,u} = \Omega_{-,v} \setminus \Omega_{+,v}$

and

$$v(y, s) \geq \beta + S(\hat{t}, s) - S(\hat{t}, \hat{s}) \quad \text{for } y \in U^{3r}, s \in (0, T). \quad (7.18)$$

Let $(\Omega_{-,u}, \Omega_{+,u}) = (U^{2r}, U^{2r} \cap (V^{2r})^c)$ and $(\Omega_{-,v}, \Omega_{+,v}) = (V^{2r}, V^{2r} \cap (U^{2r})^c)$. Suppose that $\hat{D} = [R_-, R_+]$ for some $R_+ > R_- > 0$ is a connected component of $U^{2r} \cap V^{2r}$ that contains \hat{x} . In what follows, we construct faceted test functions with these test pairs in general position at (\hat{x}, \hat{t}) and (\hat{x}, \hat{s}) , respectively.

By the definition of U and V , $u(\cdot, \hat{t}) < \alpha$ in $(U^r)^c$ and $v(\cdot, \hat{s}) > \beta$ in $(V^r)^c$. So due to the upper semicontinuity of u and the lower semicontinuity of v , there exists $\tau > 0$ such that

$$u(\cdot, t) < \alpha + S(t, \hat{s}) - S(\hat{t}, \hat{s}) \text{ in } (U^r)^c \text{ for } t \in [\hat{t} - \tau, \hat{t} + \tau], \quad (7.19)$$

$$v(\cdot, s) > \beta + S(\hat{t}, \hat{s}) - S(\hat{t}, s) \text{ in } (V^r)^c \text{ for } s \in [\hat{s} - \tau, \hat{s} + \tau], \quad (7.20)$$

Therefore, together with Corollary 5,

$$u(\cdot, t) \leq \alpha + S(t, \hat{s}) - S(\hat{t}, \hat{s}) \text{ in } (U^r)^c \cup V^{3r} \text{ for } t \in [\hat{t} - \tau, \hat{t} + \tau], \quad (7.21)$$

$$v(\cdot, s) \geq \beta + S(\hat{t}, \hat{s}) - S(\hat{t}, s) \text{ in } (V^r)^c \cup U^{3r} \text{ for } s \in [\hat{s} - \tau, \hat{s} + \tau], \quad (7.22)$$

Our goal is to construct admissible faceted test functions that correspond to facets

$(\Omega_{-,i}, \Omega_{+,i})$, $i = u, v$, which are in general position with respect to u and v at (\hat{x}, \hat{t}) .

Therefore, let ψ_u, ψ_v be the support functions constructed in 3 for pairs

$(\Omega_{-,u}, \Omega_{+,u}) = (U^{2r}, U^{2r} \cap (V^{2r})^c)$, $(\Omega_{-,v}, \Omega_{+,v}) = (V^{2r}, V^{2r} \cap (U^{2r})^c)$, respectively.

Define

$$\phi_u(x, t) = \lambda_u[\psi_u(x)]_+ - \mu_u[\psi_u(x)]_- + \alpha + S(t, \hat{s}) - S(\hat{t}, \hat{s}) \quad (7.23)$$

$$\phi_v(x, s) = \lambda_v[\psi_v(x)]_+ - \mu_v[\psi_v(x)]_- + \beta + S(\hat{t}, \hat{s}) - S(\hat{t}, s). \quad (7.24)$$

Note that Lemma 7, it suffices to construct ϕ_u, ϕ_v in the vicinity of \hat{D} . Next lemma shows that ϕ_u and ϕ_v are in general position of u and v , respectively.

Lemma 8. *There are positive constants λ_u, μ_v , chosen large enough and positive constants μ_u, λ_v , chosen small enough, so that*

$$u(x, t) \leq \phi_u(x - a, t) \quad \text{for } x \in (0, R), t \in [\hat{t} - \tau, \hat{t} + \tau], a \in [0, r], \quad (7.25)$$

$$v(x, s) \geq \phi_v(x - a, s) \quad \text{for } x \in (0, R), s \in [\hat{s} - \tau, \hat{s} + \tau], a \in [0, r] \quad (7.26)$$

Proof. Since the proofs for inequalities (7.25) and (7.26) are similar, we only prove the case of u and ϕ_u here.

We start by defining $\phi^r(x, t) = \min_{|h| \leq r} \phi_u(x - h, t) \in C(\bar{Q})$ for all $t \in [0, T]$. Then the spatial part of ϕ^r is a support function of the pair $((H_v)^{-r}, (G_u)^{-r})$. Moreover, the

statement of the lemma is clearly equivalent to $u \leq \phi^r$ for $x \in (0, R)$, $t \in [\hat{t} - \tau, \hat{t} + \tau]$.

The interval $(0, R)$ can be divided into three parts:

1. $M_1 = U^r \cap (V^{3r})^c$. Since $\psi_u > 0$ in $U^r \cap (V^{3r})^c$, we obtain

$\min_{|h| \leq r} \min_{\overline{M}_1+h} \psi_u > 0$ and we can choose λ_u large enough to satisfy $u \leq \phi^r$ in $\overline{M}_1 \times [\hat{t} - \tau, \hat{t} + \tau]$ due to boundedness of u in $[0, R)$.

2. $M_2 = U^r \cap V^{3r}$. By the definition of support functions, $\psi_u \geq 0$ on $U^r \subset U^{2r}$. Also, $u \leq \alpha + S(t, \hat{s}) - S(\hat{t}, \hat{s})$ in V^{3r} . Thus, $u \leq \phi^r$ on $M_2 \times [\hat{t} - \tau, \hat{t} + \tau]$.

3. $M_3 = (U^r)^c$. Then by (7.19), there exists some $\tau > 0$ such that

$u(x, t) - \alpha - S(t, \hat{s}) + S(\hat{t}, \hat{s}) < 0$ for $t \in [\hat{t} - \tau, \hat{t} + \tau]$ and any $x \in \overline{(U^{2r})^c}$. Since u is upper semi-continuous, we can choose $\mu_u > 0$ small enough so that

$$-\mu_u \|\psi_u\|_\infty \geq \max_{X \times [\hat{t} - \tau, \hat{t} + \tau]} u(x, t) - \alpha - S(t, \hat{s}) + S(\hat{t}, \hat{s}). \quad (7.27)$$

Thus we have $u \leq \phi^r$ with this choice of μ_u on $M_3 \times [\hat{t} - \tau, \hat{t} + \tau]$.

□

By definition, $\phi_u(\hat{x}, \hat{t}) = u(\hat{x}, \hat{t})$ and $\phi_v(\hat{x}, \hat{s}) = v(\hat{x}, \hat{s})$. Also,

$$\overline{B}_r(\hat{x}) \subset U^{2r} \cap V^{2r} \subset \Omega_{-,u} \setminus \overline{\Omega}_{+,u} \text{ and similarly, } \overline{B}_r(\hat{x}) \subset U^{2r} \cap V^{2r} = \Omega_{-,v} \setminus \overline{\Omega}_{+,v}.$$

Therefore ϕ_u is in general position of radius r with respect to u at (\hat{x}, \hat{t}) . Similarly, $-\phi_v$

is in general position of radius r with respect to $-v$ at (\hat{x}, \hat{s}) .

Therefore, by the definition of viscosity solutions together with ,

$$S_t(\hat{t}, \hat{s}) - 3 \frac{R_-^2 - R_+^2}{R_-^3 - R_+^3} \leq 0 \quad (7.28)$$

and

$$-S_s(\hat{t}, \hat{s}) - 3 \frac{R_-^2 - R_+^2}{R_-^3 - R_+^3} \geq 0. \quad (7.29)$$

Combining these two inequalities yields

$$0 < \frac{\gamma}{(T - \hat{t})^2} + \frac{\gamma}{(T - \hat{s})^2} \leq 3 \frac{R_-^2 - R_+^2}{R_-^3 - R_+^3} - 3 \frac{R_-^2 - R_+^2}{R_-^3 - R_+^3} = 0, \quad (7.30)$$

which is a contradiction.

7.2 Case II

Suppose that for arbitrarily small ξ , there exists ϵ, σ, γ , and $(x, t, y, s) \in \arg \max_{Q \times Q} \Phi_\xi$ such that $x - y \neq \xi$. Then $x - y \neq \xi$ implies that $\partial_x \Psi_\xi(\hat{x}, \hat{t}, \hat{y}, \hat{s}) = -\partial_y \Psi_\xi(\hat{x}, \hat{t}, \hat{y}, \hat{s}) \neq 0$.

First, we replace u, v with radially symmetric functions \tilde{u}, \tilde{v} with \mathbf{R}^2 -spatial dependence and drop the tildes. Denote $\hat{\Psi}_{\xi, x} := \nabla_x \Psi_\xi(\hat{x}, \hat{t}, \hat{y}, \hat{s})$, $\hat{\Psi}_{\xi, t} := \partial_t \Psi_\xi(\hat{x}, \hat{t}, \hat{y}, \hat{s})$. $\hat{\Psi}_{\xi, y}, \hat{\Psi}_{\xi, s}$ are defined similarly.

Below, we recall a few definitions from conventional theory of viscosity solutions:

Definition 10. (*parabolic superjet*) Let $u : \mathbf{R}^2 \times [0, T] \rightarrow \mathbf{R}$ and $(x, t) \in \mathbf{R}^2 \times [0, T]$. We

denote by $\mathcal{P}^{2,+}(u(x, t))$ (the parabolic superjet of u at (x, t)) the set of triples

$(\tau, p, X) \in \mathbf{R} \times \mathbf{R}^2 \times \mathbf{S}^2$ (here, \mathbf{S}^2 is a set of symmetric matrices) such that for all

$(y, s) \in \mathbf{R}^2 \times [0, T]$ in a neighborhood of (x, t) , the following inequation holds:

$$u(y, s) \leq u(x, t) + \tau(s - t) + \langle p, y - x \rangle + \frac{1}{2} \langle X(y - x), y - x \rangle + o(|s - t| + |y - x|^2). \quad (7.31)$$

Similarly, define $\mathcal{P}^{2,+}u(x, t)$ (the parabolic subjet of u at (x, t)) as the set of triples

$(\tau, p, X) \in \mathbf{R} \times \mathbf{R}^2 \times \mathbf{S}^2$ which are such that for all $(y, s) \in \mathbf{R}^2 \times [0, T]$ in a neighborhood of (x, t) ,

$$u(y, s) \geq u(x, t) + \tau(s - t) + \langle p, y - x \rangle + \frac{1}{2} \langle X(y - x), y - x \rangle + o(|s - t| + |y - x|^2). \quad (7.32)$$

Definition 11. *The closure of a parabolic superjet is defined by*

$$\overline{\mathcal{P}}_{\mathcal{O}}^{2,+}(u(x,t)) = \{(\tau, p, X) \in \mathbf{R} \times \mathbf{R}^2 \times \mathbf{S}^2 \mid \exists(x_n, t_n, \tau_n p_n, X_n) \in \mathcal{O} \times [0, T] \times \mathbf{R} \times \mathbf{R}^2 \times \mathbf{S}_2$$

such that $(\tau_n, p_n, X_n) \in \mathcal{P}_{\mathcal{O}}^{2,+}u(x_n, t_n)$ and $(x_n, t_n, u(x_n, t_n), \tau_n, p_n, X_n) \rightarrow (x, t, u(x, t), \tau, p, X)$ $\}$.

The closure of a subjet is defined similarly. Note the slight abuse of the word “closure” here. Unlike a topological closure, we also require $u(x_n, t_n) \rightarrow u(x, t)$, $x_n \rightarrow x$, $t_n \rightarrow t$.

We state the following classical result without a proof [19, Theorem 3.2] [82, Corollary 3.6].

Lemma 9. *Using the special structure of Φ_{ξ} , there exists matrices $X, Y \in \mathcal{S}^2$, $X \leq Y$ such that*

$$\left(\hat{\Psi}_{\xi,t}, \hat{\Psi}_{\xi,x}, X\right) \in \overline{\mathcal{P}}^{2,+}(u(\hat{x}, \hat{t})), \quad \left(-\hat{\Psi}_{\xi,s}, -\hat{\Psi}_{\xi,y}, Y\right) \in \overline{\mathcal{P}}^{2,-}(v(\hat{y}, \hat{s})). \quad (7.33)$$

Case i: $\hat{x} \neq 0$ and $\hat{y} \neq 0$. We first assume that $\hat{x} \neq 0$ and $\hat{y} \neq 0$. Then by Lemma 9, there exists $(l_i, p_i, X_i) \in \mathcal{P}^{2,+}(u(x_i, t_i))$ such that $(x_i, t_i) \rightarrow (\hat{x}, \hat{t})$, $l_i \rightarrow \hat{\Psi}_{\xi,t}$, $p_i \rightarrow \hat{\Psi}_{\xi,x}$, $X_i \rightarrow X$ and similarly, there exists $(h_i, q_i, Y_i) \in \mathcal{P}^{2,-}(v(y_i, s_i))$ such that $(y_i, s_i) \rightarrow (\hat{y}, \hat{s})$, $h_i \rightarrow -\hat{\Psi}_{\xi,s}$, $q_i \rightarrow -\hat{\Psi}_{\xi,y}$, and $Y_i \rightarrow Y$.

Since u, v are proper sub- and supersolutions, in view of Remark 14, we obtain

$$l_i - k(p_i, X_i) \leq 0 \quad (7.34)$$

$$-h_j - k(q_j, Y_j) \geq 0 \quad (7.35)$$

Since $p := \hat{\Psi}_{\xi,x} = -\hat{\Psi}_{\xi,y} \neq 0$, k is continuous at $(\hat{\Psi}_{\xi,x}, X)$ and $(-\hat{\Psi}_{\xi,y}, Y)$. Hence, passing to the limit $i \rightarrow \infty$ and $j \rightarrow \infty$ yields

$$\hat{\Psi}_{\xi,t} - k(\hat{\Psi}_{\xi,x}, X) \leq 0 \quad (7.36)$$

$$-\hat{\Psi}_{\xi,s} - k(-\hat{\Psi}_{\xi,y}, Y) \geq 0 \quad (7.37)$$

Furthermore, combining inequalities (7.37) and (7.36) yields

$$\hat{\Psi}_{\xi,t} + \hat{\Psi}_{\xi,s} \leq k(\hat{y}, p, Y) - k(\hat{x}, p, X) \leq 0. \text{ The last inequality is due to the ellipticity of}$$

$-k$ and the fact that $X \leq Y$. Therefore, we establish a contradiction:

$$0 < \frac{\gamma}{(T-t)^2} + \frac{\gamma}{(T-s)^2} = \hat{\Psi}_{\xi,t} + \hat{\Psi}_{\xi,s} \leq 0. \quad (7.38)$$

Case ii: $\hat{x} = 0$ or $\hat{y} = 0$. Suppose that $\hat{x} = 0$ or $\hat{y} = 0$ for all $|\xi| \leq \kappa(\epsilon)$ for which $|x - y - \xi| \neq 0$ (non-diagonal). First, let us assume

$$\left(\hat{\Psi}_{\xi,t}, \hat{\Psi}_{\xi,x}, X\right) \in \mathcal{P}^{2,+}(u(\hat{x}, \hat{t})), \quad \left(-\hat{\Psi}_{\xi,s}, -\hat{\Psi}_{\xi,y}, Y\right) \in \mathcal{P}^{2,-}(v(\hat{y}, \hat{s})). \quad (7.39)$$

- **Suppose that $\xi = 0$.** Then $\hat{x} = 0$ or $\hat{y} = 0$ would respectively lead to

$$\hat{\Psi}_{\xi,x} = -\hat{y} < 0 \text{ or } -\hat{\Psi}_{\xi,y} = \hat{x} > 0. \text{ Both of these inequalities contradict the}$$

Neumann boundary condition for sub- and super-solution (recall Remark 15).

- **Suppose that $\xi > 0$.** If $\hat{x} = 0$, then $\hat{\Psi}_{\xi,x} = -\hat{y} - \xi < 0$, which again contradicts the Neumann boundary condition for subsolution. So let us suppose that $\hat{y} = 0$. In order for u to satisfy the Neumann boundary condition for subsolution, $\hat{\Psi}_{\xi,x}$ must satisfy $\hat{\Psi}_{\xi,x} \leq 0$. Moreover, since other scenarios can fall into the cases we have already addressed, the only remaining situation to consider is when $\hat{\Psi}_{\xi,x}$ stays positive as $\xi \rightarrow 0$. We now make the ξ -dependence in \hat{x} explicit by denoting $x_\xi = \hat{x}$. Recall:

$$k(\hat{x}, \hat{\Psi}_{\xi,x}, X) = \frac{1}{x_\xi} \text{sign}(\hat{\Psi}_{\xi,x}) + 2g|\hat{\Psi}_{\xi,x}|X + \frac{g}{x_\xi} \hat{\Psi}_{\xi,x}|\hat{\Psi}_{\xi,x}|. \quad (7.40)$$

Then due to the sign of $\hat{\Psi}_{\xi,x}$ and the fact that $x_\xi \rightarrow y_\xi = 0$ as $\xi \rightarrow 0$, we obtain

$$\liminf_{\xi \rightarrow 0^+} \frac{1}{x_\xi} \text{sign}(\hat{\Psi}_{\xi,x}) + \frac{g}{x_\xi} \hat{\Psi}_{\xi,x} |\hat{\Psi}_{\xi,x}| > \liminf_{\xi \rightarrow 0} \frac{1}{x_\xi} = +\infty \quad (7.41)$$

By the boundedness of other terms, we deduce from (7.41) that

$$\hat{\Psi}_{\xi,t} - k(\hat{x}, \hat{\Psi}_{\xi,x}, X) > 0 \quad (7.42)$$

for small enough ξ and this contradicts the definition of sub-solution.

- **Suppose that $\xi < 0$.** By symmetry, the argument leading to a contradiction in this case is parallel to one for $\xi > 0$ with the role of x and y reversed.

Finally, we conclude this proof by noting that due to the nature of the Neumann boundary condition and the lower/upper semicontinuity of \overline{G} and \underline{G} (see, 15), the above argument extends to the full problem in which

$$\left(\hat{\Psi}_{\xi,t}, \hat{\Psi}_{\xi,x}, X \right) \in \overline{\mathcal{P}^{2,+}}(u(\hat{x}, \hat{t})), \quad \left(-\hat{\Psi}_{\xi,s}, -\hat{\Psi}_{\xi,y}, Y \right) \in \overline{\mathcal{P}^{2,-}}(v(\hat{y}, \hat{s})). \quad (7.43)$$

□

Chapter 8: Existence

The main objective of this section is to show the existence of proper viscosity solutions for a class of initial conditions that in particular includes a conical initial condition. To do so, we first regularize the equation so that singularities are smoothed out and the domain is restricted to a finite area. We then construct barriers to show that the solutions of the regularized equation satisfy the far field condition for all $t \geq 0$ in the limit of the infinitely large domain. Therefore, we derive (5.2) as a limit of a series of degenerate parabolic equations. Fix a continuous function $h_0(r)$, $r \in [0, \infty)$ that satisfies a far-field condition

$$|h_0(r) - (\gamma + \ell r)| \leq C e^{-Ar} \quad (8.1)$$

for some constants $\gamma \in \mathbf{R}$, $\ell < 0$, $A, C > 0$.

8.1 Regularized equations

We start by regularizing (5.2).

We consider the following equation with parameters $c, \epsilon, \delta > 0$. In $[0, R] \subset \mathbf{R}$, we define

$$a(s) = \frac{s}{(s^2 + \epsilon)^{1/2}}, \quad \psi_c(s) = \max(1/c, s), \quad (8.2)$$

and consider the equation

$$h_t = \left[g\psi_c(|h_r|) + \frac{1}{2}a'(h_r) \right] h_{rr} + \frac{g}{\delta + r} \text{sign}(h_r) \psi_c(|h_r|^2) + \frac{1}{\delta + r} a(h_r). \quad (8.3)$$

Note that $a'(s) = \frac{\epsilon}{(s^2 + \epsilon)^{3/2}}$. Equation (8.3) is accompanied by a Neumann boundary condition $h_r = -\gamma$ at $\partial B_R(0)$, $h(r, 0) = h_0(r)$. Note that (8.3) is no longer singular in the limit $|h_r| \rightarrow \infty, r \rightarrow \infty$ and $|h_r| = 0, r = 0$. The coefficient for h_{rr} is $g\psi_c(|h_r|) + \frac{1}{2}a'(h_r) > 0$ so (8.3) is uniformly parabolic and we can apply a standard theory of uniformly parabolic equations: By Theorem 12.22 of [60], there exists a solution $h(r, t; \epsilon, \delta, c, R) \in C(\bar{\Omega}) \cap C^{2,1}(\Omega)$.

8.2 Bound for h_r

In order to get some bound on h_r that are independent of ϵ, δ, c , and R , we note that $v := h_r$ is a solution of the following equation:

$$\begin{aligned} v_t = & \left[g\psi_c(|v|) + \frac{1}{2}a'(v) \right] v_{rr} + \left[g\text{sign}(v) + \frac{1}{2}a''(v) \right] (v_r)^2 \\ & + \left[\frac{2}{r + \delta}\psi_c(|v|) + \frac{1}{r + \delta}a'(v) \right] v_r - \frac{g}{(r + \delta)^2} [\psi_c(|v|) + a(v)] \end{aligned} \quad (8.4)$$

with boundary condition $v = -\gamma$ at $r = R$, $v = 0$ at $r = 0$.

Since $g\psi_c(|v|) + \frac{1}{2}a'(v) > 0$, by a classic theory of parabolic differential equations(see, [60, Theorem 12.22]), there exists a solution

$v(r, t; \epsilon, \delta, c, R) \in C([0, R]) \cap C^{2,1}(0, R)$ that is bounded uniformly in δ, c, ϵ, R by the maximum principle. Therefore, we have proven the following lemma:

Lemma 10. $-\theta \leq h_r \leq 0$ for all parameters ϵ, δ, c, R , where $\theta = \max(\|(h_0)_r\|_\infty, \gamma)$.

Remark 16. Due to the bound on v , h is also bounded locally in L^∞ and so for c small enough, we have $\psi_c(|v|) = |v|$. Thus, we may rewrite (8.3) as

$$h_t = \left[g|h_r| + \frac{1}{2}a'(h_r) \right] h_{rr} + \frac{g}{\delta + r}\text{sign}(h_r)|h_r|^2 + \frac{1}{\delta + r}a(h_r). \quad (8.5)$$

Or equivalently,

$$h_t = \frac{1}{2(r+\delta)^2} \frac{\partial}{\partial r} [(r+\delta)^2 a(h_r)] + \frac{g}{3(r+\delta)} \frac{\partial}{\partial r} [(r+\delta)|h_r|^3] \quad (8.6)$$

8.3 Application of Arzelà-Ascoli theorem

In this section, we show that the sequence of solutions from the last section converge by application of Arzelà-Ascoli theorem. We start by proving the following lemma:

Lemma 11. *There exists a constant $C > 0$ independent of ϵ, δ, R such that for $h(x, t) := (h(\cdot, \cdot; \epsilon, \delta, c, R))_{\epsilon, \delta, c, R}$, the following Hölder inequality holds:*

$$|h(x, t_2) - h(x, t_1)| \leq C |t_2 - t_1|^{1/2}. \quad (8.7)$$

Proof. Rewrite (8.6) as

$$2(r+\delta)^2 h_t = \frac{\partial}{\partial r} [(r+\delta)^2 a(h_r)] + \frac{2g(r+\delta)}{3} \frac{\partial}{\partial r} [(r+\delta)|h_r|^3]. \quad (8.8)$$

Next, we integrate both sides of (8.8) from $x \in (0, R]$ to $x+r$ and find bounds for each term. Here, $r > 0$ is to be chosen later. Since the exact values of the constants used in the bounds do not matter, we will use $C > 0$ for all the constants for the ease of notation. Each term of the right hand side of (8.8) is bounded by:

$$\begin{aligned} \int_x^{x+r} \frac{\partial}{\partial y} [(r+\delta)^2 a(h_r)] dy &= (x+r+\delta)^2 a(h_r) - (x+\delta)^2 a(h_r) \\ &\leq C [(x+r+\delta)^2 - (x+\delta)^2] \end{aligned} \quad (8.9)$$

$$\int_x^{x+r} \frac{2g(y+\delta)}{3} [(y+\delta)|h_y|^3]_y dy = C(x+r+\delta) [(x+r+\delta) - (x+\delta)] \quad (8.10)$$

because $|h_y|$ is uniformly bounded by a constant $\gamma > 0$ independent of the parameters ϵ, δ, c and R .

Also,

$$\int_x^{x+r} 2(y + \delta)^2 h_t \, dy = 2\partial_t \int_x^{x+r} (y + \delta)^2 h \, dy \quad (8.11)$$

So integrating (8.8) in time from $t = t_1$ to $t = t_2$ and using (8.9)-(8.11) yields a bound:

$$\begin{aligned} \int_x^{x+r} (y + \delta)^2 h(y, t_2) \, dy &\leq \int_x^{x+r} (y + \delta)^2 h(y, t_1) \, dy \\ &\quad + C \{ [(x + r + \delta)^2 - (x + \delta)^2] + r(x + r + \delta) \} \end{aligned} \quad (8.12)$$

On the other hand, because $h(y, t)$ is Lipschitz uniformly in the parameters ϵ, δ, c, R , we have

$$\left| \int_x^{x+r} (y + \delta)^2 h(y, t) \, dy - h(x, t) \int_x^{x+r} (y + \delta)^2 \, dy \right| \leq Cr^3. \quad (8.13)$$

So

$$\begin{aligned} |h(x, t_2) - h(x, t_1)| &\leq Cr + (t_2 - t_1) \left[\int_x^{x+r} (y + \delta)^2 \, dy \right]^{-1} \times \\ &\quad C \{ [(x + r + \delta)^2 - (x + \delta)^2] + r(x + r + \delta) \} \end{aligned} \quad (8.14)$$

$$\begin{aligned} &\leq Cr + |t_2 - t_1| \left[\int_x^{x+r} (y + \delta)^2 \, dy \right]^{-1} \times \\ &\quad C \{ (x + r + \delta)^2 + r(x + r + \delta) \}. \end{aligned} \quad (8.15)$$

By choosing $r = (t_2 - t_1)^{1/2}$, we obtain

$$\begin{aligned} |h(x, t_2) - h(x, t_1)| &\leq C|t_2 - t_1|^{1/2} + |t_2 - t_1| \left[\int_x^{x+r} (y + \delta)^2 \, dy \right]^{-1} \times \\ &\quad C \{ (x + r + \delta)^2 + r(x + r + \delta) \} \end{aligned} \quad (8.16)$$

Note that

$$\int_x^{x+r} (y + \delta)^2 dy \geq \int_0^r y^2 dy = \frac{1}{3}r^3 \quad (8.17a)$$

$$\int_x^{x+r} (y + \delta)^2 dy \geq (x + \delta)^2 r. \quad (8.17b)$$

Therefore, if $x + \delta \leq |t_2 - t_1|^{1/2} = r$, then by using (8.17a),

$$\begin{aligned} |h(x, t_2) - h(x, t_1)| &\leq C|t_2 - t_1|^{1/2} + C \frac{|t_2 - t_1|}{r^3} \{|t_2 - t_1| + |t_2 - t_1|\} \\ &\leq C|t_2 - t_1|^{1/2} \end{aligned} \quad (8.18)$$

And if $x + \delta \geq |t_2 - t_1|^{1/2} = r$, then by using (8.17b),

$$\begin{aligned} |h(x, t_2) - h(x, t_1)| &\leq C|t_2 - t_1|^{1/2} + \frac{|t_2 - t_1|}{(x + \delta)^2 r} \{C(x + r + \delta)^2 + Cr(x + r + \delta)^2\} \\ &\leq C|t_2 - t_1|^{1/2} + \frac{|t_2 - t_1|}{(x + \delta)^2 r} \{C(x + \delta)^2 + Cr(x + r + \delta)\} \\ &\leq C \left(|t_2 - t_1|^{1/2} + |t_2 - t_1| \frac{(x + r + \delta)}{(x + \delta)^2} \right) \\ &\leq C \left(|t_2 - t_1|^{1/2} + |t_2 - t_1| \frac{1}{(x + \delta)} \right) \\ &\leq C|t_2 - t_1|^{1/2} \end{aligned} \quad (8.19)$$

□

Therefore, with this Hölder bound in the time variable we conclude that we may apply Arzelà-Ascoli's theorem. So $(h(\cdot, \cdot; \epsilon, \delta, c, R))_{\epsilon, \delta, c, R}$ is in a compact subset of $C(\mathcal{K})$ for any $\mathcal{K} \subset\subset C(\mathbf{R}^3)$. By this compactness, we can extract a converging sequence from

$(h(\cdot, \cdot; \epsilon, \delta, c, R))_{\epsilon, \delta, c, R}$ with a limit $h(y, t)$.

Remark 17. An important consequence of the maximum principle for $h_r(\cdot, \cdot; \epsilon, \delta, c, R)$ is that (1) If the initial data for $h_0(t)$ is monotone, then $h(r, t)$ stays monotone (2) $|h_r|$ also stays bounded.

8.4 Far-field condition

In this section, we construct barriers in order to show that the function $h(y, t)$ found in the previous section satisfies the far-field condition.

Consider an ansatz $v(r, t) = \gamma + \ell r + C e^{-Ar+Bt}$ where $A, C > 0$, $0 > \ell$, $\gamma \in \mathbf{R}$ are constants used from the equation (8.1) and $B > 0$ is to be chosen. Then we have

$$v_t = C B e^{-Ar+Bt} \quad (8.20)$$

$$v_r = \ell - C A e^{-Ar+Bt} \quad (8.21)$$

$$v_{rr} = C A^2 e^{-Ar+Bt}. \quad (8.22)$$

Applying the ansatz to the left-hand side of (8.3) yields an expression

$$\mathcal{K} = K_1 + K_2 + K_3, \quad (8.23)$$

where

$$K_1 = \left[g|v_r| + \frac{1}{2} \frac{\epsilon}{(|v_r|^2 + \epsilon)^{3/2}} \right] v_{rr}, \quad (8.24a)$$

$$K_2 = \text{sign}(v_r) \frac{g}{\delta + r} v_r^2, \quad (8.24b)$$

$$K_3 = \frac{1}{\delta + r} \frac{v_r}{(v_r^2 + \epsilon)^{1/2}}. \quad (8.24c)$$

Note that we have the following inequalities: $\frac{1}{r+\delta} \leq 1/\delta$, $\frac{\epsilon}{(|v_r|^2 + \epsilon)^{3/2}} \leq \frac{\epsilon}{\ell^3}$,

$\frac{v}{\sqrt{|v|^2 + \epsilon}} \leq \max(1, \epsilon^{-1})$, $v_r \leq 0$, $v_{rr} \geq 0$. So

$$K_1 \leq \left[g|\ell - C A e^{-Ar+Bt}| + \frac{1}{2} \frac{\epsilon}{\ell^3} \right] v_{rr} = \left[g(-\ell + C A e^{-Ar+Bt}) + \frac{1}{2} \frac{\epsilon}{\ell^3} \right] C A^2 e^{-Ar+Bt}, \quad (8.25)$$

$$K_2 = -\frac{g}{\delta+r}v_r^2 \leq 0, \quad (8.26)$$

and

$$K_3 = \frac{1}{(\delta+r)} \frac{v_r}{(v_r^2 + \epsilon)^{1/2}} \leq 0. \quad (8.27)$$

Therefore, combining equations (8.25)-(8.27) with (8.23) yields

$$\begin{aligned} v_t - \mathcal{K} &= v_t - K_1 - K_2 - K_3 \\ &\geq v_t - K_1 \\ &\geq \left[B + g\ell A^2 - gCA^3 - \frac{\epsilon}{|\ell|^3} A^2 \right] Ce^{-Ar+Bt}. \end{aligned} \quad (8.28)$$

Choose $B \geq -g\ell A^2 + gCA^3 + \frac{A^2}{|\ell|^3}$. Then for all $\epsilon \leq 1$, (8.28) is nonnegative. Thus, we found a super solution v of (8.3) that is chosen independent of ϵ , δ , and R . It can be similarly shown that $u = (\gamma + \ell r) - Ce^{-Ar+Bt}$ is a subsolution for the same choice of B . Since $u(r, 0) \leq h_0(r) \leq v(r, 0)$, by the maximum principle for the solution $h(r, t; \epsilon, \delta, R)$ of the problem (8.3), we attain that

$$u(r, t) \leq h(r, t; \epsilon, \delta, R) \leq v(r, t) \quad (8.29)$$

for all $\epsilon, \delta, R > 0$. Since the choice of u and v do not depend on the parameters ϵ, δ, R , by passing (8.29) to the limit $\epsilon, \delta \rightarrow 0$ and $R \rightarrow \infty$, we conclude that the limit $h(r, t)$ from the previous section satisfy the far-field condition.

8.5 Proper viscosity solution

Away from $r = 0$, (8.30) is parabolic. So by a classical theory of second order parabolic equations (see, [60, Theorem 12.22]), we have the following lemma:

Lemma 12. *Suppose that $u_{\epsilon,\delta}(r,t)$ is a sequence of solutions to (8.6). In the limit $\delta \rightarrow 0$, $u_{\epsilon,\delta}(r,t)$, $r \in (0, R)$, $t \in (0, T)$, approach locally uniformly to $u_\epsilon \in C^2((0, R) \times (0, T))$, which satisfies a parabolic equation*

$$u_t = \left[g|u_r| + \frac{1}{2}a'(u_r) \right] u_{rr} + \frac{g}{r} \text{sign}(u_r)|u_r|^2 + \frac{1}{r}a(u_r) \quad (8.30)$$

in classical sense. Moreover, $u_\epsilon \in C^0([0, R] \times (0, T)) \cap \text{Lip}([0, R] \times (0, T))$ and u_ϵ also satisfies the Neumann condition $u_r(0, t) = 0$ in the viscosity sense for all $t > 0$.

Proof. We only check the viscosity Neumann condition of Lemma 12 since the rest of the above statement is classical. Let ϕ be a C^2 -test function such that $\max(u_\epsilon - \phi)$ is achieved at $(0, \hat{t})$ and suppose by contradiction that $-\partial_r \phi(0, \hat{t}) > 0$. Then by the convergence of maximum points [13, 34], there exist sequences $t^\delta \rightarrow \hat{t}$ and $r^\delta \rightarrow 0$ such that $u_{\epsilon,\delta} - \phi$ achieves its maximum at (r^δ, t^δ) where $u_{\epsilon,\delta}$ is the solution of (8.3). Now, for small enough δ , $-\partial_r \phi(r^\delta, t^\delta) > 0$ by the continuity of ϕ . So r^δ cannot be 0 for a small enough δ because this would contradict the Neumann condition for $u_{\epsilon,\delta}$. Therefore, for small enough $\delta > 0$, we have $r^\delta \neq 0$. Again by continuity, we also have $-\partial_r \phi(r^\delta, t^\delta) > \eta > 0$. However, this implies that

$$-\frac{1}{r^\delta + \delta} \partial_r \phi(r^\delta, t^\delta) \rightarrow +\infty \quad \text{as } \delta \rightarrow 0. \quad (8.31)$$

Note that when evaluating (8.3) at (r^δ, t^δ) and $h = \phi$, other terms in equation (8.3) are either bounded or have the same sign as (8.31). Since the classical solution $u_{\epsilon,\delta}$ is also a subsolution of (8.3), the limit (8.31) contradicts the definition of subsolution.

Therefore, with this contradiction, we conclude that $-\partial_r \phi(0, \hat{t}) < 0$ and u_ϵ satisfies the Neumann condition in the sense of subsolution. We can similarly show that u_ϵ satisfies the Neumann condition in the sense of supersolution. Therefore, u_ϵ satisfies the Neumann condition in the viscosity sense. □

Finally, we conclude this chapter by showing that the limit of the solutions to (8.30) is indeed a proper viscosity solution of the problem (5.2). We follow an argument parallel to the proof for the stability theorem in [31, Theorem 5.2].

Theorem 7. *Suppose that $u_m : [0, R] \rightarrow \infty$ is a solution to*

$$u_t = \left[g|u_r| + \frac{1}{2}a'_m(u_r) \right] u_{rr} + \frac{g}{r} \text{sign}(u_r)|u_r|^2 + \frac{1}{r}a_m(u_r). \quad (8.32)$$

with

$$a_m(s) = \frac{s}{(s^2 + m^{-2})^{1/2}}, \quad m \rightarrow \infty \quad (8.33)$$

If u_m is converging as $m \rightarrow \infty$ with a limit u , then u is a proper viscosity solution to (5.2).

To check the conventional test, one follows the usual procedure (see, [19, Lemma 6.1]).

So here, we focus on the faceted test.

Proof. Let $\phi(r, t) = f(r) + g(t)$, $r \in [0, R]$, be an admissible test function in a general position of radius $\eta > 0$ at (\hat{r}, \hat{t}) with respect to u . By definition, f is a Lipschitz support function of some test pair (Ω_-, Ω_+) with some Lipschitz constant $L > 0$. If $\hat{r} = 0$ (this is only possible if $\Omega_+ = \emptyset$), then by making η smaller if necessary, we notice that $\phi(r, t)$ is also in general position of u at some $r \in \Omega_-$ nearby 0. Therefore, we may assume $\hat{r} \neq 0$ without loss of generality. Observe that the definition also ensures $f(\hat{r} - z) = 0$ for all $|z| \leq \eta$. We set $\delta = \eta/4$.

The main idea of this proof is to construct admissible test functions for u_m that converge to $\phi(r, t)$ in some sense. In order to make sense of this convergence while addressing the singularity in $r^{-2}\partial(r^2 f_r/|f_r|)$ when $f_r = 0$, we turn to resolvent problems. Rather than directly using the convergence of the sequence of solutions u_m of (8.32) to the solution u of (5.2), we will compare the respective resolvent problems of (8.32) and (5.2).

To that end, define a singular energy $E : L^2(B_R(0)) \rightarrow \mathbf{R} \cup \{+\infty\}$ where $B_R(0) \subset \mathbf{R}^3$.

$$E(\psi) = \begin{cases} \int \left(\frac{1}{2} |\nabla \psi|^2 + \frac{g}{3} |\nabla \psi|^3 \right) dx & \text{for } \psi \in BV(B_R(0)) \cap L^2(B_R(0)) \text{ and } |\nabla \psi| \in L^3(B_R(0)), \\ +\infty & \text{otherwise} \end{cases}, \quad (8.34)$$

and a smooth approximation of E parameterized by $m \in \mathbb{N}$:

$$E_m(\psi) = \begin{cases} \int \left(\frac{1}{2} \sqrt{|\nabla \psi|^2 + m^{-2}} + \frac{g}{3} |\nabla \psi|^3 \right) dx & \text{for } \psi \in H^1(B_R(0)), |\nabla \psi| \in L^3(B_R(0)) \\ +\infty & \text{otherwise} \end{cases}. \quad (8.35)$$

Then for any $\psi \in \mathcal{D}(\partial E_m)$, the subdifferential $\partial E_m(\psi)$ is a singleton and its only element (thus, clearly this is the canonical restriction $\partial^0 E_m$) has a formula

$$\partial^0 E_m(\psi) = -\operatorname{div} \left[\frac{\nabla \psi}{2(|\nabla \psi|^2 + m^{-2})^{1/2}} + g |\nabla \psi| \nabla \psi \right]. \quad (8.36)$$

In the rest of this section, we replace the support function $f : [0, R] \rightarrow \mathbf{R}$ with a radially symmetric function $\tilde{f}(x, t) = f(|r|, t)$ and drop the tilde from \tilde{f} for the ease of notation.

The following lemma whose proof is provided in [31] provides a priori gradient bounds for the solutions of the resolvent problems, which will be crucial in passing to the limit $m \rightarrow 0$.

Lemma 13. *Let $f(x) \in Lip(B_R(0))$. Then for positive constants m, τ, ϵ , the resolvent problems:*

$$f_\tau + \tau \partial E(f_\tau) \ni \epsilon f \quad (8.37)$$

$$f_{\tau,m} + \tau \partial E_m(f_{\tau,m}) \ni \epsilon f \quad (8.38)$$

admit unique Lipschitz continuous solutions f_τ and $f_{\tau,m}$ respectively. Also these solutions satisfy Lipschitz bounds

$$\|\nabla f_\tau\|_\infty, \|\nabla f_{\tau,m}\|_\infty \leq \epsilon \|\nabla f\|_\infty. \quad (8.39)$$

Moreover, $f_{\tau,m} \in C^{2,\alpha}(B_R(0))$ for some $\alpha > 0$.

Define

$$h_\tau = \frac{f_\tau - \epsilon f}{\tau}, \quad h_{\tau,m} = \frac{f_{\tau,m} - \epsilon f}{\tau} = -\partial^0 E_m(f_{\tau,m}), \quad (8.40)$$

where the last equality comes from the fact that $\partial^0 E_m(f_{\tau,m})$ is a singleton. If furthermore, $f \in \mathcal{D}(\partial E)$, then also

$$h_\tau \rightarrow -\partial^0 E(\epsilon f) \quad \text{strongly in } L^2(B_R(0)) \text{ as } \tau \rightarrow 0. \quad (8.41)$$

Roughly speaking, $f_{\tau,m}$, f_τ play the role of approximate support functions.

Since ϕ is in general position of radius η with respect to u , there is room for perturbation. For $\delta := \eta/4$, let z be a vector satisfying $|z| < \delta$ and

$$f_\tau(\hat{x} - z) = \min_{B_\delta(\hat{x})} f_\tau. \quad (8.42)$$

Then by [31, Lemma 5.4], we obtain a bound

$$u(x, t) - \epsilon \inf_{|z| < \delta} f(x - z) - g(t) < u(\hat{x}, \hat{t}) - g(\hat{t}) \quad t \in [\hat{t} - \eta, \hat{t} + \eta] \setminus \hat{t}, \quad (8.43)$$

whenever $x \in U^\eta \cap Z^\eta$, where $U := \{u(\cdot, \hat{t}) \geq u(\hat{r}, \hat{t})\}$ and $Z := \{f \leq 0\}$.

Since f_τ uniformly converges to ϵf , the bound (8.43) implies that

$u(x, t) - f_\tau(x - z) - g(t)$ achieves a maxima on $(U^\eta \cap Z^\eta) \times [\hat{t} - \delta, \hat{t} + \delta]$ for small enough τ . Let (x_τ, t_τ) , $x_\tau \neq 0$, be a point of maxima for

$$(x, t) \mapsto u(x, t) - f_\tau(x - z) - g(t). \quad (8.44)$$

Subsequently, by the uniform convergence $f_{\tau, m} \rightarrow f_\tau$, there exists a sequence

$(x_{\tau, m}, t_{\tau, m}) \xrightarrow{m \rightarrow 0} (x_\tau, t_\tau)$ such that the mapping

$$(x, t) \mapsto u_m(x, t) - f_{\tau, m}(x - z) - g(t) \quad (8.45)$$

attains its maxima at $(x_{\tau, m}, t_{\tau, m})$. Here, let m be small enough so that $x_{\tau, m} \neq 0$.

Then since u_m is a viscosity solution to a regularized problem, with a test function

$$f_{\tau, m} \in C^{2, \alpha},$$

$$g'(t_{\tau, m}) + \partial E_m(h_{\tau, m})(x_{\tau, m} - z) + \frac{g}{|x_{\tau, m}|} |\nabla f_{\tau, m}(x_{\tau, m} - z)| \nabla f_{\tau, m}(x_{\tau, m} - z) \cdot \nu_r \leq 0. \quad (8.46)$$

By definition of $h_{\tau, m}$, this is equivalent to

$$g'(t_{\tau, m}) - h_{\tau, m}(x_{\tau, m} - z) + \frac{g}{|x_{\tau, m}|} |\nabla f_{\tau, m}(x_{\tau, m} - z)| \nabla f_{\tau, m}(x_{\tau, m} - z) \cdot \nu_r \leq 0. \quad (8.47)$$

Now, by the Lipschitz bound (8.39), there exists a vector p_τ such that a subsequence of

$\nabla f_{\tau, m}(x_{\tau, m} - z)$ converges to p_τ and $|p_\tau| \leq \epsilon \|\nabla f\|_\infty = \epsilon L$. Since $\hat{x} \neq 0$, x_τ is also

nonzero for sufficiently small τ by the virtue of the continuity of g and the rest of the

left-hand side of (8.47) at x_τ . Therefore, in the limit of $m \rightarrow \infty$, we obtain

$$g'(t_\tau) - h_\tau(x_\tau - z) + \frac{g}{|x_\tau|} |p_\tau| p_\tau \cdot \nu_r \leq 0. \quad (8.48)$$

Next, the following lemma [31, Lemma 5.5] provides a bound for $h_\tau(x_\tau - z)$.

Lemma 14.

$$h_\tau(x_\tau - z) \leq h_\tau(\hat{x} - z) = \min_{\overline{B}_\delta(\hat{x})} h_\tau \quad (8.49)$$

Applying Lemma 14 to (8.48), we arrive at

$$g'(t_\tau) - \min_{\overline{B}_\delta(\hat{x})} h_\tau + \frac{g}{|x_\tau|} |p_\tau| p_\tau \nu_r \leq g'(t_\tau) - h_\tau(x_\tau - z) + \frac{g}{|x_\tau|} |p_\tau| p_\tau \nu_r \leq 0. \quad (8.50)$$

Furthermore, since $|p_\tau| < \epsilon L$, we can choose a subsequence that converges to a limit \hat{p} as $a \rightarrow 0$. Thus, in the limit of $\tau \rightarrow 0$,

$$g'(\hat{t}) - \liminf_{\tau \rightarrow 0} \min_{\overline{B}_\delta(\hat{x})} h_\tau + \frac{g}{|\hat{x}|} |\hat{p}| \hat{p} \cdot \nu_r \leq 0. \quad (8.51)$$

Finally, we take $\epsilon \rightarrow 0$ in (8.51). By Lemma 13, $h_\tau \rightarrow -\partial^0 E(\epsilon f)$ in L^2 as $\tau \rightarrow 0$. On the other hand, $\overline{B}_\delta(\hat{x})$ is contained in the facet $\Omega_- \setminus \Omega_+$, so for any $x \in \overline{B}_\delta(\hat{x})$, we also have

$$-\partial^0 E(\epsilon f)(x) = \Lambda(\Omega_-, \Omega_+) = 3 \frac{R_-^2 - R_+^2}{R_-^3 - R_+^3}. \quad (8.52)$$

Furthermore, $|\hat{p}| \leq \epsilon L \rightarrow 0$ as $\epsilon \rightarrow 0$. Hence (8.51) approaches

$$g'(\hat{t}) - 3 \frac{R_-^2 - R_+^2}{R_-^3 - R_+^3} \leq 0 \quad (8.53)$$

as $\epsilon \rightarrow 0$.

Therefore, h satisfies the faceted test with respect to an arbitrary faceted test function $\phi(x, t)$. Consequently, h is a proper viscosity sub-solution; furthermore, it can be similarly shown that h is also a super-solution. Hence, h is indeed a proper viscosity solution. \square

Appendix A: Computations for facets in (1+1)D

A.1 Second-order difference scheme

Consider the difference scheme

$$\psi_{j+1} - 2\psi_j + \psi_{j-1} = f_j, \quad j = 0, \dots, N-1; \quad \psi_{-1} = 0 = \psi_N, \quad (\text{A.1})$$

where f_j can be time dependent but the time is suppressed since it is immaterial here.

By multiplying (A.1) by s^j and summing over j we have

$$s^{-1}[\Psi(s) - \psi_0 + \psi_N s^N] - 2\Psi(s) + s[\Psi(s) + \psi_{-1}s^{-1} - \psi_{N-1}s^{N-1}] = F(s),$$

where $F(s)$ is defined in (2.25). Thus, we obtain

$$\Psi(s) = \frac{\psi_0 - \psi_{-1}s - \psi_N s^N + \psi_{N-1}s^{N+1} + sF(s)}{(1-s)^2} = \frac{\mathcal{P}(s)}{(1-s)^2}, \quad (\text{A.2})$$

which leads to (2.25) by virtue of the termination conditions. The point $s = 1$ is a removable singularity provided $\mathcal{P}(1) = 0 = \mathcal{P}'(1)$, which yield (2.26).

The coefficient of s^j in $\Psi(s)$ is given by (2.20). By restricting the contour Γ in the interior of the unit disk ($|\zeta| < 1$) and eliminating analytic terms, we have

$$\psi_j = \frac{1}{2\pi i} \oint_{\Gamma} \frac{\psi_0 + \zeta F(\zeta)}{(1-\zeta)^2} \frac{d\zeta}{\zeta^{j+1}}, \quad j = 0, \dots, N-1. \quad (\text{A.3})$$

Recalling the binomial expansion $(1-\zeta)^{-2} = \sum_{k=0}^{\infty} (1+k)\zeta^k$, we find the series

$$\frac{\psi_0 + \zeta F(\zeta)}{(1-\zeta)^2} = \psi_0 + \sum_{l=0}^{\infty} \zeta^{l+1} \left[l+2 + \sum_{p=0}^l (1+l-p)f_p \right]. \quad (\text{A.4})$$

The coefficient of ζ^j is singled out for $l = j - 1$; thus, by (A.3) we recover (2.27). The derivation of (2.38) and (2.39) follows from the same procedure.

A.2 Extensions

In this section we discuss two possible extensions of our formulation. First, we address different laws of nearest-neighbor step interactions; in this case, the slope behavior, i.e., the exponent $1/2$ (see Remarks 3 and 6), at facet edges is modified accordingly. Second, we propose a “*toy model*” where the kinetics of attachment-detachment for extremal steps are different from the kinetics for other steps. Our discussion aims to indicate the role that individual steps may play in the derivation of boundary conditions in the continuum setting.

Another plausible extension concerns the presence of an Ehrlich-Schwoebel barrier, by which the attachment-detachment law for all steps is characterized by different kinetic rates, say k_u and k_d , for up- and down-steps [20, 93]. In this case, the effective kinetic rate for the adatom flux is the harmonic average of k_u and k_d [64]. Our analysis remains essentially intact, leading to the same form of continuum laws. This case is not discussed any further.

A.2.1 Multipole nearest-neighbor step interactions

In this section, we discuss continuum-scale implications of the step energy [64]

$$E_N(\{x_j\}_{j=0}^N) = \frac{1}{\alpha} \sum_{i=0}^{N-1} \left(\frac{\epsilon}{x_{i+1} - x_i} \right)^\alpha = \frac{1}{\alpha} \sum_{i=0}^{N-1} m_i^\alpha \quad \alpha > 1, \quad (\text{A.5})$$

which in principle includes step multipole interactions for integer $\alpha \geq 2$ [78]; $\alpha = 2$ for dipole step interactions. The j th-step chemical potential is

$$\mu_j = \frac{\delta E_N}{\delta x_j} = \epsilon^{-1} (m_j^{\alpha+1} - m_{j-1}^{\alpha+1}), \quad j = 1, \dots, N-1; \quad (\text{A.6})$$

in addition, $\mu_0 = \epsilon^{-1} m_0^{\alpha+1}$ and $\mu_N = -\epsilon^{-1} m_{N-1}^{\alpha+1}$. Formulas for the adatom flux and step velocity ensue from Section 2.1 via $m_j^3 \mapsto m_j^{\alpha+1}$ in μ_j .

For instance, in DL kinetics the discrete scheme for steps now reads

$$\begin{aligned} \frac{\dot{m}_j}{m_j^2} = & -\epsilon^{-4} [m_{j+1}(m_{j+2}^{\alpha+1} - 2m_{j+1}^{\alpha+1} + m_j^{\alpha+1}) - 2m_j(m_{j+1}^{\alpha+1} - 2m_j^{\alpha+1} + m_{j-1}^{\alpha+1}) \\ & + m_{j-1}(m_j^{\alpha+1} - 2m_{j-1}^{\alpha+1} + m_{j-2}^{\alpha+1})], \quad j = 0, \dots, N-1; \end{aligned} \quad (\text{A.7a})$$

$$m_{-1} = 0 = m_N, \quad m_{-2}, m_{N+1} : \text{finite}. \quad (\text{A.7b})$$

Thus, the discrete self-similar slopes read $m_j(t) = [(\alpha + 3)t + K]^{-\frac{1}{\alpha+3}} M_j$.

To proceed along the lines of Section 2.3, let $\psi_j = M_j^{\alpha+1}$; or, more generally, $\psi_j(t) = m_j(t)^{\alpha+1}$. Our manipulations for ψ_j remain intact. The analogue of Proposition 2 contains the relation (cf. (2.37))

$$m(h)^{\alpha+1} = C_1 h - C_2 \int_0^h \frac{z(h-z)}{m(z)} dz + \int_0^h \int_0^z \frac{(h-z)(z-\zeta)}{m(z)m(\zeta)} d\zeta dz, \quad (\text{A.8})$$

where C_1 and C_2 are subject to the vanishing of slope and flux at $h = 1$.

Iterations of (A.8) yield a formal expansion of the slope near the facet edge ($h = 0$).

Accordingly, we obtain $m(h(x, t), t) = \mathcal{O}((x - x_f(t))^{1/\alpha})$ as $x \rightarrow x_f(t)$, the position of a facet edge, for sufficiently long times. This behavior manifests the intimate connection of step interaction law and near-facet expansion at equilibrium [10].

A.2.2 Special kinetics of extremal step

In this section we explore the following scenario. Suppose the attachment-detachment law for extremal steps ($j = 0, N$) involve kinetic rates, say k_L for $j = 0$ and k_R for

$j = N$, which may be different from k . So, according to linear kinetics, the fluxes impinging on these steps are

$$-\varphi_0 = 2k_L(\rho_0 - \rho_0^{\text{eq}}) \quad x = x_0 ; \quad \varphi_{N-1} = 2k_R(\rho_{N-1} - \rho_N^{\text{eq}}) \quad x = x_N . \quad (\text{A.9})$$

At the remaining steps, the fluxes have rate $2k$. We study whether k_L or k_R can possibly distort nontrivially the previous boundary conditions in the macroscopic limit, *assuming this limit is well defined*. Without loss of generality, set $k_R = k \neq k_L$ and define

$\beta = k_L/k > 0$; hence, we restrict attention to the left facet edge ($h = 0$). It is tempting

to claim that, in the limit $\epsilon \downarrow 0$, the detail of (A.9) *disappears* and we recover a

continuum-scale boundary condition of zero slope and flux. We discuss formally why this claim is consistent with steps if $\beta = \mathcal{O}(1)$. The situation is subtler if $\beta = \mathcal{O}(\epsilon^\gamma)$, $\gamma > 0$.

The 0-th terrace adatom flux is $\varphi_0 = -\epsilon^{-1}(\bar{k}\epsilon)m_0(\rho_1^{\text{eq}} - \rho_0^{\text{eq}})/(\bar{k}\epsilon + m_0)$ where

$\bar{k} = (k^{-1} + k_L^{-1})^{-1}$. We focus on ADL kinetics, where surface processes are limited by atom attachment-detachment at steps, and scale time by $k\epsilon$. The motion laws for the discrete slopes are described by (2.13a) along with the *partially modified* termination

conditions

$$m_{-1}^3 + (1 - \beta)(m_1^3 - 2m_0^3) = 0 = m_N^3 , \quad (\text{A.10a})$$

$$m_0^3 - 2m_{-1}^3 + m_{-2}^3 = 0 = m_{N-1}^3 - 2m_N^3 + m_{N+1}^3 . \quad (\text{A.10b})$$

Equations (A.10b) state that the auxiliary discrete fluxes vanish, in accord with (2.13b);

hence, we expect that the boundary conditions for the continuum-scale flux are intact.

By contrast, (A.10a) indicates a nonzero m_{-1} , which in turn suggests the possibility of a nonzero continuum-scale slope as $h \downarrow 0$. (Note, however, that in view of (A.10a) the mirror symmetry of the system is removed.)

We proceed to convert (2.13a) to sum equations via generating polynomials from

Appendix A.2.3; let $\psi_j = m_j^3$. After some algebra, we find (cf. (2.48))

$$\begin{aligned} \psi_j = & \frac{1}{6} \left\{ \beta(\psi_1 - 2\psi_0)j^2(j+3) + 2[\psi_0 + \psi_1 - 2(\beta-1)(\psi_1 - 2\psi_0)]j + 6\psi_0 \right. \\ & \left. + \epsilon^4 \sum_{p=0}^{j-2} (j-p-1)(j-p)(j-p+1)(d/dt)\psi_j(t)^{-1/3} \right\}, \end{aligned} \quad (\text{A.11})$$

where, with $F(s) = \epsilon^4 \sum_{j=0}^{N-1} s^j (d/dt)\psi_j(t)^{-1/3}$, the requisite coefficients are

$$\beta(\psi_1 - 2\psi_0) = \frac{-NF(1) + F'(1)}{N+1},$$

$$\begin{aligned} 2(N+1)[\psi_0 + \psi_1 - 2(\beta-1)(\psi_1 - 2\psi_0)] = & \left(2N^2 - N + 6\frac{\beta-1}{\beta} \frac{N}{N+1} \right) F(1) \\ & + \left(2N^2 - 5N + 2 - 6\frac{\beta-1}{\beta} \frac{1}{N+1} \right) F'(1) - 3(N-1)F''(1) + F'''(1), \end{aligned}$$

$$\begin{aligned} 6(N+1)\psi_0 = & \left(2N^2 + N - 6N \frac{\beta-1}{\beta} \frac{N}{N+1} \right) F(1) + \left(2N^2 - 5N \right. \\ & \left. + 6\frac{\beta-1}{\beta} \frac{N}{N+1} \right) F'(1) - 3(N-1)F''(1) + F'''(1). \end{aligned}$$

Note the term ψ_0 entering the right-hand side of (A.11). *The question arises as to whether $\psi_0 = \mathcal{O}(1)$ as $\epsilon \downarrow 0$ by manipulation of β .*

Consider the limit of (A.11) as $N \rightarrow \infty$ with $\epsilon(N+1) = 1$. By inspection of the preceding formulas and repetition of the procedure of Section 2.3.2.2, we infer that any contribution of β is negligible if $\beta = \mathcal{O}(1)$. In this case, the macroscopic laws are identical to those for $\beta = 1$ (Section 2.3.2.2); so, the slope *and* flux vanish at the facet edges. These conditions appear to persist provided $\beta > \mathcal{O}(N^{-3})$. In particular, the flux vanishes at $h = 0, 1$ for any $\beta > 0$ (provided the continuum limit is meaningful). A possibility for nonzero slope as $h \downarrow 0$ may arise if $\beta = \mathcal{O}(N^{-3})$.

Entertaining the scenario of a small, extreme β , suppose $\beta = \check{\beta}/N^3$, $\check{\beta} = \mathcal{O}(1) > 0$, while the macroscopic limit makes sense, e.g., $N^{4-n}F^{(n)}(1) \rightarrow \int_0^1 z^{n-1} \partial_t [m(z, t)^{-1}] dz = \mathcal{O}(1)$ as $N \rightarrow \infty$; $n = 1, 2, 3, 4$ and $F^{(n)}(s)$ denotes the n th-order derivative of $F(s)$. By

dominant balance we wind up with

$$m(h, t)^3 = C_0(t) + C_1(t)h - C_3(t)h^3 + \frac{1}{6} \int_0^h (h-z)^3 \partial_t [m(z, t)^{-1}] dz ; \quad (\text{A.12})$$

cf. (2.53). The coefficients $C_0(t)$, $C_1(t)$, $C_3(t)$ are found to be

$$C_0(t) = \lim_{\epsilon \downarrow 0} \psi_0(t) = \check{\beta}^{-1} \int_0^1 (1-z) \partial_t [m(z, t)^{-1}] dz ,$$

which signifies the nonzero value of the continuum slope as $h \downarrow 0$, and

$$\begin{aligned} C_1(t) &= \lim_{\epsilon \downarrow 0} \frac{\psi_1(t) + \psi_0(t) - 2(\beta - 1)[\psi_1(t) - 2\psi_0(t)]}{3\epsilon} \\ &= \frac{1}{6} \int_0^1 [(1 - 6\check{\beta}^{-1})(1-z) - (1-z)^3] \partial_t [m(z, t)^{-1}] dz , \\ C_3(t) &= - \lim_{\epsilon \downarrow 0} \frac{\beta[\psi_1(t) - 2\psi_0(t)]}{6\epsilon^3} = \frac{1}{6} \int_0^1 (1-z) \partial_t [m(z, t)^{-1}] dz . \end{aligned}$$

Note that if $\check{\beta} \gg 1$, (A.12) reduces to the macroscopic limit of Section 2.3.2.2.

A sufficiently small β forces the microscale flux at the top step to become small; thus, the motion of the extremal step tends to be frozen and the density of steps increases in the vicinity of the left facet edge. Interestingly, our heuristic analysis indicates the critical scaling $\mathcal{O}(N^{-3})$ for β .

A.2.3 Fourth-order difference scheme

Next, consider the difference scheme (2.46). The generating polynomial, $\Psi(s)$, introduced in (2.21) satisfies

$$\begin{aligned} &s^{-2}(\Psi - \psi_0 - \psi_1 s + \psi_N s^N + \psi_{N+1} s^{N+1}) - 4s^{-1}(\Psi - \psi_0 + \psi_N s^N) \\ &+ 6\Psi - 4s(\Psi + \psi_{-1} s^{-1} - \psi_{N-1} s^{N-1}) + s^2(\Psi + \psi_{-2} s^{-2} + \psi_{-1} s^{-1} \\ &- \psi_{N-1} s^{N-1} - \psi_{N-2} s^{N-2}) = F(s) = \sum_{j=0}^{N-1} f_j s^j . \end{aligned}$$

In view of termination conditions (2.46b), we thus find

$$\Psi(s) = \frac{\mathcal{P}(s)}{(1-s)^4}, \quad (\text{A.13a})$$

where the numerator is

$$\begin{aligned} \mathcal{P}(s) = & \psi_0 + (\psi_1 - 4\psi_0)s + \psi_0s^2 + \psi_{N-1}s^{N+1} + (\psi_{N-2} - 4\psi_{N-1})s^{N+2} \\ & + \psi_{N-1}s^{N+3} + s^2F(s). \end{aligned} \quad (\text{A.13b})$$

Clearly, the point $s = 1$ must be a removable singularity in (A.13a); thus, we should have

$\mathcal{P}(1) = \mathcal{P}'(1) = \mathcal{P}''(1) = \mathcal{P}'''(1) = 0$, which entail a system of equations for the parameters $\psi_0, \psi_1, \psi_{N-2}, \psi_{N-1}$:

$$\begin{aligned} \psi_1 - 2\psi_0 + \psi_{N-2} - 2\psi_{N-1} &= -F(1), \\ \psi_1 - 2\psi_0 + (N+2)(\psi_{N-2} - 2\psi_{N-1}) &= -2F(1) - F'(1), \\ 2\psi_0 + (N+1)(N+2)\psi_{N-2} - 2(N^2 + 3N + 1)\psi_{N-1} &= -2F(1) \\ &\quad - 4F'(1) - F''(1), \\ N(N+1)(N+2)\psi_{N-2} - 2(N^2 - 1)(N+3)\psi_{N-1} &= -6[F'(1) \\ &\quad + F''(1)] - F'''(1). \end{aligned} \quad (\text{A.14})$$

The solution of this system leads to formulas (2.49).

Next, we determine ψ_j in terms of ψ_0, ψ_1 with recourse to (2.20); Γ is a contour enclosing 0 in the interior of the unit disk. By removing the analytic part of the integrand, we have (for $j = 0, \dots, N-1$)

$$\psi_j = \frac{1}{2\pi i} \oint_{\Gamma} \frac{\psi_0 + (\psi_1 - 4\psi_0)\zeta + \psi_0\zeta^2 + \zeta^2F(\zeta)}{(1-\zeta)^4} \frac{d\zeta}{\zeta^{j+1}}. \quad (\text{A.15})$$

By virtue of the binomial expansion

$$(1-\zeta)^{-4} = \frac{1}{3!} \sum_{l=0}^{\infty} (l+1)(l+2)(l+3)\zeta^l \quad |\zeta| < 1,$$

the integrand in (A.15) has residue equal to

$$\frac{1}{3!} \left[\psi_0(j+1)(j+2)(j+3) + (\psi_1 - 4\psi_0)j(j+1)(j+2) + \psi_0(j-1)j(j+1) + \sum_{p=0}^{j-2} (j-1-p)(j-p)(j-p+1)f_p \right].$$

By separating distinct powers of j in the first line, we obtain (2.48).

A.3 Iterations of integral equations

In this appendix, we discuss the integral equations of Section 2.3, especially the use of iterations for formally constructing expansions of solutions near facet edges. The case with evaporation-condensation serves as a paradigm for validation of the iteration procedure, since a simple exact, global similarity solution for the slope is derived independently.

A.3.1 Evaporation-condensation

Iteration scheme. Consider the sequence $\{m^{(n)}(h)\}_{n=0}^{\infty}$ defined by (2.31). On the basis of the proposed scheme, we compute

$$\begin{aligned} n = 1 : \quad m^{(1)}(h) &= \left(C_1 h - \frac{9}{10} C_1^{-1/3} h^{5/3} \right)^{1/3} \\ \Rightarrow m^{(1)}(h) - m^{(0)}(h) &= -\frac{3}{10} C_1^{-1} h + \mathcal{O}(h^{5/3}) \quad \text{as } h \downarrow 0. \end{aligned} \quad (\text{A.16})$$

More generally, the difference $\delta m^{(n)} = m^{(n)} - m^{(n-1)}$ satisfies

$$\delta m^{(n)} [m^{(n)2} + m^{(n)}m^{(n-1)} + m^{(n-1)2}] (h) = \int_0^h \frac{(h-z)\delta m^{(n-1)}(z)}{m^{(n-1)}(z)m^{(n-2)}(z)} dz \quad (\text{A.17})$$

for $n = 2, \dots$; $m^{(n)}(h) \sim (C_1 h)^{1/3}$ for every n as $h \downarrow 0$. By inspection of (A.16) and

(A.17), we see that $\delta m^{(n)}(h) \sim a_n h^{b_n}$. For instance, for $n = 2$ we compute

$a_2 = -(9/280)C_1^{-7/3}$, $b_2 = 5/3$ and

$$m^{(2)} \sim m^{(1)}(h) - \frac{9}{280}C_1^{-7/3}h^{5/3} = \left(C_1h - \frac{9}{10}C_1^{-1/3}h^{5/3}\right)^{1/3} - \frac{9}{280}C_1^{-7/3}h^{5/3},$$

which immediately leads to the three-term expansion (2.32) for $m(h)$. Higher-order terms are generated in an analogous fashion, but of course the algebra becomes increasingly cumbersome with the order, n .

Global similarity solution. It is rather fortuitous that $m(h)$ can be determined globally, thus rendering possible a comparison with expansion (2.32). By $\psi(h) = m(h)^3$, the governing ODE is $\psi'' = -\psi^{-1/3}$, where the prime denotes the derivative in h . If $\psi(0) = 0 = \psi(1)$, by symmetry we can restrict $\psi(h)$ in $(0, 1/2)$ where $\psi'(h) \geq 0$ and $\psi'(1/2) = 0$. The ODE is split into the system

$$\psi' = w, \quad w' = -\psi^{-1/3}, \quad (\text{A.18})$$

to which we associate a constant of motion via the ‘‘energy’’

$$\mathcal{E}(h) = \frac{1}{2}w(h)^2 + \frac{3}{2}\psi(h)^{2/3}; \quad \mathcal{E}'(h) = 0. \quad (\text{A.19})$$

Thus, solutions of (A.18) can be parametrized by the constant $c = \mathcal{E}(h)$.

Suppose that we look for solutions consistent with integral equation (2.18). So, we require that ψ , w solve (A.18) for $h \in (0, 1/2)$ under the conditions

$$\psi(0) = 0, \quad w(1/2) = 0. \quad (\text{A.20})$$

By definition of \mathcal{E} and w we compute $h(m)$ by

$$h = \int_0^\psi \frac{d\xi}{\sqrt{2c - 3\xi^{2/3}}} = \frac{c}{\sqrt{3}} \left(\sin^{-1} \tilde{m} - \tilde{m} \sqrt{1 - \tilde{m}^2} \right); \quad \tilde{m} = m \sqrt{\frac{3}{2c}} \quad (\text{A.21})$$

and $0 \leq h \leq 1/2$ along with $w = d\psi/dh \geq 0$. The solution $h(m)$ for $1/2 < h \leq 1$ is obtained by reflection. In principle, (A.21) (and its reflection) can be inverted to

generate $m(h)$. The constant c can be found by setting $h = 1/2$ in (A.21) and using the definition of $\mathcal{E}(h)$ and $w(1/2) = 0$. Thus, we deduce

$$\frac{1}{2} = \int_0^{\psi(1/2)} \frac{d\xi}{\sqrt{2c - 3\xi^{2/3}}} , \quad c = 3\psi(1/2)^{2/3}/2 \Rightarrow c = \sqrt{3}/\pi , \quad (\text{A.22})$$

and $m(1/2) = 3^{-1/4}2^{1/2}\pi^{-1/2}$.

We proceed to generate a power series of $m(h)$ in h by inversion of (A.21). We write the Maclaurin expansion

$$\pi h = \sum_{l=1}^{\infty} \frac{\Gamma(\frac{1}{2} + l)}{l! \Gamma(\frac{1}{2})} \frac{4l}{4l^2 - 1} \tilde{m}^{2l+1} \quad \tilde{m} < 1 ,$$

where $\Gamma(z)$ is the usual Gamma function. The inversion of the last series up to three terms yields

$$\tilde{m}(h)^3 = \frac{3\pi h}{2} - \frac{3}{10} \left(\frac{3\pi h}{2} \right)^{5/3} - \frac{3}{280} \left(\frac{3\pi h}{2} \right)^{7/3} + \mathcal{O}(h^3) \quad \text{as } h \downarrow 0 . \quad (\text{A.23})$$

This expansion is in agreement with (2.32) provided $C_1 = 3^{1/4}2^{1/2}\pi^{-1/2}$. It is worthwhile noting that the complete h -expansion produced by inversion of the exact solution is convergent in a neighborhood of $h = 0$.

A.3.2 DL kinetics

Consider scheme (2.42). Because of the increasingly elaborate algebra, we compute up to three terms for $m(h(\eta))$.

$$\begin{aligned} m^{(1)}(h)^3 &= C_1 h - \int_0^h \frac{h-z}{(C_1 z)^{1/3}} C_2 z \, dz = C_1 h - \frac{9}{40} \frac{C_2}{C_1^{1/3}} h^{8/3} , \quad (\text{A.24}) \\ \varphi^{(1)}(h) &= C_2 h - \int_0^h \frac{h-z}{(C_1 z)^{1/3}} \, dz = C_2 h - \frac{9}{10} C_1^{-1/3} h^{5/3} ; \\ \Rightarrow \frac{\varphi^{(1)}(h)}{m^{(1)}(h)} &= \frac{C_2}{C_1^{1/3}} h^{2/3} - \frac{9}{10} C_1^{-2/3} h^{4/3} + \mathcal{O}(h^{7/3}) \quad h \downarrow 0 . \end{aligned}$$

Accordingly, an approximation for $m^{(2)}(h)$ comes from

$$\begin{aligned} m^{(2)}(h)^3 &= C_1 h - \int_0^h (h-z) \frac{\varphi^{(1)}(z)}{m^{(1)}(z)} \\ &= C_1 h - \frac{9}{40} \frac{C_2}{C_1^{1/3}} h^{8/3} + \frac{3^4}{700} C_1^{-2/3} h^{10/3} + \mathcal{O}(h^{13/3}), \end{aligned} \quad (\text{A.25})$$

which leads to (2.43) where $m(h(\eta)) = h'(\eta)$. By integrating in η we find

$$\bar{\eta} = \frac{3}{2} C_1^{-1/3} h^{2/3} + \frac{9}{280} \frac{C_2}{C_1^{5/3}} h^{7/3} - \frac{9}{700} C_1^{-2} h^3 + \mathcal{O}(h^4) \quad h \downarrow 0.$$

The inversion of this expansion yields

$$h(\eta) = \left(\frac{2}{3}\right)^{3/2} C_1^{1/2} \bar{\eta}^{3/2} - \frac{2}{315} C_2 \bar{\eta}^4 + \frac{8}{4725} \bar{\eta}^5 + \mathcal{O}(\bar{\eta}^{13/2}), \quad (\text{A.26})$$

which is reduced to (2.44) through differentiation.

Appendix B: Evaporation model as limit of BCF-type model in radial setting

In this chapter, we discuss we discuss the source of the geometric factor by deriving M2 as a special case of surface diffusion in the BCF framework; M1 follows from simplification of this model.

First, we provide a modified evaporation-condensation model, M3, which is derived as a special limit of surface diffusion in the context of BCF theory [6, 84] in the presence of desorption and an inverse ES effect. M3 is subsequently simplified to model M2. Outside the facet, these models reduce to the same PDE for the slope profile.

Let C_i be the concentration of adatoms on the i th terrace, $r_{i-1} < r < r_i$, and t_{ds} be a typical desorption time. In juxtaposition to our ad hoc models M1 and M2, here we adopt the viewpoint that the step velocity is driven by changes in the adatom flux across terraces. So, we start with a diffusion equation for the concentration, C_i , of adatoms including desorption under the quasi-steady approximation:

$$\partial_{rr}C_i + r^{-1}\partial_r C_i - \kappa^2 C_i = 0 \quad r_{i-1} < r < r_i , \quad (\text{B.1})$$

where $\kappa^2 = (D_s t_{\text{ds}})^{-1}$ ($\kappa > 0$). Equation (B.1) has the general solution [100]

$$C_i(r) = A_i I_0(\kappa r) + B_i K_0(\kappa r) , \quad (\text{B.2})$$

where $I_0(z)$ and $K_0(z)$ are modified Bessel functions of zeroth order; and A_i and B_i are integration constants to be determined from the boundary conditions at the bounding

step edges. The requisite conditions are

$$-\mathcal{J}_i(r, t) = k_u(C_i - C_i^{\text{eq}}), \quad r = r_i, \quad (\text{B.3a})$$

$$\mathcal{J}_i(r, t) = k_d(C_i - C_{i+1}^{\text{eq}}), \quad r = r_{i+1}, \quad (\text{B.3b})$$

where $\mathcal{J}_i(r, t) = -D_s \partial_r C_i(r, t)$ is the adatom flux on the i th terrace, k_u (k_d) is the kinetic rate for atom attachment/detachment at an up-step (down-step), and C_i^{eq} is the equilibrium concentration at the i th step edge. By (B.2) and (B.3), we obtain

$$\begin{aligned} A_i &= \frac{1}{\mathcal{D}_i} \left\{ -\frac{k_u}{D_s \kappa} C_i^{\text{eq}} \left[K'_0(\kappa r_{i+1}) + \frac{k_d}{D_s \kappa} K_0(\kappa r_{i+1}) \right] \right. \\ &\quad \left. - \frac{k_d}{D_s \kappa} C_{i+1}^{\text{eq}} \left[K'_0(\kappa r_i) - \frac{k_u}{D_s \kappa} K_0(\kappa r_i) \right] \right\}, \\ B_i &= \frac{1}{\mathcal{D}_i} \left\{ \frac{k_d}{D_s \kappa} C_{i+1}^{\text{eq}} \left[I'_0(\kappa r_i) - \frac{k_u}{D_s \kappa} I_0(\kappa r_i) \right] \right. \\ &\quad \left. + \frac{k_u}{D_s \kappa} C_i^{\text{eq}} \left[I'_0(\kappa r_{i+1}) + \frac{k_d}{D_s \kappa} I_0(\kappa r_{i+1}) \right] \right\}, \end{aligned}$$

where the prime denotes differentiation with respect to the argument and

$$\begin{aligned} \mathcal{D}_i &= \left[I'_0(\kappa r_i) - \frac{k_u}{D_s \kappa} I_0(\kappa r_i) \right] \left[K'_0(\kappa r_{i+1}) + \frac{k_d}{D_s \kappa} K_0(\kappa r_{i+1}) \right] \\ &\quad - \left[I'_0(\kappa r_{i+1}) + \frac{k_d}{D_s \kappa} I_0(\kappa r_{i+1}) \right] \left[K'_0(\kappa r_i) - \frac{k_u}{D_s \kappa} K_0(\kappa r_i) \right]. \end{aligned} \quad (\text{B.4})$$

The step velocity law for surface diffusion reads [6, 53]

$$\dot{r}_i = \frac{\Omega}{a} (\mathcal{J}_{i-1} - \mathcal{J}_i) \quad r = r_i. \quad (\text{B.5})$$

By (B.2), the step velocity becomes

$$\dot{r}_i = -\frac{\Omega}{a} \kappa D_s [A_{i-1} I'_0(\kappa r_i) + B_{i-1} K'_0(\kappa r_i) - A_i I'_0(\kappa r_i) - B_i K'_0(\kappa r_i)]. \quad (\text{B.6})$$

We now simplify the right-hand side of (B.6) under the conditions

$$k_u t_{\text{ds}} \ll r_i, \quad \kappa r_i \ll 1, \quad k_u \ll k_d, \quad |r_i - r_{i-1}| \ll \kappa t_{\text{ds}}. \quad (\text{B.7})$$

Note that the second inequality implies that the diffusion length $\sqrt{D_s t_{\text{ds}}}$ is large compared to the step radius. The third inequality expresses an inverse ES effect. Thus, we obtain the simplified step motion law

$$\dot{r}_i = -\frac{\Omega}{t_{\text{ds}}} \frac{r_i + r_{i-1}}{2r_i} \frac{r_i - r_{i-1}}{a} C_i^{\text{eq}}, \quad (\text{B.8})$$

which reveals the (geometric) structure of the discrete mobility if C_i^{eq} is affine in the step chemical potential, μ_i . Now recall the usual Gibbs-Thomson relation [53],

$C_i^{\text{eq}} = C_s \exp(\mu_i/\mathcal{T}) \sim (C_s/\mathcal{T})(\mathcal{T} + \mu_i)$ for $|\mu_i| \ll \mathcal{T}$ where \mathcal{T} is Boltzmann's energy (or absolute temperature in appropriate units); evidently, M2 results from (B.8) by removal of the constant \mathcal{T} [cf. (3.7)].

Appendix C: On discrete equations with $g = 0$ in radial setting

In this appendix, we solve exactly the equations of motion (3.15) with $g = 0$ for the two top steps, aiming to obtain a recursion relation for the time differences $\delta_n = t_n - t_{n-1}$. Our results enable us to check the accuracy of our numerical scheme for solving the step ODEs. We employ units with $\nu\Omega g_1 = 1 = a$.

C.1 Model M1

First, consider times $t_{n-1} < t < t_n$ for fixed collapse number n ($n \geq 1$). For $g = 0$, (3.15) reduce to

$$\dot{r}_i = -\frac{r_i - r_{i-1}}{r_i} \quad i \geq n. \quad (\text{C.1})$$

In particular, for $i = n$ we have $\dot{r}_n = -1$ by which

$$r_n(t) = t_n - t, \quad t_{n-1} < t \leq t_n. \quad (\text{C.2})$$

We proceed to determine $r_{n+1}(t)$, which satisfies $r_{n+1}\dot{r}_{n+1} = -r_{n+1} + t_n - t$ in view of (C.2). We seek a solution in parametric form by using another independent variable, say, τ . Let $t_n - t \equiv \sigma(\tau)$ and $r_{n+1}(t) \equiv \sigma(\tau)p(\tau)$ where σ and p are to be determined. The ODE for $r_{n+1}(t)$ yields

$$\frac{\dot{\sigma}}{\sigma} = -\frac{\dot{p}p}{p^2 - p + 1}, \quad (\text{C.3})$$

which can be integrated exactly; $\dot{\sigma} \equiv d\sigma/d\tau$. By setting $p(\tau) = \tau$ (without loss of

generality), we find $\sigma(\tau)$ and thereby compute t and r_{n+1} as functions of τ :

$$\begin{aligned} r_{n+1}(t(\tau)) &= C(\tau^2 - \tau + 1)^{-1/2} \tau e^{\mathcal{K}(\tau)}, \\ t(\tau) &= t_n - C(\tau^2 - \tau + 1)^{-1/2} e^{\mathcal{K}(\tau)}, \end{aligned} \quad (\text{C.4})$$

where $\tau > \tau_*$ (and τ_* depends on n) and

$$\mathcal{K}(\tau) = \frac{1}{2\sqrt{3}} \tan^{-1} \left[\frac{\sqrt{3}(1-2\tau)}{1+2\tau-2\tau^2} \right]. \quad (\text{C.5})$$

The (in principle n -dependent) constants C and τ_* are determined by the initial conditions $t(\tau_*) = t_{n-1}$ and $r_{n+1}(t(\tau_*)) = r_{n+1}(t_{n-1}) \equiv \mathfrak{R}_n$. Thus, we obtain

$$\begin{aligned} t(\tau) &= t_n - \delta_n \left(\frac{\tau_*^2 - \tau_* + 1}{\tau^2 - \tau + 1} \right)^{1/2} e^{\mathcal{K}(\tau) - \mathcal{K}(\tau_*)}, \\ r_{n+1}(t(\tau)) &= \delta_n \left(\frac{\tau_*^2 - \tau_* + 1}{\tau^2 - \tau + 1} \right)^{1/2} \tau e^{\mathcal{K}(\tau) - \mathcal{K}(\tau_*)}, \end{aligned} \quad (\text{C.6})$$

where

$$\tau_* = \frac{\mathfrak{R}_n}{\delta_n}. \quad (\text{C.7})$$

As the n th step collapses, $t \uparrow t_n$ and thus $\tau \rightarrow \infty$; the radius $r_{n+1}(t_n)$ follows from (C.6).

Now consider times $t_n < t < t_{n+1}$, after the n th step collapses. Then, $r_{n+1}(t) = t_{n+1} - t$.

By continuity of $r_{n+1}(t)$ and use of (C.6), we find the recursion relation

$$\frac{\delta_{n+1}}{\delta_n} = \sqrt{\tau_{*,n}^2 - \tau_{*,n} + 1} e^{-\mathcal{K}(\tau_{*,n})}, \quad (\text{C.8})$$

where $\tau_{*,n} \equiv \tau_* = \mathfrak{R}_n / \delta_n = r_{n+1}(t_{n-1}) / \delta_n$.

It is of interest to discuss implications of (C.8) in the limit $n \rightarrow \infty$, under the

assumption that $\delta_{n+1} / \delta_n \gtrsim 1$. By (C.8), $\tau_{*,n}$ cannot approach 0. If in addition δ_{n+1} / δ_n is

assumed to be bounded with n , as is presumably the case for an initial conical profile

(where $r_i(0)$ is linear in i), we assert that $\tau_{*,n}$ must approach a finite value: $\tau_{*,n} \rightarrow \tau_o$ as

$n \rightarrow \infty$. Thus, τ_o obeys

$$(\tau_o^2 - \tau_o + 1)^{1/2} e^{-\mathcal{K}(\tau_o)} = 1. \quad (\text{C.9})$$

By numerically solving this transcendental equation, we find $\tau_o \approx 1.66$, in agreement with our (independent) numerical simulations for (3.15).

C.2 Model M2

Consider times $t_{n-1} < t < t_n$ for fixed collapse number n ($n \geq 1$). For $g = 0$, (3.15)

reduce to

$$\dot{r}_i = -\frac{r_i + r_{i-1}}{2r_i} \frac{r_i - r_{i-1}}{r_i} \quad i \geq n. \quad (\text{C.10})$$

In particular, for $i = n$ we have $\dot{r}_n = -1/2$ by which

$$r_n(t) = \frac{1}{2}(t_n - t), \quad t_{n-1} < t \leq t_n. \quad (\text{C.11})$$

We proceed to determine $r_{n+1}(t)$, which satisfies

$8r_{n+1}^2 \dot{r}_{n+1} = -(2r_{n+1} + t_n - t)(2r_{n+1} - (t_n - t))$ in view of (C.11). As before, we seek a solution in parametric form by using an independent variable τ . The ODE for $r_{n+1}(t)$ yields

$$\frac{\dot{\sigma}}{\sigma} = -\frac{\dot{p}p^2}{p^3 - (2p+1)(2p-1)/8},$$

where $\sigma(\tau)$, $p(\tau)$ are the functions defined as in the case M1. By integrating the above equation exactly and by setting $p(\tau) = \tau$, we find $\sigma(\tau)$ and thereby compute t and r_{n+1} as functions of τ . Accompanied by initial conditions $t(\tau_*) = t_{n-1}$ and

$r_{n+1}(t(\tau_*)) = r_{n+1}(t_{n-1}) \equiv \mathfrak{R}_n$, these solutions become

$$\begin{aligned} t(\tau) &= t_n - \delta_n e^{\mathcal{K}(\tau) - \mathcal{K}(\tau_*)}, \\ r_{n+1}(t(\tau)) &= \delta_n \tau e^{\mathcal{K}(\tau) - \mathcal{K}(\tau_*)}, \end{aligned} \quad (\text{C.12})$$

where $\tau > \tau_*$ (and τ_* depends on n) and

$$\begin{aligned}\mathcal{K}(\tau) &= - \sum_U \omega \frac{\ln(\tau - \omega_i)}{3\omega_i}, \\ U &= \{\omega : 8\omega^3 - 4\omega^2 + 1 = 0\}, \\ \tau_* &= \frac{\mathfrak{R}_n}{\delta_n}.\end{aligned}$$

As the n th step collapses, $t \uparrow t_n$ and thus $\tau \rightarrow \infty$; the radius $r_{n+1}(t_n)$ follows from (C.12).

Now, consider times $t_n < t < t_{n+1}$, after the n th step collapses. Then,

$r_{n+1}(t) = \frac{1}{2}(t_{n+1} - t)$. By continuity of $r_{n+1}(t)$ and use of (C.12), we find the recursion relation

$$\frac{\delta_{n+1}}{\delta_n} = 2 \prod_{\omega_i \in U} (\tau_* - \omega_i)^{\frac{\omega_i}{3\omega_i - 1}}, \quad (\text{C.13})$$

where $\tau_{*,n} \equiv \tau_* = \mathfrak{R}_n/\delta_n = r_{n+1}(t_{n-1})/\delta_n$.

By (C.8), $\tau_{*,n}$ cannot approach 0. If in addition δ_{n+1}/δ_n is assumed to be bounded with n , as is presumably the case for an initial conical profile (where $r_i(0)$ is linear in i), we assert that $\tau_{*,n}$ must approach a finite value: $\tau_{*,n} \rightarrow \tau_o$ as $n \rightarrow \infty$. Thus, τ_o obeys

$$2 \prod_{\omega_i \in U} (\tau_o - \omega_i)^{\frac{\omega_i}{3\omega_i - 1}} = 1.$$

By numerically solving this transcendental equation, we find $\tau_o \approx 0.94$, in agreement with our (independent) numerical simulations for (3.15). Finally, using this result, we obtain $\mathbf{g} = \lim_{t \rightarrow \infty} \mathcal{G}(t) = \lim_{t_n \rightarrow \infty} \frac{r_{n+2}(t_n) + r_{n+1}(t_n)}{2r_{n+2}(t_n)} = 0.77$.

Appendix D: Continuum solutions for $g = 0$ in radial setting

In this appendix, we provide some detailed derivations of formulas needed in section 3.4.5.

Consider the PDE solution (3.45). The differentiation of height continuity, equation (3.36), with respect to t under initial data (3.42) entails

$$\dot{h}_f(t) = -\dot{r}_f(t) - \frac{1}{r_f(t)} + \frac{t}{r_f(t)^2} \dot{r}_f(t) . \quad (\text{D.1})$$

Accordingly, generalized condition (3.40) on $\xi(\cdot, t)$ yields an ODE for $r_f(t)$:

$$\dot{r}_f(t) = \frac{[2\tilde{\mathcal{G}}(t) - 1]r_f}{r_f^2 - t} ; \quad r_f(0) = r_{f0} . \quad (\text{D.2})$$

Once $r_f(t)$ is computed, $h_f(t)$ can be found via (3.36) and (3.45).

Next, specify values of $\tilde{\mathcal{G}}(t)$ by Remark 7. For $\tilde{\mathcal{G}} = 1$, $r_f(t)$ satisfies

$$\dot{r}_f = \frac{r_f}{r_f^2 - t} ; \quad r_f(0) = r_{f0} . \quad (\text{D.3})$$

This ODE is solved exactly by inversion, $r_f \mapsto T(r_f) = t$:

$$t = T(r_f) = - (r_{f0}^3/3) r_f^{-1} + r_f^2/3 . \quad (\text{D.4})$$

Hence, r_f satisfies the cubic polynomial equation $r_f^3 - 3tr_f - r_{f0}^3 = 0$ and turns out to be [7] $r_f(t) = [r_{f0}^3/2 + \vartheta(t)]^{1/3} + [r_{f0}^3/2 - \vartheta(t)]^{1/3}$ where $\vartheta(t) = \sqrt{r_{f0}^6/4 - t^3}$ (the positive square root is taken for $t < 2^{-2/3}r_{f0}^2$). For $t > 2^{-2/3}r_{f0}^2$, the solution reads

$$r_f(t) = 2\sqrt{t} \cos\left(\frac{1}{3} \tan^{-1} \frac{\sqrt{4t^3 - r_{f0}^6}}{r_{f0}^3}\right) . \quad (\text{D.5})$$

Equation (D.5) leads to asymptotic formula (3.47). The facet height is furnished by height continuity, $h_f(t) = h_{f0} + r_{f0} - r_f - t/r_f$; in particular, we wind up with (3.48).

Now set $\tilde{\mathcal{G}}(t) = \mathbf{c} \neq 1$. Then, again by inversion, (D.2) is exactly solved by

$$t = T(r_f) = (4\mathbf{c} - 1)^{-1} r_f^2 \left[1 - \left(\frac{r_{f0}}{r_f} \right)^{(4\mathbf{c}-1)/(2\mathbf{c}-1)} \right]. \quad (\text{D.6})$$

This equation no longer leads to a polynomial in r_f , in contrast to (D.4). We have been unable to invert (D.6) analytically. Nonetheless, we can obtain an asymptotic formula for r_f in the limit $t \rightarrow \infty$. Notably, growth of a real, nonnegative $r_f(t)$ as $t \rightarrow \infty$ implies $\mathbf{c} > 1/2$. For these values of \mathbf{c} , the first term on the right-hand side of (D.6) dominates for large enough t . A more precise argument to deduce the growth of $r_f(t)$ can be sketched as follows. As $t \rightarrow \infty$, we have either $r_f \rightarrow +\infty$ or $r_f \downarrow 0$ (since $r_f \geq 0$). Suppose that $r_f(t)$ decays as $t \rightarrow \infty$. Consider large t . For $\mathbf{c} < 1/4$, (D.6) would entail $(1 - 4\mathbf{c})t \sim r_{f0}^{(4\mathbf{c}-1)/(2\mathbf{c}-1)} r_f^{1/(1-2\mathbf{c})}$, a contradiction. A similar contradiction is encountered if $1/4 \leq \mathbf{c} < 1/2$. For $\mathbf{c} > 1/2$, by (D.6) $r_f(t)$ would not be compatible with a real solution. Therefore, $r_f(t) \rightarrow +\infty$ as $t \rightarrow \infty$, which implies (3.50) with $\mathbf{c} > 1/2$. In the exceptional case with $\mathbf{c} = 1/2$, by (D.2) $r_f(t) \equiv r_{f0}$ for all $t \geq 0$; there is no facet evolution.

Appendix E: Formal boundary layer analysis for facets in radial setting

In this appendix, we provide heuristic derivations of formulas presented in section 3.5.3 by invoking elements of singular perturbation theory [45]. Self similarity is not needed for our main arguments.

First, $m(r, t)$ is recast to a form that manifests the boundary layer width. Inside the boundary layer (inner region), write

$$m(r, t) = a_0(t)f_0(\zeta, t) , \quad \zeta = \frac{r - r_f(t)}{g^\alpha w(t)} = \mathcal{O}(1) . \quad (\text{E.1})$$

The substitution of (E.1) into PDE (3.24) yields

$$\begin{aligned} \dot{a}_0 f_0 + a_0 \partial_t f_0 - g^{-\alpha} \frac{a_0}{w} (\dot{r}_f + g^\alpha \dot{w} \zeta) \partial_\zeta f_0 &= - \frac{1}{(r_f + g^\alpha w \zeta)^2} \\ &+ g^{1-2\alpha} \frac{a_0^2}{w^2} \partial_\zeta \{ (r_f + g^\alpha w \zeta)^{-1} \partial_\zeta [(r_f + g^\alpha w \zeta) f_0^2] \} . \end{aligned}$$

By treating ζ as well as a_0 , f_0 , w , r_f and their derivatives as $\mathcal{O}(1)$ quantities for $0 < g \ll 1$, we observe that the $\mathcal{O}(g^{-\alpha})$ term on the left-hand side of the last equation must be balanced by the $\mathcal{O}(g^{1-2\alpha})$ term; thus, $\alpha = 1$, as claimed in (3.58).

The resulting equation for f_0 reads

$$\partial_{\zeta\zeta}(f_0^2) = -\ell \partial_\zeta f_0 \quad \zeta > 0 ; \quad \ell := w \dot{r}_f / a_0 . \quad (\text{E.2})$$

Now let us match $a_0(t)f_0(\zeta, t)$ as $\zeta \rightarrow \infty$ with the outer solution for m given by (3.46) as $r \downarrow r_f(t)$, assuming there is a region where the two solutions overlap. Accordingly, we

choose to set $a_0(t)$ equal to $1 - t/r_f^2$, as displayed in (3.59), while we take

$$f_0 \rightarrow 1 \quad \text{as } \zeta \rightarrow \infty . \quad (\text{E.3})$$

By integrating (E.2), in view of (E.3), we obtain

$$(f_0^2)_\zeta = \ell(1 - f_0) \quad \zeta > 0 ; \quad f_0 = 0 \quad \text{as } \zeta \downarrow 0 . \quad (\text{E.4})$$

Here, we impose the condition of slope continuity at the facet edge. We henceforth consider $\partial_t f_0 \equiv 0$ and set $\ell = \text{const}$. By (E.4), we obtain $2f_0 + \ln(1 - f_0) = -\ell\zeta$, which must be reconciled with (E.3). Thus, $\ell > 0$; without loss of generality, set $\ell = 1$. This value leads to formula (3.60). It is of some interest to note that

$$f_0(\zeta) = 1 + W(-e^{-1-\zeta/2}) \quad \text{where } W(x) \text{ is the Lambert function [15].}$$

By definition of ℓ in (E.2), we extract a formula for the boundary layer width in accord with (3.58). This finding concludes our computation of the inner solution for m . As usual, a composite formula can be constructed by adding the outer solution (3.46) to the inner solution, $a_0(t)f_0(\zeta)$, and subtracting their common limit (valid in the overlap region where $\zeta \rightarrow \infty$) [45]; cf. (3.59).

Appendix F: On near-facet expansion for $\mathbf{m}(\eta)$

In this appendix, we provide the coefficients c_l for the sum S_k introduced in (3.57) with $k = 13$. In this vein, we also invoke the coefficients, d_l , of expansion $\mathcal{M}_1(s) \sim \sum_{l=1}^k d_l s^l$. By dominant balance in the similarity ODE (3.53) along with the facet condition (3.54) and after some algebra we derive the following formulas. Set $\tilde{g} = g/\tilde{\mathfrak{g}}$.

$$\begin{aligned}
d_0 &= c_0 = 0, & d_1 &= (\eta_f \tilde{g})^{-1}, & c_1 &= \sqrt{d_1}, & d_2 &= -c_1 \eta_f / (3\tilde{g}), & c_2 &= d_2 / (2c_1), \\
d_3 &= -\frac{\eta_f c_2}{4\tilde{g}} + \frac{1}{2\tilde{g}\eta_f^2} + \frac{c_1^2}{2\eta_f}, & c_3 &= \frac{d_3 - c_2^2}{2c_1}, & d_4 &= -\frac{4}{15\eta_f^2} \left(\frac{3\eta_f^2 c_1 + 3\eta_f^3 c_3}{4\tilde{g}} + 3d_2 \eta_f \right), \\
c_4 &= \frac{d_4 - 2c_2 c_3}{2c_1}, & d_5 &= -\frac{1}{6\eta_f^2} \left(\frac{3c_2 \eta_f^2 + 2c_4 \eta_f^3}{2\tilde{g}} + 6d_3 \eta_f \right), & c_5 &= \frac{d_5 - 2c_2 c_4 - c_3^2}{2c_1}, \\
d_6 &= -\frac{4}{35\eta_f^2} \left(\frac{3c_1 \eta_f + 9c_3 \eta_f^2 + 5c_5 \eta_f^3}{4\tilde{g}} + 5d_2/4 + 10d_4 \eta_f \right), & c_6 &= \frac{d_6 - 2c_2 c_5 - 2c_3 c_4}{2c_1}, \\
d_7 &= -\frac{1}{12\eta_f^2} \left(\frac{3c_2 \eta_f + 6c_4 \eta_f^2 + 3c_6 \eta_f^3}{2\tilde{g}} + 3d_3 + 15d_5 \eta_f \right), & c_7 &= \frac{d_7 - 2c_2 c_6 - 2c_3 c_5 - c_4^2}{2c_1}, \\
d_8 &= -\frac{4}{63\eta_f^2} \left(\frac{c_1 + 9c_3 \eta_f + 15c_5 \eta_f^2 + 7c_7 \eta_f^3}{4\tilde{g}} + 21d_4/4 + 21d_6 \eta_f \right), \\
c_8 &= (d_8 - 2c_2 c_7 - 2c_3 c_6 - 2c_4 c_5) / (2c_1), \\
d_9 &= -\frac{1}{20\eta_f^2} \left(\frac{c_2 + 6c_4 \eta_f + 9c_6 \eta_f^2 + 4c_8 \eta_f^3}{2\tilde{g}} + 8d_5 + 28d_7 \eta_f \right), \\
c_9 &= (d_9 - 2c_2 c_8 - 2c_3 c_7 - 2c_4 c_6 - c_5^2) / (2c_1), \\
d_{10} &= -\frac{4}{99\eta_f^2} \left(\frac{3c_3 + 15c_5 \eta_f + 21c_7 \eta_f^2 + 9c_9 \eta_f^3}{4\tilde{g}} + 45d_6/4 + 36d_8 \eta_f \right), \\
c_{10} &= (d_{10} - 2c_2 c_9 - 2c_3 c_8 - 2c_4 c_7 - 2c_5 c_6) / (2c_1),
\end{aligned}$$

$$\begin{aligned}
d_{11} &= -\frac{1}{30\eta_f^2} \left(\frac{2c_4 + 9c_6\eta_f + 12c_8\eta_f^2 + 5c_{10}\eta_f^3}{2\tilde{g}} + 15d_7 + 45d_9\eta_f \right), \\
c_{11} &= (d_{11} - 2c_2c_{10} - 2c_3c_9 - 2c_4c_8 - 2c_5c_7 - c_6^2)/(2c_1), \\
d_{12} &= -\frac{4}{143\eta_f^2} \left(\frac{5c_5 + 21c_7\eta_f + 27c_9\eta_f^2 + 11c_{11}\eta_f^3}{4\tilde{g}} + 77d_8/4 + 55d_{10}\eta_f \right), \\
c_{12} &= (d_{12} - 2c_2c_{11} - 2c_3c_{10} - 2c_4c_9 - 2c_5c_8 - 2c_6c_7)/(2c_1), \\
d_{13} &= -\frac{1}{42\eta_f^2} \left(\frac{3c_6 + 12c_8\eta_f + 15c_{10}\eta_f^2 + 6c_{12}\eta_f^3}{2\tilde{g}} + 24d_9 + 66d_{11}\eta_f \right), \\
c_{13} &= (d_{13} - 2c_2c_{12} - 2c_3c_{11} - 2c_4c_{10} - 2c_5c_9 - 2c_6c_8 - c_7^2)/(2c_1).
\end{aligned}$$

Bibliography

- [1] H. Attouch, A. Damllamian 1977, *Application des methods de convexite et monotonie a l'etudé de certaines equations quasi lineares*, Proc. Roy. Soc. Edinburgh, 79A, 107-129.
- [2] F. Andreu, J. M. Maçon 2008, *The Total Variation Flow*, lecture notes from the course given in the summer school “Calculus of Variations”, Rome.
- [3] F. Andreu, C. Ballester, V. Caselles and J. M. Maçon 2001, *Minimizing total variation flow*, Diff. and Int. Eq. 14, 321-360.
- [4] H. Al Hajj Shehadeh 2010, *The Evolution of a Crystal Surface: Step ODEs, PDEs and Self-similarity*, Courant Institute, New York University, Ph.D. Thesis.
- [5] H. Al Hajj Shehadeh, R. V. Kohn, and J. Weare 2011, *The evolution of a crystal surface: Analysis of a one-dimensional step train connect two facets in the ADL regime*, Physica D, 240, pp. 1771–1784.
- [6] W. K. Burton, N. Cabrera, F. C. Frank, 1951 *The growth of crystals and the equilibrium structure of their surfaces*, Philos. Trans. Roy. Soc. London Ser. A, 243, 299-358.
- [7] G. Birkhoff and S. MacLane 1959, *A Survey of Modern Algebra*, MacMillan, New York.
- [8] H. P. Bonzel, E. Preuss and B. Steffen 1984, *The dynamical behavior of periodic surface profiles on metals under the influence of anisotropic surface-energy*, Appl. Phys. A-Mater., 35, 1–8.
- [9] A. Bonito, R. H. Nochetto, J. Quah, D. Margetis 2009, *Self-organization of decaying surface corrugations: A numerical study*, Phys. Rev. E 79, 050601.
- [10] H. P. Bonzel 2003, *3D equilibrium crystal shapes in the new light of STM and AFM*, Phys. Rep. 385, 1–67.

- [11] G. F. Carrier, M. Krook, C. E. Pearson 1966, *Functions of a Complex Variable: Theory and Technique*, McGraw-Hill, New York.
- [12] A. Chame, S. Rousset, H. P. Bonzel, and J. Villain 1996/97, *Slow dynamics of stepped surfaces*, Bulgarian Chem. Commun., 29, 398–434.
- [13] Y.-G. Chen, Y. Giga, S. Goto 1991, *Remarks on Viscosity Solutions for Evolution Equations*, Proc. Japan Acad., 67, 323-328.
- [14] E. A. Coddington and N. Levinson 1955, *Theory of Ordinary Differential Equations*, McGraw-Hill, Boston, MA, pp. 13–15.
- [15] R. M. Corless, G. H. Gonnet, D. E. G. Hare, D. J. Jeffrey, and D. E. Knuth 1996, *On the Lambert W function*, Adv. Comput. Math., 5, 329–359.
- [16] W. E, N. K. Yip 2001, *Continuum theory of epitaxial growth. I*, J. Stat. Phys., 104, 221–253.
- [17] G. Ehrlich and F. Hudda 1966, *Atomic view of surface diffusion: Tungsten on tungsten*, J. Chem. Phys., 44, 1039–1099.
- [18] L.-Q. Chen 2002, Annual Rev. Materials Res., 32, 113.
- [19] M. Crandall, H. Ishi, and P.-L. Lions 1992, *User’s guide to viscosity solution of second order partial differential equations*, Bulletin Of The American Mathematical Society, 27, Num. 1, 1-67.
- [20] G. Ehrlich and F. Hudda 1966, *Atomic view of surface self-diffusion: tungsten on tungsten*, J. Chem. Phys., 44, 1039.
- [21] R. L. Schwoebel and E. J. Shipsey 1966, *Step motion on crystal surfaces*, J. Appl. Phys., 37, 3682–3686.
- [22] J. W. Evans, P. A. Thiel, M. C. Bartelt 2006, *Morphological evolution during epitaxial thin film growth: Formation of 2D islands and 3D mounds*, Surf. Sci. Rep. 61, 1–128.
- [23] L.-C. Evans 2002, *Partial Differential Equations*, AMS, Providence, RI.
- [24] L.-C. Evans, J. Spruck 1991, *Motion of level sets by mean curvature I*, J. Diff. Geometry 33, 635-681.
- [25] L.-C. Evans, J. Spruck 1992, *Motion of level sets by mean curvature II*, Trans. Amer. math. Soc, 330, 321-332.
- [26] P.-W. Fok 2006, *Simulation of Axisymmetric Stepped Surfaces with a Facet*, Massachusetts Institute of Technology Ph.D Thesis, Cambridge, MA.

- [27] P.-W. Fok, R. R. Rosales, and D. Margetis 2007, *Unification of step bunching phenomena on vicinal surfaces*, Phys. Rev. B, 76, 033408.
- [28] P.-W. Fok, R. R. Rosales, and D. Margetis 2008, *Facet evolution on supported nanostructures: Effect of finite height*, Phys. Rev. B, 78, 235401.
- [29] M.-H. Giga and Y. Giga 1998, *Evolving graphs by singular weighted curvature*, Arch. Rational Mech. Anal. 141, 2, 117-198.
- [30] M.-H. Giga, Y. Giga, R. Kobayashi 2001, *Very singular diffusion equations*, Adv. Stud. Pure Math., 31, 93-126.
- [31] M.-H. Giga, Y. Giga, and N. Pózar 2014, *Periodic total variation flow of non-divergence type in \mathbf{R}^n* , J. Math. Pures Appl., 102, 203–233.
- [32] Y. Giga, Y. Kashima, M.-H. Sato 2005, *Viscosity solutions with shocks for second order equations*, Research Institute for Math. Sciences Kokyuroku, Kyoto University **1428**, 41–57.
- [33] Y. Giga, R. Kohn 2011, *Scale-invariant extinction time estimates for some singular diffusion equations*, Discr Cont Dyn Sys A 30, 509-535.
- [34] Y. Giga 2003, *Shocks and very strong vertical diffusion*, in Lectures on Partial Differential Equations: Proceedings in honor of Louis Nirenberg’s 75th Birthday, New Studies in Advance Mathematics, International Press, Somerville, MA, Vol.2, 95–102.
- [35] Y. Giga 2003, *Singular diffusivity-facets, shocks and more*, in Applied Mathematics Entering the 21st Century, Invited Talks from the ICIAM 2003 Congress, SIAM, Philadelphia, PA, 121–138.
- [36] M.-H. Giga and Y. Giga 2003, *Minimal vertical singular diffusion preventing overturning for the Burgers equation*, in Recent Advances in Scientific Computing and Partial Differential Equations, Contemp. Math. 330, AMS, Providence, RI, 73–88.
- [37] D. T. J. Hurle 1993, *Handbook of Crystal Growth*, North Holland, Amsterdam.
- [38] M.-H. Giga, Y. Giga, and R. Kobayashi 2001, *Very singular diffusion equations*, Adv. Stud. Pure Math., 31, 93–126.
- [39] T. Michely, J. Krug 2004, *Islands, Mounds and Atoms: Patterns and Processes in Crystal Growth Far From Equilibrium*, Springer, Berlin.
- [40] E. Gruber and W. Mullins 1967, *On the theory of anisotropy of crystalline surface tension*, J. Phys. Chem. Solids, 28, 875–887.

- [41] J. K. Hale 1969, *Ordinary Differential Equations*, Willy-Interscience, Providence, RI, 12–22.
- [42] C. Herring 1950, *Effect of change of scale on sintering phenomena*, J. Appl. Phys., 21, 301–303.
- [43] C. Herring 1951, *Some theories on the free energies of crystal surfaces*, Phys. Rev., 82, 87–93.
- [44] B. R. Hunt, R. L. Lipsman, J. E. Osborn, and J. Rosenberg 2005, *Differential Equations with Matlab*, Wiley, New York.
- [45] M. H. Holmes 1998, *Introduction to Perturbation Methods*, Springer, New York.
- [46] Y. Homma, H. Hibino, T. Ogino, and N. Aizawa 1998, *Sublimation of a heavily boron-doped Si(111) surface*, Phys. Rev. B, 58:13146(13150).
- [47] Z. Hu, J. Lowengrub, S. Wise, and A. Voigt 2012, Physica D **241**, 77.
- [48] N. Israeli, H.-C. Jeong, D. Kandel, J. D. Weeks 2000, *Dynamics and scaling of one-dimensional surface structures*, Phys. Rev. B, 61, 5698–5706.
- [49] N. Israeli and D. Kandel 1999, *Profile of a decaying crystalline cone*, Phys. Rev. B, 60, 5946–5962.
- [50] N. Israeli and D. Kandel 2000, *Decay of one-dimensional surface modulations*, Phys. Rev. B, 62, 13707–13717.
- [51] H.-C. Jeong, J.D. Weeks 1995, Phys. Rev. Lett., 75, 4456.
- [52] C. Jayaprakash, W. F. Saam, S. Teitel 1983, *Roughening and facet formation in crystals*, Phys. Rev. Lett. 50, 2017–2020.
- [53] H.-C. Jeong and E. D. Williams 1999, Surf. Sci. Rep., **34**, 171.
- [54] M. Kalff, G. Comsa, and T. Michely 1998, Phys. Rev. Lett. **81**, 1255.
- [55] R. Kobayashi and Y. Giga 1999, *Equations with singular diffusivity*, J. Stat. Phys., 95, 1187–1220.
- [56] R. V. Kohn, T. S. Lo, and N. K. Yip 2002, *Continuum limit of a step flow model of epitaxial growth*, Statistical Mechanical Modeling in Materials Science, MRS Symposia Proceedings, Materials Research Society, Warrendale, PA, 701, T1.7.1–T1.7.7.

- [57] P. Lax 1973, *Hyperbolic Systems of Conservation Laws and the Mathematical Theory of Shock Waves*, SIAM, Philadelphia, PA.
- [58] P. Lax and B. Wendroff 1960, *Systems of conservation laws*, Commun. Pure Appl. Math., 13, 217–237.
- [59] R. J. LeVeque 2005, *Numerical Methods for Conservation Laws*, Birkhäuser, Basel, 2nd Ed., Chap. 12.
- [60] G. Lieberman 1996, *Second order parabolic differential equations*, World Scientific, Singapore.
- [61] V. I. Marchenko and A. Ya. Parshin 1980, *Elastic properties of crystal surfaces*, Sov. Phys. JETP, 52, 129–131.
- [62] D. Margetis, M. J. Aziz, and H. A. Stone 2005, *Continuum approach to self-similarity and scaling in morphological relaxation of a crystal with a facet*, Phys. Rev. B, 71, 165432.
- [63] D. Margetis, P.-W. Fok, M. J. Aziz, and H. A. Stone 2006, *Continuum theory of nanostructure decay via a microscale condition*, Phys. Rev. Lett., 97, 096102.
- [64] D. Margetis and R. V. Kohn 2006, *Continuum relaxation of interacting steps on crystal surfaces in 2+1 dimensions*, Multiscale Model. Simul., 5, 729–758.
- [65] D. Margetis and K. Nakamura 2011, *From crystal steps to continuum laws: Behavior near large facets in one dimension*, Physica D, 240, 1100–1110.
- [66] T. Michely and J. Krug 2004, *Islands, Mounds and Atoms: Patterns and Processes in Crystal Growth Far From Equilibrium*, Springer, Berlin.
- [67] C. Misbah, O. Pierre-Louis, and Y. Saito 2010, *Crystal surfaces in and out of equilibrium: A modern view*, Rev. Mod. Phys., 82, 981–1040.
- [68] W. W. Mullins 1958, *The effect of thermal grooving on grain boundary motion*, Acta Metall., 6, 414–427.
- [69] D. Margetis and K. Nakamura 2012, *Homogenization of composite vicinal surfaces: Evolution laws in 1 + 1 dimensions*, Physica D **241**.
- [70] D. Margetis 2009, *Homogenization of reconstructed crystal surfaces: Ficks law of diffusion*, Phys. Rev. E **79**, 052601.
- [71] D. Margetis, P.-W. Fok, M. J. Aziz, H. A. Stone 2006, *Continuum Theory of Nanostructure Decay Via a Microscale Condition*, Phys. Review Letters, 97, 096102.

- [72] D. Margetis, A. E. Tzavaras 2009, *Kinetic hierarchies and macroscopic limits for crystalline steps in 1+1 dimensions*, Multisc. Model. Simul. 7,1428–1454.
- [73] K. Nakamura, D. Margetis 2013, *Discrete and continuum relaxation dynamics of faceted crystal surface in evaporation models*, Multiscale Modeling & Simulation, Vol. 11(1), 244–281.
- [74] D. Margetis, and K. Nakamura 2012, *Homogenization of composite vicinal surfaces: Evolution laws in 1+1 dimensions*, Physica D, 241, 1179–1189.
- [75] P. Müller, A. Saúl 2004, *Elastic effects on surface physics*, Surface Science Reports, 54, 157258.
- [76] J. P. Schneider, K. Nakamura, and D. Margetis 2014, *Role of chemical potential in relaxation of faceted crystal structure*, Phys. Rev. E, 89, 062408.
- [77] K. Nakamura, and D. Margetis 2013, *Phase field model for reconstructed stepped surface*, Phys. Rev. E, 88(1), 014401.
- [78] R. Najafabadi and J. R. Srolovitz 1994, *Elastic step interactions on vicinal surfaces of fcc metals*, Surf. Sci., 317, 221–234.
- [79] P. Nozières 1987, *On the motion of steps on a vicinal surface*, J. Phys. France, 48, 1605–1608.
- [80] A. Pimpinelli, V. Tonchev, A. Videcoq, and M. Vladimirova 2002, *Scaling and universality of self-organized patterns on unstable vicinal surfaces*, Phys. Rev. Lett., 88, 206103.
- [81] I. V. Odisharia 2006, *Simulation and analysis of the relaxation of a crystalline surface*, Courant Institute, New York University Ph.D Thesis, New York, NY.
- [82] M. Ohnuma and K.Sato 1997, *Singular degenerate parabolic equations with applications to the p -Laplace diffusion equation*, Comm. Partial Differential Equations 22, no.3-4, 381–411.
- [83] M. Ozdemir and A. Zangwill 1990, *Morphological equilibration of a corrugated crystalline surface*, Phys. Rev. B, 42, 5013–5024.
- [84] A. Pimpinelli and J. Villain 1998, *Physics of Crystal Growth*, Cambridge University Press, Cambridge, UK.
- [85] R.J. Phaneuf, N.C. Bartelt, E.D. Williams, W.Swiech, E. Bauer 1993, *The Crossover from Metastable to Unstable Facet Growth on Si(111)*, Phys. Rev. Lett. 71, 2284–2287.

- [86] M. Pulvirenti 1995, *Kinetic limits for stochastic particle systems*, Lecture Notes in Mathematics, 1627, 96–126, Springer, Berlin, 1996.
- [87] A. Rettori, J. Villain 1988, *Flattening of grooves on a crystal surface: A method of investigation of surface roughness*, J. Phys. France 49, 257–267.
- [88] O. Pierre-Louis 2005, *Dynamics of crystal steps*, C. R. Phys. 6, 11–21.
- [89] J. Quah, L. P. Liang, and D. Margetis 2010, J. Phys. A: Math. Theor., **43**, 455001.
- [90] A. Rettori and J. Villain 1988, *Flattening of grooves on a crystal surface: A method of investigation of surface roughness*, J. Phys. France, 49, 257–267.
- [91] M. Sato 2007, *Effect of step permeability on step instabilities due to alternation of kinetic coefficients on a growing vicinal face*, Eur. Phys. J. B, 59, 311–318.
- [92] W. Selke and P.M. Duxbury 1995, *Equilibration of crystal surfaces*, Phys. Rev. B, 52, 17468–17479.
- [93] R. L. Schwoebel, E. J. Shipsey 1966, *Step motion on crystal surfaces*, J. Appl. Phys. 37, 3682–3686.
- [94] V. B. Shenoy, L. B. Freund 2002, *A continuum description of the energetics and evolution of stepped surfaces in strained nanostructures*, J. Mech. Phys. Solids 50, 1817–1841.
- [95] V. B. Shenoy, A. Ramasubramaniam, H. Ramanarayan, D. T. Tambe, W.-L. Chan, E. Chason 2004, *Influence of step-edge barriers on the morphological relaxation of nanoscale ripples on crystal surfaces*, Phys. Rev. Lett. 92, 256101.
- [96] H. Spohn 1991, *Large Scale Dynamics of Interacting Particles*, Springer, Berlin.
- [97] H. Spohn 1993, *Surface dynamics below the roughening transition*, J. Phys. France, 3, 69–81.
- [98] H. A. Stone, M. J. Aziz, D. Margetis 2005, *Grooving of a grain boundary by evaporation-condensation below the roughening transition*, J. Appl. Phys. 97, 113535.
- [99] Y.-H. Tsai, Y. Giga and S. Osher 2003, *A level set approach for computing discontinuous solutions of Hamilton-Jacobi equations*, Math. Comp., 72, 159–181.
- [100] G. N. Watson 1995, *A Treatise on the Theory of Bessel Functions*, Cambridge University Press, 2nd Ed., Cambridge, UK, 77–78.
- [101] Y. Xiang 2002, *Derivation of a continuum model for epitaxial growth with elasticity on vicinal surface*, SIAM J. Appl. Math. 63, 241–258.